An embedded system for the multiparametric analysis of biological signals : application to the pancreatic biosensor of insulin demand

Antoine Pirog

université de BORDEAUX

Thèse de Doctorat
de l'Université de Bordeaux

École doctorale des Sciences Physiques et de l'Ingénieur

Spécialité Électronique

Préparée au Laboratoire IMS

Par Antoine Pirog

An embedded system for the multiparametric analysis of biological signals: application to the pancreatic biosensor of insulin demand

---

Sous la direction de Sylvie Renaud **et de** Yannick Bornat

Après l'avis de Olivier Romain **et de** Blaise Yvert

Soutenue le 1er Décembre 2017

Devant le comité d'examen formé de:

M. Olivier Romain	Université de Cergy-Pontoise	Rapporteur
M. Blaise Yvert	INSERM	Rapporteur
M. Bogdan Catargi	Centre Hospitalier Universitaire de Bordeaux	Examinateur
Mme. Michela Chiappalone	Istituto Italiano di Tecnologica (IIT)	Examinatrice
M. Fabrice Morin	Technische Universität München (TUM)	Examinateur
M. Patrik Rorsman	Oxford University	Examinateur
Mme Sylvie Renaud	Bordeaux INP	Directrice de Thèse
M. Yannick Bornat	Bordeaux INP	Co-encadrant

Thèse réalisée
dans le laboratoire **IMS**
au sein de l'équipe **Elibio**.

Université de Bordeaux Laboratoire IMS
CNRS UMR-5218 351,
cours de la Libération
33405 TALENCE Cedex

"Well, I am a dilettante. It's only in England that dilettantism is considered a bad thing. In other countries it's called interdisciplinary research."

- Brian Eno

Abstract

Extracellular recording of electrical activity is a widespread technique in neurosciences, but only recently has it been applied to pancreatic islets and beta cells. The ease of use of Microelectrode Arrays (MEAs) has opened new perspectives for the electrophysiology of pancreatic cells, including screening methods for clinics and biosensor approaches for the artificial pancreas. This thesis is a contribution to the design and characterization of a hybrid biosensor composed of pancreatic cells cultured on an MEA and dedicated processing electronics. This device is the product of multi-disciplinary projects conducted at IMS (Bioelectronics group), partnered with CBMN (Cell biology and Biosensors team), both at the University of Bordeaux. Projects also involved the endocrinology service of university hospitals in Bordeaux, Montpellier, Grenoble, and Geneva.

The covered projects include:

— ISLET-CHIP (French ANR 2013-PRTS-0017), investigating a method of evaluating the quality of a preparation prior to its transplantation in type-I diabetic patients.
— BIODIA (EU FEDER), characterizing islet electrical response to glucose, hormone, and drug stimuli for screening, cell differentiation, and closed-loop approaches.
— DIAGLYC (French regional grant 2017 1R30 226), investigating the use of the hybrid biosensor as an artificial pancreas front-end sensor.

The thesis tackles the biosensor in both its electronic and biological aspects, its integration in applicative experimental setups, and experimental results. It also addresses the modeling of a closed regulation loop for type-I diabetic patients.

First, the electronic processing platform is described. It is a custom board performing multichannel acquisition and digital signal processing. It is built around an FPGA (Field Programmable Gate Array) that makes its processing architecture versatile and evolutive. It is capable of measuring, displaying and storing multichannel data. Computation was optimized for low-processing latencies compatible with closed-loop configurations. Both its processing algorithms and architecture are detailed.

Then, experimental results using this system and its algorithms are shown to illustrate islet response to glucose, drug, and hormone stimuli. Islet activity is quantified by analyzing Action Potentials (APs), and more importantly Slow Potentials (SPs), a novel electrical signature exclusively measured on pancreatic islets. These measurements in both steady state and dynamic regime help characterize the biosensor response, but also shed light on the endogenous algorithms of islets of Langerhans.

Finally, approaches for integrating the biosensor in an artificial pancreas are investigated. The measured glucose and hormone responses are modeled and simulated in a full-body glucose-insulin system. This concept is novel in that the sensor in charge of measuring insulin demand in the body is not only sensitive to glucose, but also to blood hormones.

Key words

Biological signals, FPGA, Diabetes, Bioelectronics,

Résumé

L'enregistrement extracellulaire d'activité électrique est une technique très répandue en neurosciences, mais son application aux îlots pancréatiques et cellules bêta n'est que très récente. La facilité d'utilisation des MEAs (Microelectrode Arrays, Matrices de Microélectrodes) a ouvert de nouvelles perspectives à l'électrophysiologie des cellules bêta, dont des méthodes de criblage en clinique ou des approches biocapteur pour le pancréas artificiel. Cette thèse contribue à la conception et la caractérisation d'un biocapteur hybride composé de cellules pancréatiques cultivées sur un MEA et d'un système électronique de traitement du signal. Le système ainsi réalisé est le fruit de collaborations et projets pluridisciplinaires menés à l'IMS (groupe bioélectronique), en partenariat avec le CBMN (biologie cellulaire et biocapteurs), tous deux au sein de l'Université de Bordeaux. Les projets faisaient également appel au service d'endocrinologie des Hôpitaux Universitaires de Bordeaux, Montpellier, Grenoble et Genève.

Les projets en question incluent :

— ISLET-CHIP (ANR 2013-PRTS-0017), qui explore une méthode pour évaluer la qualité d'un greffon pancréatique destiné à des patients diabétiques de type I.
— BIODIA (EU FEDER), qui caractérise la réponse électrique d'îlots à des stimuli de glucose, hormones et médicaments pour des applications de criblage, différentiation cellulaire, et en boucle-fermée.
— DIAGLYC (Bourse régionale 2017 1R30 226), qui étudie l'utilisation du biocapteur hybride comme un capteur pour le pancréas artificiel.

La thèse aborde le biocapteur dans ses aspects à la fois électronique et biologique, son intégration dans des expériences appliquées, et ses résultats expérimentaux. Elle s'intéresse également à la modélisation d'une boucle de régulation chez le patient diabétique de type I.

D'abord, le système d'analyse électronique est décrit. Issue de l'équipe Elibio, il réalise acquisition multicanaux et traitement du signal numérique. Il est construit autour d'un FPGA (Field Programmable Gate Array) qui rend son architecture de calcul polyvalente et évolutive. Il est capable de mesurer, afficher, et enregistrer des données multicanaux. Le calcul embarqué est optimisé pour de faibles latences de calcul, compatibles avec des applications en boucle fermée. La thèse décrit ses algorithmes de traitement et son architecture.

Des résultats expérimentaux utilisant le système et ses algorithmes sont ensuite montrés pour illustrer la réponse des îlots à des stimuli de glucose, médicaments et hormones. L'activité des îlots est quantifiée en analysant leurs APs (Action Potentials, Potentiels d'Action), et plus notoirement leurs SPs (Slow Potentials, Potentiels Lents), une nouvelle signature électrique exclusivement mesurée sur les îlots pancréatiques. Ces mesures, en régimes statique et dynamique, contribuent non seulement à caractériser la réponse du biocapteur, mais aussi à mettre en évidence les algorithmes internes des îlots de Langerhans.

Enfin, des approches pour l'intégration du biocapteur dans un pancréas artificiel sont étudiées. Les réponses au glucose et aux hormones sont modélisées et simulées dans un modèle des interactions glucose-insuline dans le corps entier. Ce concept est novateur dans le sens où le capteur en charge de mesurer le besoin d'insuline n'est pas seulement sensible au glucose, mais aussi aux hormones présentes dans le sang.

Mots-clés

Signaux biologiques, FPGA, Diabète, Bioélectronique

Remerciements

Le travail qui sera présenté dans cet ouvrage est le fruit de trois ans de recherches. Bien entendu ceci n'est pas l'œuvre d'une personne seule, et beaucoup de crédit revient à tous ceux qui m'ont entouré professionnellement et, particulièrement dans une aventure de longue haleine telle que celle-ci, personnellement. Bien que le reste du manuscrit soit en anglais, mais je me permets ces mots dans ma langue maternelle.

D'abord, je me dois de remercier les deux directeurs de l'IMS qui se sont succédés durant ma thèse, les professeurs Claude Pellet et Yann Deval, pour m'avoir accueilli au sein du laboratoire. Ma gratitude va tout particulièrement à Yann Deval pour ses cours hauts en couleur lorsque j'étais son élève, ainsi que pour ses mots sincères à l'obtention de ma thèse.

Mes remerciements sincères vont ensuite à Messieurs Olivier Romain et Blaise Yvert, rapporteurs de cette thèse, pour leur relecture et commentaire, irrécusables autant de justesse que d'autorité.

Merci ensuite aux membres du jury pour avoir accepté d'assister à la soutenance, et pour s'être déplacés, de près ou de loin, pour examiner mes travaux. Merci à Fabrice Morin pour sa minutie et son exhaustivité dans le commentaire, et à Patrik Rorsman, *physiologist extraodinaire*, pour son interprétation – revendiquée – de *Dr. Jekyll and Mr. Hyde*. Bien sûr je remercie chaleureusement Michela Chiappalone pour avoir si promptement accepté de participer à cette soutenance et de l'avoir ensuite fait avec tant d'intérêt et de sincérité. Merci également pour son accueil à Gènes lors de notre première rencontre il y a maintenant plus de trois ans. Enfin merci à Bogdan Catargi pour avoir si agréablement présidé la soutenance, muni de son habituelle légèreté frisant l'impesanteur.

Enfin, je remercie les différents acteurs des projets ISLET-CHIP, BIODIA et DIAGLYC à Bordeaux, Genève, Montpellier et Grenoble, ainsi que ceux qui y contribueront par la suite, particulièrement David Henry et Jérôme Cieslak.

*
* *

Chaleureusement, je remercie mes encadrants de thèse Sylvie Renaud et Yannick Bornat. Merci à Sylvie pour ses conseils réfléchis et apaisants, sa direction toujours empreinte de bienveillance et de sagesse – qui en était autant une direction que la main assurée d'un parent qui accompagne son bambin sur son premier tour à vélo – et une implacable volonté de me préserver devant les innombrables sollicitations et mon ignorance du mot "non". Sans mentionner un magnifique bonnet vert canard tricoté main. Merci à Yannick pour son accessibilité – plus de sa personne que de son calendrier, je le concède – son pointillisme infatigable, son œil acéré, son intérêt érudit pour la photographie, le cinéma douteux, les boisson houblonnées et la gaufre, mais avant tout merci à lui pour sa décontraction, devant même sa ridicule charge de travail. Merci à vous deux pour votre encadrement impeccable. J'ai eu le luxe, grâce à vous, de réaliser ma propre vision de la thèse malgré ma propension au désordre. J'ai réellement apprécié la confiance que vous m'avez accordée et la pédagogie dont vous avez fait preuve. Avec vous le jeune stagiaire qui est arrivé dans l'équipe il y a bientôt quatre ans a bien changé !

Il me reste ensuite à remercier les autres titulaire d'Elibio, Noëlle Lewis et Gilles N'Kaoua. Merci à Noëlle pour si bien contribuer à l'atmosphère du doux cocon Elibio, ainsi qu'à sa plus pragmatique attention aux deadlines qui a sans doute pallié à ma phobie administrative. Enfin, une oraison jaculatoire pour Gilles et son inébranlable décontraction. Aussi, pour ses boutades frivoles qu'il débite à chaque occasion qui se présente (trois). Reste un rockeur Gilles, ça te va si bien.

Avant mes contemporains, je tiens à exprimer toute mon affection et ma gratitude pour mes aînés. A commencer par François, que je remercie pour la quotidienne ambiance musicale, diversifiée et symptomatique d'un rare cas d'érudition. Merci à toi pour avoir insufflé en moi les bases d'un doctorat bien vécu, dans le plaisir d'une franche camaraderie et d'une décontraction teintée d'un bon stoïcisme des familles. Ensuite Florian, chercheur modèle, penseur acharné, rigoureux, et malgré tout d'une présence absolument apaisante et rassurante. Merci aussi à Ashwin et ses talents de cuisinier et à Adeline et son patronyme qui sent bon la mère patrie.

Place maintenant à mes contemporains d'Elibio. Jonathan, collègue galérien aux mains râpeuses et au cœur tendre. J'ai pris un vrai plaisir de partager avec toi ces quelques années et leur dose quotidienne de travail, difficultés, échecs, frustrations, procrastinations, stress, deadlines, et occasionnelles réussites. Ensuite, plutôt petite jeune que contemporaine, Amélie, que Jonathan et moi abandonnons simultanément, non sans crainte de précipiter chez elle un incurable sentiment d'abandon. Merci à toi pour cette amitié d'une inexplicable force, pour les nombreux moments de détente et de divertissements qui ont pu graviter autour de toi, et pour la ténacité dont tu as pu faire preuve face à deux doctorants au bord de la démence. Même si nous ne nous sommes vraiment croisés qu'un an dans l'équipe, nous l'avons rempli plus que de raison et il est maintenant difficile d'imaginer la vie au labo autrement !

Enfin, merci aux "petites mains" électroniciennes qui ont contribué / contribueront à mon travail : Clément Hognon pour être venu prêter main forte à l'approche des derniers mois de thèse, et Loïc Olçomendy pour reprendre le flambeau et continuer mon travail le temps d'une thèse supplémentaire ; courage à toi pour reconquérir les nombreux aspects de cette recherche et mener à bien ses perspectives.

*
* *

Bien sûr, ce travail, tentaculaire par sa diversité, n'aurait pas pu être mené sans la collaboration proche avec les membres du laboratoire CBMN. Merci d'abord à Jochen Lang, premier représentant du *"Wir machen keine halben Sachen"* de ces remerciements. Merci à lui pour son accueil, sa clairvoyance, sa détermination, et son conseil toujours opportun. Merci ensuite à Matthieu Raoux pour sa grande gentillesse, sa convivialité, son esprit politique taquin, et par dessus tout son rôle central dans la bonne entente – humaine et professionnelle – entre les équipes de deux disciplines *exolingues*.

Je remercie ensuite chaleureusement Romain, pourfendeur de souris, camarade de paillasse, et premier membre de notre *gang* de jeunes, pour avoir partagé et noyé à de nombreuses reprises la peine d'une journée infructueuse devant des cultures capricieuses. J'ai consciencieusement apprécié le temps passé avec toi à déconner au laboratoire où en dehors. Dans ce même environnement, je remercie la belle Éléonore pour une riche rencontre autour d'un stage, et pour sa superbe – et regrettée – compagnie pendant mes premiers pas dans les expériences d'électrophysiologie. Enfin sa successeure, la magnifique (puisqu'il faut faire dans la surenchère) Manon. Utilisatrice prosélyte de Multimed, merci à toi pour tes nombreux, *nombreux* retours qui ont sans doute causé la vaste majorité de mon travail au-delà des horaires "décents". Outre cette pique, merci à toi pour ta rigueur à toute épreuve, ton implication admirable, et à titre plus personnel, pour le temps passé en ta délicieuse compagnie. Je te souhaite toute la réussite que tu mérites pour ta thèse fraîchement commencée.

Merci enfin à tous ceux que j'ai pu croiser, quotidiennement ou moins, dans les couloirs du CBMN : Julien et sa barbe très abondante, Fanny pour la qualité de son héritage et son accueil attentionné à Genève, Isma et sa personne si *perky*, Ariana et son grand sourire, sans oublier Myriam, Eileen, Pier, Alexandra, et Etienne.

*
* *

Je remercierai ensuite les personnes qui n'ont pas directement contribué à mon travail, mais que j'ai croisées régulièrement aux abords du laboratoire et du campus. Ceux-là par leurs positions de conseils, aides et amis gagnent leur place dans mon souvenir à la sortie de la thèse.

D'abord les voisins d'étage, que je remercierai pour des motifs occasionnellement professionnels, mais principalement personnels. Merci d'abord aux membres de l'équipe AS2N : aux permanents Sylvain Saïghi, Jean Tomas et Timothée Levi ; aux "anciens" de la belle époque Gwendal et Matthieu ; aux petits jeunes Manuel, Farad et Charly. Merci ensuite aux membres de BioEm : Bernard Veyret, Isabelle Lagroye, Yann Percherancier, Emma, Rémy, et Ian, mon second contemporain et amateur de bonne chair (*pun intended*). Enfin, merci aux membres de l'équipe capteurs ; Jean-Luc, Simon, Krishna et Samuel. Deux mentions spéciales : l'une pour Luigi, bel italien, *di notte leoni, di giorno coglioni*, mais toujours avec classe *(che non è acqua)* ; l'autre pour Katrin, seconde représentante teutonne du *"Wir machen keine halben Sachen"*, et pas des moindres puisque celle-ci se réfère à la taille de son verre.

Merci ensuite aux personnes qui ont endossé des rôles plus administratifs : Merci d'abord à Simone, qui a tenu l'accueil pendant ma thèse et bien d'autres avant, et qui a tenu sa réputation de rendre à tous la vie plus simple et plus agréable ; ensuite à notre gestionnaire bien-aimée Valérie pour l'organisation des nombreux déplacements, ses airs de "maman cool", et son goût pour la musique ; également à Brigitte Bordes qui a suivi avec beaucoup de minutie les aspects administratifs de la thèse du côté de l'école doctorale ; enfin à Sophie, qui a su maintenir avec zèle nos espaces de travail immaculés.

Je tiens également à remercier les personnes avec qui j'ai enseigné à l'ENSEIRB-MATMECA durant la thèse : Arnaud Curutchet et Nathalie Deltimple pour l'électronique analogique, et Patrice Tesson pour l'électromagnétisme. Bien sûr, merci à Christophe Jego pour avoir si bien orchestré la répartition des cours chaque année. Pour finir, merci à mes élèves pour leurs retours – conscients ou non – qui m'ont donné la confiance et l'envie de me lever aux aurores pour leur enseigner les rudiments des matières déjà nommées.

*
* *

Viennent finalement mes remerciements purement personnels. Ma vie en dehors du laboratoire étant, aux dires de beaucoup, plus remplie que celle du thésard standard, ils sont probablement plus nombreux que de raison. Je citerai les Pennarun, Ariane et Christian, Cécile et Quentin, Claire et Alex ; le groupe des erasmus, Sergio la belle blonde, Lucie, Amélie, Nadia, Edoardo, Anna, et tous les autres ; les colocs d'Amélie, Vanille et Alizée ; la famille des N'Kaoua, Hervé, Bernard, Ilan, Benjamin, qui ont constitué un bout d'entourage musical complètement décomplexant. Pour les moments plus difficiles je remercie chaleureusement Yoann et Jean ; Yoann, bon vivant en toutes circonstances, et très apte à changer efficacement les idées par tous les moyens, solides ou liquides ; Jean, amateur érudit de musique, bruit, littérature, langues, technologies, programmation, et globalement trop de sujets que l'on partage, merci pour les nombreuses sessions de remontage de moral. Por la helpo, kiun vi alportis al mi, dankon de la fundo de mia koro !

Merci infiniment à mes colocs et *bandmates*, Germain et Alexis, pour plus de cinq ans de vie commune et de musique : Germain, fier breton, beau comme une star des 60s, merci pour ton ouverture, ton raffinement, et ce que je devrai qualifier d'un sens du devoir que jamais je n'atteindrai ; Alexis, *my brother from another mother*, musicien extraordinaire, scientifique plus que correct, acharné politique, et globalement ce qu'il se fait de plus proche d'un humaniste moderne, merci pour la compagnie musicale et pour les projets d'un avenir incertain mais ô combien satisfaisant. Merci aussi à Léopold, dernier bandmate et occasionnel coloc, talentueux batteur, pour ces quelques années de renouveau musical et ton insaisissable personnalité qui fait toujours sourire. Ensemble nous avons réussi à autoproduire entièrement un album en plein milieu de nos thèses, et ça reste de loin l'aventure la plus mémorable de ces trois dernières années.

A Amélie, merci pour quatre ans passés ensemble, pour ton amour, pour ta bienveillance, pour ton aide précieuse et généreuse, et plus généralement pour être une personne absolument magnifique en tous aspects. Merci bien sûr à ta petite famille, Nathalie, Olivier, Guillhem, Myriam et Jake, pour me donner ce sentiment d'appartenance familiale si sincère.

Enfin, merci à mes parents, pour leur soutien, si j'en suis ici aujourd'hui c'est en grande partie de leur fait.

Contents

List of Figures 19

List of Tables 21

Abbreviations 24

Introduction 25

1 Scientific context 27
- 1.1 Type 1 Diabetes Mellitus . . . 27
  - 1.1.1 Epidemiology and prevalence . . . 28
  - 1.1.2 Pathophysiology . . . 28
  - 1.1.3 Existing treatments . . . 29
- 1.2 Continuous Glucose Monitors . . . 30
  - 1.2.1 Principle . . . 30
  - 1.2.2 Artificial pancreas . . . 30
  - 1.2.3 Limitations . . . 31
- 1.3 Electrophysiology of the pancreatic β cell . . . 32
  - 1.3.1 General electrophysiology . . . 32
  - 1.3.2 Transient ion mechanisms in the β cell . . . 32
  - 1.3.3 Measurement techniques . . . 33
- 1.4 Biosensors . . . 37
  - 1.4.1 Designing the transducer . . . 37
  - 1.4.2 Applications . . . 37
- 1.5 Research context . . . 38
  - 1.5.1 Research projects for diabetes . . . 39

2 Multimed, the measuring device 41
- 2.1 Introduction . . . 41
- 2.2 Hardware . . . 42
  - 2.2.1 Architecture . . . 42
  - 2.2.2 Interfaces . . . 44
- 2.3 The FPGA as a core processing unit . . . 46
- 2.4 VHDL architecture . . . 46
  - 2.4.1 The philosophy behind the architecture . . . 46
- 2.5 The processing algorithms . . . 48
  - 2.5.1 Wavelet filters . . . 48
  - 2.5.2 IIR filters . . . 48
  - 2.5.3 Adaptive threshold: standard deviation estimator . . . 49
  - 2.5.4 ISI processing: spike cleaning and burst detection . . . 49
  - 2.5.5 Detection of Slow-Potentials . . . 49
  - 2.5.6 Amplitude measurements . . . 50
  - 2.5.7 Frequency and FOPP measurements . . . 50
  - 2.5.8 Electrode sorting . . . 52

2.5.9 Spatial averaging . . . 55
2.6 Complete processing architecture . . . 55
2.7 Hardware implementation . . . 56
2.7.1 Integration and communication . . . 56
2.7.2 Parallelization and serialization of computation . . . 57
2.7.3 Implementation costs and performance . . . 57
2.8 Functional blocks . . . 60
2.8.1 Recording . . . 60
2.9 Graphical User Interface . . . 60
2.9.1 Communication layer . . . 60
2.9.2 Graphical interface layer . . . 61
2.10 Hardware support . . . 63
2.10.1 Complete setup . . . 63
2.11 Modularity and Evolutivity . . . 63
2.11.1 Macro-module aspect . . . 63
2.11.2 Technology transfer . . . 64

3 Experiments and results **67**
3.1 Materials and methods . . . 67
3.1.1 Electrophysiology material . . . 68
3.1.2 Biological materials . . . 70
3.1.3 Routine setups and protocols . . . 71
3.1.4 Analysis methods . . . 72
3.2 Glucose dose-response . . . 72
3.2.1 Action Potential frequency dependence . . . 73
3.2.2 Slow-Potential frequency dependence . . . 73
3.2.3 Asymmetry in glucose dose-responses . . . 73
3.3 Hormone dose-response . . . 73
3.3.1 Adrenaline . . . 73
3.3.2 GLP-1 . . . 76
3.4 A general analysis of pancreatic signals . . . 77
3.4.1 Correlation between Action Potentials and Slow Potentials . . . 78
3.4.2 Biphasic activity . . . 79
3.4.3 Correlation between Slow Potentials . . . 79
3.5 Functional experiments . . . 79
3.5.1 Blind experiments . . . 81
3.5.2 Quality control of pancreatic islets . . . 83
3.6 Discussion . . . 84
3.6.1 Introducing Glucose-equivalents . . . 84
3.6.2 Towards a data-based biosensor model . . . 86

4 Towards the artificial pancreas **89**
4.1 Simulation environment . . . 90
4.1.1 Models for whole-body glucose-insulin dynamics . . . 90
4.1.2 Python integration of the T1DMS model . . . 90
4.2 Integrating the biosensor . . . 94
4.2.1 SP generation . . . 94
4.2.2 SP response static model . . . 95
4.2.3 Hysteresis model . . . 95
4.2.4 Dynamic model . . . 95
4.2.5 Glucose-equivalents . . . 97
4.2.6 Simulation results . . . 98
4.3 Perspectives . . . 103
4.3.1 Robust controllers and model identification . . . 103
4.3.2 Supervised closed-loop on mice . . . 103

Conclusion **107**

A SP detection validation on β cell signals **113**

B Electrode sorting validation data **115**

C Storage formats **117**
C.1 Raw data . . . 117
C.2 Processed data . . . 117
C.3 Processed data IDs and properties . . . 119

D Functional Blocks **123**
D.0.1 Spatial display of detected events . . . 123
D.1 High-level communication interfaces . . . 124
D.1.1 Microcontroller-VHDL blocks communication . . . 124
D.1.2 Microcontroller-User communication . . . 124

E Configuring Multimed **125**
E.1 Summary . . . 125
E.2 Detail . . . 127
E.2.1 Acquisition configuration . . . 127
E.2.2 Recording setup . . . 127
E.2.3 Wavelet coefficient configuration . . . 127
E.2.4 Wavelet levels configuration . . . 127
E.2.5 Interspike interval configuration . . . 127
E.2.6 Adaptive threshold configuration . . . 127
E.2.7 AP frequency measurement configuration . . . 128
E.2.8 FOPP measurement configuration . . . 128
E.2.9 SP timeout configuration . . . 128
E.2.10 SP detection threshold configuration . . . 128
E.2.11 SP filter configuration . . . 128
E.2.12 SP frequency measurement configuration . . . 128
E.2.13 Displayed channel selection . . . 128
E.2.14 Sortin LUT configuration . . . 128
E.2.15 Electrode sorting . . . 128

F Setting up Multimed **131**
F.1 Instructions . . . 131
F.2 Safety precautions . . . 131

G Event correlation computation method **133**

H Revised quality control protocol **135**

I Model equations and parameters **137**

Bibliography **141**

List of Figures

1.1 Personalities known to have developed Type 1 Diabetes Mellitus (T1D). 28
1.2 A Deltec Cozmo insulin pump with its infusion set 30
1.3 The six stages of artificial pancreas development as classified by the Juvenile Diabetes Research Foundation (JDRF). 31
1.4 Context and mechanisms of pancreatic β cells. 34
1.5 Different techniques for recording cell activity, intra- and extra-cellular. 35
1.6 Principle of Microelectrode Array (MEA) measurements. 36

2.1 The Multimed hardware and its key components. 45
2.2 MCS hardware used in conjunction with Multimed. 45
2.3 The Multimed VHDL (VHSIC Hardware Description Language) architecture. . 47
2.4 IIR filters cutoff frequencies with respect to k 51
2.5 Slow Potential (SP) detection scheme. 51
2.6 SP frequency measurement performance on a 0.5 Hz sine wave. 52
2.7 Electrode sorting architecture. 54
2.8 Sorting results on three different experiments. 55
2.9 Complete processing architecture. 56
2.10 Inter-module communication schemes. 59
2.11 Graphical User Interface (GUI) layout. 62
2.12 Complete measurement setup scheme. 63
2.13 Pictures of two different measurement setups. 65

3.1 Two planar MEAs used in ISLET-CHIP 69
3.2 Human islets are sampled from preparations destined for transplantation. . . . 71
3.3 Action Potentials (APs) activate at post-prandial glucose levels in mouse islets. 74
3.4 Electrical activity recorded on mouse islets and real-time SP frequency measurement, showing SPs modulated by glucose concentration. 75
3.5 Human islets show glucose-dependent SPs. 75
3.6 Asymmetrical response of SP frequency to small glucose steps in the physiological range (3-11 mmol/l). 76
3.7 SPs of mouse islet cells are inhibited by Adrenaline. 77
3.8 SPs of mouse islets are excited by GLP-1. 77
3.9 Tendency of APs recorded on mouse islets to fire during the falling phase of SPs. 78
3.10 Signals recorded on murine islets show a two-phase activity when stimulated by a glucose step. 80
3.11 Changes in electrical coupling in pancreatic islets during Glucose-induced biphasic response on acphdmea. 81
3.12 Blind experiment. SP frequency was measured online on a microfluidic MEA (μ-MEA), in response to 3 different unknown glucose concentrations. 82
3.13 Islet quality control protocol. 85
3.14 SP frequency measured in real-time during a quality control experiment on whole human islets at the Geneva University Hospital. 86

4.1 Whole body model used as a simulation environment. 92
4.2 Original Glucose-Insulin model ported to Python 2.7 for a non-diabetic person. 93
4.3 Model of average and normalized SPs. **A**: One period of the modeled SP at 1 Hz. **B**: 0-0.5 Hz ramp of SPs. 94
4.4 Static model of SP response to glucose. 95
4.5 Preisach hysteresis model fitted to SP frequency response to small steps of glucose. 96
4.6 Glucose equivalent principle and identification. 99
4.7 Derived glucose equivalent models. **A** and **B**: GLP-1-dependent glucose equivalents. **C** and **D**: Adrenaline-dependent glucose equivalents. 100
4.8 Simulations of *in silico* T1D patients. 102
4.9 Integration of a Glucose- and Hormone-sensitive regulation scheme including the biosensor model and a $\mathcal{H}_\infty$ controller embedded in the T1DM simulator. . 104
4.10 Controllable open-loop experiment scheme. 105

A.1 Validation of SP detection on mouse whole islets. 114

B.1 Validation of sorting algorithms on test signals. 116

C.1 **A**: Raw data format. 16-bit data is big-endian. **B**: Processed data format. . . . 118
C.2 State machine of the recording buffer used to handle multiple sources. 121

D.1 Memory configurations for two different MEA layouts. 123
D.2 Instruction addressing scheme 124

F.1 Complete setup scheme 132

G.1 Illustration of the method used to compute temporal event correlation, and its matrix representation. 134

H.1 Revised islet quality control protocol. 136

List of Tables

2.1 Mainstream electrophysiology DAQ and processing systems. 43
2.2 Indicative Resource uptake per module. Percentages are device utilization (Xilinx Spartan-6), except for LUT-FF pairs that are a fraction of utilized LUTs. LUT: Lookup Table; FF: Flip-Flop; RAM: Random Access Memory; FIFO: First In First Out. 58
2.3 Processing latency of modules and their sub-modules for N channels (generic case) and 64 channels (present case). 59

3.1 Summary of the blind experiment. 82

C.1 Processed data storage format 119

E.1 Configuration commands of Multimed: Glycaemia V1.3.1 126
E.2 Format of the electrode sorting configuration two-byte argument 129

I.1 Model parameters 138

Abbreviations

ADC	Analogue-to-Digital Converter
ANN	Artificial Neural Network
AP	Action Potential
APD	Artificial Pancreas Device
API	Application Programming Interface
ASCII	American Standard Code for Information Interchange
ASIC	Application-Specific Integrated Circuit
AST	Aquitaine Science Transfert
ATP	adenosine triphosphate
CBMN	Institute of Chemistry & Biology of Membranes & Nano-objects
CCK	cholesystokinin
CGM	Continuous Glucose Monitor
CNT	carbon nanotubes
CPG	Central Pattern Generator
CPU	Central Processing Unit
CSII	Continuous Subcutaneous Insulin Injection
DAQ	Data Acquisition
DDE	Delay Differential Equation
DIV	Days In Vitro
DSP	Digital Signal Processor
DWT	Discrete Wavelet Transform
FDA	Food and Drug Administration
FIFO	First In First Out
FOPP	Fraction Of Plateau Phase
FPGA	Field Programmable Gate Array
GIP	glucose-dependent insulinotropic peptide
GLP-1	Glucagon-like peptide-1
GPU	Graphical Processing Unit
GUI	Graphical User Interface
HD-MEA	High-Definition MEA
IDE	Integrodifferential Equation
IEQ	Islet Equivalent
IIR	Infinite Impulse Response
IMS	Integration: from Material to Systems
I/O	Input/Output
IP	intraperitoneal
ISG	Insulin Secretory Granule
ISR	Insulin Secretion Rate
IV	intravenous
JDRF	Juvenile Diabetes Research Foundation
JTAG	Joint Test Action Group
LED	Light-Emitting Diode

LFP	Local Field Potential
LUT	Lookup Table
MCS	Multi Channel Systems
MDI	Multiple Daily Injections
MEA	Microelectrode Array
MIMO	Multiple Inputs Multiple Outputs
MISO	Multiple Inputs Single Output
MPC	Model Predictive Control
ODE	Ordinary Differential Equation
OS	Operating System
PD	Proportionate Derivative
PDE	Partial Differential Equation
PEDOT	poly(3 4-ethylenedioxythiophene)
PEDOT-CNT	PEDOT-carbon nanotubes
PEDOT:PSS	PEDOT-polystyrene sulfonate
PGA	Programmable Gain Amplifier
PI	Proportionate Integrative
PID	Proportionate Integrative Derivative
PYY	peptide YY
RAM	Random Access Memory
RRP	Readily Releasable Pool
SC	subcutaneous
SD	Secure Digital
SDE	Stochastic Differential Equation
SEM	Standard Error of the Mean
SIP	System-In-Package
SISO	Single Input Single Output
SMA	SubMiniature version A
SMBG	Self-monitoring of blood glucose
SNN	Silicon Neural Network
SNR	Signal-to-Noise Ratio
SP	Slow Potential
STDP	Spike-Timing-Dependent Plasticity
SWT	Stationary Wavelet Transform
T1D	Type 1 Diabetes Mellitus
T2D	Type 2 Diabetes
TRS	Tip Ring Sleeve
UART	Universal Asynchronous Receiver/Transmitter
μ-MEA	microfluidic MEA
USB	Universal Serial Bus
VGA	Video Graphics Array
VHDL	VHSIC Hardware Description Language
VIP	vasoactive intestinal peptide
XML	Extensible Markup Language

Introduction

"I think the popular view of Science is a solid body of truth, shared by a whole lot of learned men in a room, all agreeing on the answers to the questions of how the Universe works. Whereas nothing could be further from the truth. The one truth that I see emerging from the History of Science is that experiment has always surprised theorists."

- Brian May

Bioelectronics is a field of research in which biological materials interact with electronic systems, generally with the final goal of supplanting an impaired body function.

To achieve that, bioelectronics takes advantage of cells having measurable electrical activity. With the joint efforts of many areas of expertise including biology, electronics, medicine, chemistry, cognitics, etc. it aims at, on one end, acquiring information regarding body state, performing *decision-making*, and on the other end executing an action (a *stimulus*) in return. Studies in bioelectronics include developing techniques to record electrical biological signal, understanding the *electrophysiological* mechanisms behind it, model cell and cell network behaviour, design embedded systems for prosthetics, conceive bio-compliant ways of electrically stimulating tissues, or design physiologically-accurate controllers that transparently restore body functions.

The best-known applications of bioelectronic techniques are those of neurosciences, where *action potentials* fired by neurons are recorded and studied to explain mechanisms of the brain and the nerve system. Prior to neurosciences, the pioneering application of bioelectronics was the electrical stimulation of nerves and muscles, which gave birth to the pacemaker. Driven by an aging population and a general fascination for these science-fiction-like disciplines, more and more advances are being made. Well mastered techniques can now supplant failing organs: pacemakers assist a million failing hearts every year, deep brain stimulation negates Parkinson's disease tremors, cochlear implants restore hearing in the deaf, mind-controlled prosthetics start to appear, and retinal implants progressively give sight to the blind.

Despite the main body of bioelectronic research being focused on the brain and the nerve system, other cells have measurable electrical activity: this thesis explores the extracellular measurement of pancreatic islets, and more specifically that of its insulin secreting β cells. Just like neurons signal communication with action potentials, pancreatic β cells signal insulin release with action potentials as well as a unique group signature called slow potentials. These activities are modulated by the different nutrients and hormones present in the body and can

be utilized to acquire information regarding body state and, for example, supplant a failing pancreas.

Type 1 Diabetes Mellitus (T1D) in an autoimmune disease in which β cells are attacked and destroyed by the organism. In the absence of these cells, the body cannot secrete insulin and regulate its glucose levels. The patient must therefore manually and accurately dose and inject him/herself with insulin, to avoid life-threatening hyper- and hypoglycaemia. Bioelectronics has brought solutions to this disease by automating part of the self-management process (measuring glucose, and dosing and injecting insulin). A device capable of assisting a T1D patient in these tasks is referred to as an *artificial pancreas*, even though it does not currently possess all the sensitivities of the actual organ. Indeed, artificial pancreas sensors only measure glucose levels, and other factors influencing glycaemia and insulin secretion must be compensated manually.

The novel method investigated in the following study proposes to utilize pancreatic islets as a sensing material, and transducing their electrical activity into an image of insulin demand. An embedded electronic system is proposed to measure multi-site islet activity and integrate multiple parameters regarding their activity patterns. The biosensor thus formed has of course applications in hormone- and nutrient- sensitive sensing of insulin demand for the artificial pancreas, drug screening for pharmacological applications, and islet screening for clinical applications.

This thesis studies the utilisation of such a biosensor, focusing on the design and utilization of the electronic transducer. The first chapter introduces the scientific context. It explains the pathophysiology of T1D, the electrophysiology of the impaired cells, and techniques for measuring their electrical activity. It finally presents the concept of a biosensor for insulin demand using pancreatic cells and its possible applications. The second chapter gives a detailed description of the processing electronics developed to transduce multichannel cell activity. The FPGA-based hardware platform is described, as well as the processing architecture and algorithms implemented to satisfy the specificities of electrical cell activity. The third chapter gives experimental results obtained on murine and human cells. Modulation of electrical cell activity by glucose and hormones is studied and analyses of the observed phenomena are provided. The fourth chapter utilizes the established experimental results to produce a model of the biosensor. This model is simulated within a whole-body glucose-insulin system to demonstrate its ability to be used as a sensor for the artificial pancreas. Finally, an alternate measurement is proposed to account for the biosensor's multiple sensitivities while maintaining compatibility with glucose-dependent insulin dosage tables.

Chapter 1

Scientific context

The fact that we live at the bottom of a deep gravity well, on the surface of a gas covered planet going around a nuclear fireball 90 million miles away and think this to be normal is obviously some indication of how skewed our perspective tends to be.

- Douglas Adams, *The Salmon of Doubt: Hitchhiking the Galaxy One Last Time*

1.1 Type 1 Diabetes Mellitus

Type 1 Diabetes Mellitus (T1D) is an autoimmune disease targeting pancreatic β cells and leading to absolute insulin deficiency. Its prevalence is constantly rising as it concerns 5-10% of the current 371 million patients suffering from all forms of diabetes, expected to rise to 592 million by 2035 worldwide. T1D is without question one of the most common chronic diseases of childhood [1, 2]: it is most often diagnosed in children/young adults, generally presenting with a trio of symptoms (polydypsia [1], polyphagia [2], polyuria [3]) alongside overt hyperglycaemia [3]. Because of its early development, it was also classified in the past as "juvenile diabetes". It is a currently incurable disease and requires lifelong exogenous insulin replacement. While modern medicine has treatment options, good practice of the techniques, and provides near-normal life conditions to patients, it remains a disease with fatal consequences if neglected or treated incorrectly (Fig. 1.1).

T1D is not to be confused with Type 2 Diabetes (T2D), which is characterized by the body developing insulin resistance and losing the ability to respond to insulin. Generally the body compensates by producing more insulin, which over time strains β cells and destroys them. Both diseases can be differentiated by opposing characteristics: T1D is (a) often diagnosed in childhood, (b) not associated with excess body weight, (c) associated with high ketone levels at diagnosis, (d) treated with insulin injection, and (e) cannot be controlled without insulin therapy, while T2D is (a) usually diagnosed in over 30 year-olds, (b) is often associated with excess body weight, (c) is often associated with high blood pressure and/or cholesterol levels, (d) is usually treated initially without medication, and (e) sometimes can be controlled with interrupted medication.

1. excessive thirst
2. excessive hunger
3. excessive urination

Figure 1.1 – Personalities known to have developed T1D. From left to right: Singer, guitarist and composer **David Crosby** performing on stage at age 74; Actress **Mary Tyler Moore** at age 31 on the Dick Van Dyke Show, deceased in 2017 at age 80 from pneumonia; Drummer **Brad Wilk** performing on stage at age 44; Drummer **John Rutsey** (middle) in the original line-up of the Canadian band Rush, deceased at age 55 from a heart attack precipitated by diabetes.

1.1.1 Epidemiology and prevalence

T1D is widely accepted as a complex disease, and while it is common grounds that its development has both genetic and environmental causes, its detailed origins are an on-going debate. It most often presents at two peaks during childhood and adolescence [3]: one between 5 and 7 years of age, and the other at or near puberty [4]. It seems to affect men and women equally (though debate exists with a slightly increased prevalence towards male gender [5, 6]).

Environmental causes It is often said that the prevalence of T1D is increased in certain ethnic groups. Because of the lack of global studies however, geographic and ethnic incidence has been unclear in the past. Only recently have studies unveiled precise observations: in the United States, the highest rates were observed for non-Hispanic white youth (24.8 per 100,000 per year among those <10 years of age) [7], and at a global level, the incidence of T1D positively correlates to the distance north of the equator, with more that 350-fold variations [1, 8, 9]. The disorder is most common in Finland (60 cases per 100,000), Sardinia (40 cases per 100,000), and Canada, Great Britain, New Zealand, Norway, Portugal, Sweden (>20 cases per 100,000), and the least common in China, India, and Venezuela (0.1 cases per 100,000) [8–10].

Genetic causes Genetic factors also contribute to the incidence of the disease, as shown by an increased risk of developing the disease if a first-degree relative has it: people with a T1D first-degree relative have a 1 in 20 risk of developing it, whereas the risk in the United States is on 1 in 300 [11]. In addition, monozygotic twins have a 30 to 50% disease concordance, while dizygotic twins only have a 6 to 10% disease concordance. [3]. However, new T1D cases are diagnosed in people with no known family history for the disease in 85% of the cases [3]. While genes have been associated with the likeliness of the disease [12], not a single one has been identified as either necessary or sufficient to predict the disease [3].

1.1.2 Pathophysiology

As previously mentioned, T1D is an autoimmune disease that targets pancreatic β cells, which are responsible for insulin secretion. Insulin is the hormone necessary to get glucose (sugars broken down by the body) from the bloodstream and into the cells, to metabolize it into energy. In the absence of insulin, glucose accumulates in the bloodstream and increases risks of

cardiovascular diseases, nerve damage, kidney damage, retina blood vessel damage, cataract, feet problems caused by poor blood flow, bone and joint problems, and teeth infections.

It is still unclear why β cells are specifically targeted by the autoimmunity, as well as what the mechanisms inducing it are [13, 14]: whether it is molecular mimicry [4], breakdown in central tolerance [5], sensitivity of β cells to free-radical damage, local viral infection, or other causes [15] has been and is still under debate.

With the lack of access to the pancreas, T1D is generally identified with the presence of specific autoantibodies, but post-mortem examinations or biopsies [6] are the only means of witnessing actual β cell damage and studying it. The inflammatory lesion is characterized by a decrease or absence of β cells (pseudo-atrophic islets, devoid of insulin-producing cells), and an infiltrate composed of T-lymphocytes, B-lymphocytes, and macrophages. T1D usually presents once 80 to 90% of the β cells have been destroyed [16].

1.1.3 Existing treatments

While many forms of treatment exist for T1D, strategies can be summed up into two main categories: insulin therapy and transplantation. The wide majority of T1D patients are treated with insulin therapy, which involves performing regular glucose measurements (referred to as Self-monitoring of blood glucose (SMBG)) using needles to sample a drop of blood and performing the measurement with enzymatic glucose sensors. The resulting indication of blood glucose helps determine the dose of insulin to be administered subcutaneously. This method of administration is usually called Multiple Daily Injections (MDI), and is the most widespread method of self-management. In addition to SMBG, patients need to account for and anticipate meals, physical activity, stress, and their sleep schedule to modulate insulin dosage accordingly. The goal of insulin therapy is to provide insulin in as physiologic a manner as possible, which is why different types of insulin exist and help patients regulate their glucose levels more efficiently: slow-acting insulins are administered as boluses, maintaining insulin at basal levels while fast-acting insulins are injected shortly before meals (pre-prandial) to compensate for sugar intake.

Treatment aims at keeping glucose within target levels and limit hyperglycaemia and more importantly hypoglycaemia and its dire consequences; while hyperglycaemia is dangerous in the long term (increased risks of cardiovascular disease, diabetic foot infections, diabetic retinopathy, etc.), hypoglycaemia can rapidly cause confusion, loss of consciousness, and ultimately death. For that reason, insulin injections must result from careful assessment of current and future situations, which is a known source of errors for children and adolescents with lower experience and education of the disease [17, 18].

Many commercial products (Roche Accu-Check, Insulet OmniPod, Medtronic 530G, Animas Vibe) aim at facilitating self-management with automatic Continuous Glucose Monitors (CGMs) and dosage directions adapted to the context. In the same direction, the Continuous Subcutaneous Insulin Injection (CSII) regimen is being developed, proposing insulin pumps (Fig. 1.2) that perform equally to MDI once metabolic control is achieved [19]. This tendency of automating insulin therapy introduces the concept of artificial pancreas, which will be discussed further in the next section.

Patients with severe cases of T1D can also be treated with a pancreas transplant. While it is possible to transplant a whole pancreas, the method of interest in this manuscript is islet cell transplant, where islets of Langerhans are isolated and injected into the portal vein (*Edmonton Protocol*), where the main body of insulin secretion should normally originate. Although this procedure had problems in the past, it has benefited from new techniques and better immunosuppressive drugs to prevent islet rejection. In a study from one of our partners, in which 44 patients received a total islet mass of roughly 10,000 IEQ (islet equivalent) per kilogram of body mass (requiring 2 to 4 donors) [20], 33 (75%) of the patients experienced insulin

4. sharing of antigenic properties
5. a failure to establish immunity to self-antigens
6. which are mostly not considered ethically feasible for safety reasons

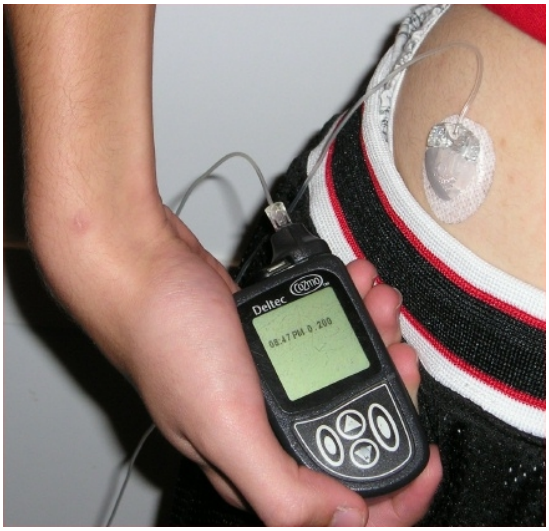

Figure 1.2 – A Deltec Cozmo insulin pump with its infusion set

independence during the five-year follow-up period (median duration of insulin independence: 19.25 months).

Still, only the most severe cases of T1D benefit from pancreas transplants because of the lack of accessibility to donors. Current research is therefore mostly oriented towards automation of insulin therapy, to facilitate treatment for adults, but also for children and adolescents who usually require closer medical surveillance [17, 18].

1.2 Continuous Glucose Monitors

1.2.1 Principle

In diabetes treatment, CGM coupled with insulin delivery (sensor-augmented pump) has provided powerful means in improving therapeutic outcomes and quality of patient's life [21]. CGM in diabetes relies on subcutaneous glucose measuring via electrochemical electrodes and the use of algorithms to predict insulin dosage [22, 23]. It has made a considerable way since its initial introduction in a clinical setting in the 1970s [21, 24, 25], brought down size and provided autonomy and comfort to the patients and carers. Moreover, a number of studies have clearly shown that CGM reduces hyperglycaemia as compared to other therapies and is thus expected to reduce the dire long-term complications of T1D [25, 26].

CGMs measure interstitial glucose levels every 1-5 minutes and provide efficient directions, alarms, and tendency graphs to the patient to help with avoiding hyper- or hypoglycaemic events. It however has some drawbacks. First, there is a time lag between glucose levels in capillary blood and interstitial space, causing readings to differ from classic (capillary) methods. Secondly, both due to the hyper-availability of data and interstitial measurement delay, patients may overtreat hyperglycaemia (*stacking* insulin doses) [19]. This is why, paradoxically, these devices designed to simplify everyday life for T1D patients are only recommended by the Endocrine Society [27] in adult patients who have demonstrated proficiency in self-management. Intermittent use of CGM is only suggested for patients with suspected nocturnal hypoglycaemia, postprandial hyperglycaemia, hypoglycaemic unawareness, and patients with important changes to their diabetes regimen.

1.2.2 Artificial pancreas

With the development of automation in both glucose monitoring and insulin injection, closed-loop systems appeared including a CGM in constant communication with an infusion

pump. In addition to these, a blood glucose meter is utilized for calibration. Regulation algorithms (controllers) are run on external processors, reading information from the CGM and producing dosing instructions for the infusion pump [27]. The closed-loop system formed is referred to as an Artificial Pancreas Device (APD).

APDs are in constant development and were classified by the Juvenile Diabetes Research Foundation (JDRF) into 6 categories based on their level of automation (Fig. 1.3). The first generation (stages 1-3) of APDs are non-closed-loop in that they only have automatic insulin delivery interruption when a risk of hypoglycaemia arises. Second generation APDs (stages 4-5) have automated insulin delivery. Stage 4 (current state of practice) are hybrid systems that have automated glucose regulation at all times but require manual intervention to announce meals or exercise. Stage 5 are fully automated insulin delivery systems. Third generation APDs (stage 6) are fully automated dual hormone closed-loops: in addition to insulin, they have a glucagon pump that helps treat severe risks of hypoglycaemia.

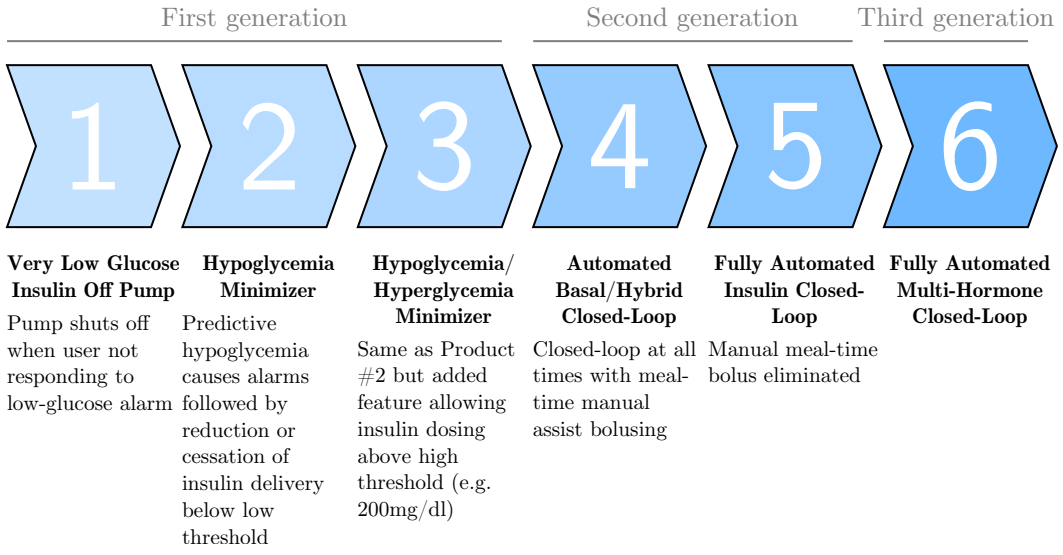

Figure 1.3 – The six stages of artificial pancreas development as classified by the JDRF.

1.2.3 Limitations

CGM and linked drug delivery is a modern approach to measure blood glucose and achieve body homeostasis in chronic diseases. In the healthy body, most of the relevant physiological parameters are controlled within a tight range and only minor excursions are tolerated. Potent hormones play a major role in achieving homeostatic control and deviation results in long-term damage of the organism, marked acute impairment, or even death [28].

In diabetes therapy, currently used CGMs rely on electrochemical enzyme-linked electrodes to measure glucose levels. Several important signals are therefore not integrated in the measurement: first, lipids represent a varying part of nutrition, and certain triglycerides arrive early in the general circulation and also stimulate insulin secretion to attain lipid homeostasis [29–31]; Second, hormonal signals translate the general body state (exercise, stress) and strongly influence insulin secretion. Specifically, secretion during the circadian cycle is modulated through incretins [32], and physical or emotional stress signal a lesser demand in insulin through adrenaline [33].

The main sources to take into account in the glucose regulation process are meals, physical activity, sleep, and stress. Yet, sensors are still only sensitive to glucose, limiting automation to meal compensation, and ignoring exercise, sleep, and stress. While biometric variables, such as heart rate, can be monitored to collect information regarding patient physiological state,

the most reliable sources of information remain hormone levels.

The main issue in continuous therapy design concerns the body status sensor: ideal sensors should be multiparametric and provide direct integration of all insulin-modulating variables. Clearly, the best indicator of insulin demand in the body, healthy or diseased, is the organ itself, and more specifically the β cell, responsible for insulin secretion and multivariable integration of body state.

1.3 Electrophysiology of the pancreatic β cell

Pancreatic β cells are found in pancreatic islets (or islets of Langerhans, Fig. 1.4). These islets are 20 to 40 µm in diameter, 3 million in number [34], and contain α cells (20%) producing glucagon, β cells (65-80%) producing insulin, δ cells (<10%) producing somatostatin, γ cells (<5%) producing pancreatic polypeptide, and ϵ cells (<1%) producing ghrelin.

Pancreatic β cells are responsible for producing, storing, and releasing insulin. Similarly to neurons, they are excitable cells, meaning they have measurable electrical activity and can be electrically stimulated to produce *Action Potentials*.

1.3.1 General electrophysiology

Electrophysiology is a branch of physiology that studies the electrical properties of biological cells. Indeed, biological cells and tissues exhibit electrical activity which principles differ from silicon-based electronics: while electronic components deal with electrical currents generated by flows of freely moving electrons, currents in electrophysiology are generated by ions. Ions, like electrons, are carriers of electric charge that can freely transit and accumulate, in turn generating currents and potentials.

Cell membranes are dotted with ion channels, complex pore-forming proteins that allow specific ions to pass through the membrane (Fig. 1.4C). Some of these channels are opened or closed by cell events (see next section) while others are constantly open and act as ion pumps. For instance, the sodium/potassium (Na/K) pump pushes two potassium ions (K^+) into the cell for every three sodium (Na^+) it pumps out. This unbalanced double gradient results in a net loss of positive charges within the cell. This in turn generates what is called the resting membrane potential, a baseline difference in electric potential across the plasma membrane ranging between -60 and -80 mV.

1.3.2 Transient ion mechanisms in the β cell

In β cells, glucose is transported through the membrane by the GLUT2 transporter and metabolized through a process called glycolysis. This process results in a net increase of high-energy adenosine triphosphate (ATP) molecules. This rise in ATP causes ATP-dependent potassium (K^+) channels to close, causing the membrane to become less permeable to K^+ ions that consequently build up inside the cell. The resulting depolarization causes Voltage-dependent calcium (Ca^{2+}) channels to open an the positive ion influx causes the membrane to further depolarize. Calcium ions in turn precipitate exocytosis, a process in which vesicles containing Insulin Secretory Granules (ISGs) fuse with the membrane and release insulin outside the cell. [35]. Membrane repolarization is achieved thanks to the combined activation of calcium- and voltage- dependent potassium channels [36], as well as the time-dependent inactivation of sodium and calcium channels [36]. The excess of calcium ions is also transported out of the cell by pumps and removal of Ca^{2+} sequestrated in insulin granules by exocytosis [37].

This process not only liberates insulin, but also causes a typical electrical variation of cell membrane called the Action Potential (AP). The described exocytosis and AP generation mechanisms are summarized in Fig. 1.4C-D. This process is extremely fast and happens in a few tens of milliseconds, and up to 12 times per second in secretory conditions [38].

Cell activity is moreover modulated by a myriad of other mechanisms and molecules (hormones, neurotransmitters, nutrients). Certain molecules can further modulate ion channels

and contribute to polarizing states: inhibitors of secretion adrenaline (epinephrine) and somatostatin cause K_{ATP} channels to open and hyperpolarize the cell [39]. Potentiators of secretion also exist, including Glucagon-like peptide-1 (GLP-1), glucose-dependent insulinotropic peptide (GIP), cholesystokinin (CCK), peptide YY (PYY), and oxyntomodulin, which are released from the gut in response to food transit [40]. They are responsible for the increase of insulin release in response to food intake versus an identical change in glycaemia imposed by intravenous injection of sugar [41]. Other potentiators of secretion include vasoactive intestinal peptide (VIP), fatty acids, and acetyl choline.

Another mechanism consists in groups of β cells communicating through gap junctions (or Connexin 36, Cx_{36} in Fig. 1.4C). These channels let Ca^{2+} ions transit from one cell to another and synchronize insulin secretion as well as electrical activity. The complex summation of ionic fluxes in the extracellular space causes slower (<1 Hz) variations in the potential in the vicinity of cells, represented in Fig. 1.4E, and called a *slow potential*. This phenomenon was first reported in [42] and characterised in [43]. Its shape and properties are reportedly unique to pancreatic islets.

The charges in transit across the membrane cause variations in potential that can be measured with conductive electrodes. If this potential is measured inside the cell, the measurement is described as *intracellular*, and exhibits traces resembling that of Fig. 1.4D. If, on the contrary, the potential is measured outside the cell (in its vicinity), the measurement is described as *extracellular* and reflects the group behaviour of all nearby cells, exhibiting activity resembling that of Fig. 1.4E. The next section describes the techniques that can be used to obtain such measurements.

1.3.3 Measurement techniques

Cell activity can be measured with various techniques. Some focus on measuring membrane potential, while others measure ion fluxes, membrane capacitance variations, or even optical cues reflecting internal behaviour. Due to the nature of this study (see section 1.5), the description of measurement techniques is restricted to those reflecting transmembrane ionic currents. The section first gives a historical background on the patch-clamp technique, and draws its limits to introduce multielectrode extracellular techniques.

Patch-clamp techniques

The study of cell mechanisms and ion fluxes has been catalysed by the development in the late 1970s of the patch-clamp technique. It is an electrophysiology technique that allows high-resolution current recordings of whole cells or excised cellular patches. Its resolution is even sufficient to capture single-channel opening events. Voltage-clamp was most notably utilized by Alan Lloyd Hodgkin and Andrew Huxley in 1952 to reveal the ion channel events of APs [44], which awarded them the Nobel Prize in Physiology and Medicine in 1963. Since then, immense improvements to the technique have been made in resolution [45], seal quality and signal-to-noise ratio [46].

The principle of patch-clamping (Fig. 1.5A) is sealing a glass or quartz micropipette onto cell membrane by applying suction, hence isolating (with a seal measured in MΩ, or giga-seal in GΩ [46]) all local ion fluxes into the pipette. A chlorided silver electrode records the resulting potential variations. The technique has several variations, depending on what needs to be studied: (a) the cell-attached patch, where the pipette is sealed to the membrane while keeping it intact; (b) the inside-out patch, identical to the cell-attached patch, except the patch is excised from the main body of the cell; (c) the whole-cell patch, where sufficient suction is applied to rupture the membrane and gain access to the intracellular space; (d) the outside-out patch, identical to whole-cell patch except the patch is excised and sampled from the main body of the cell; (e) the perforated patch, similar to whole-cell patch, except the membrane is not perforated, but chemically made porous to gain access to the intracellular space.

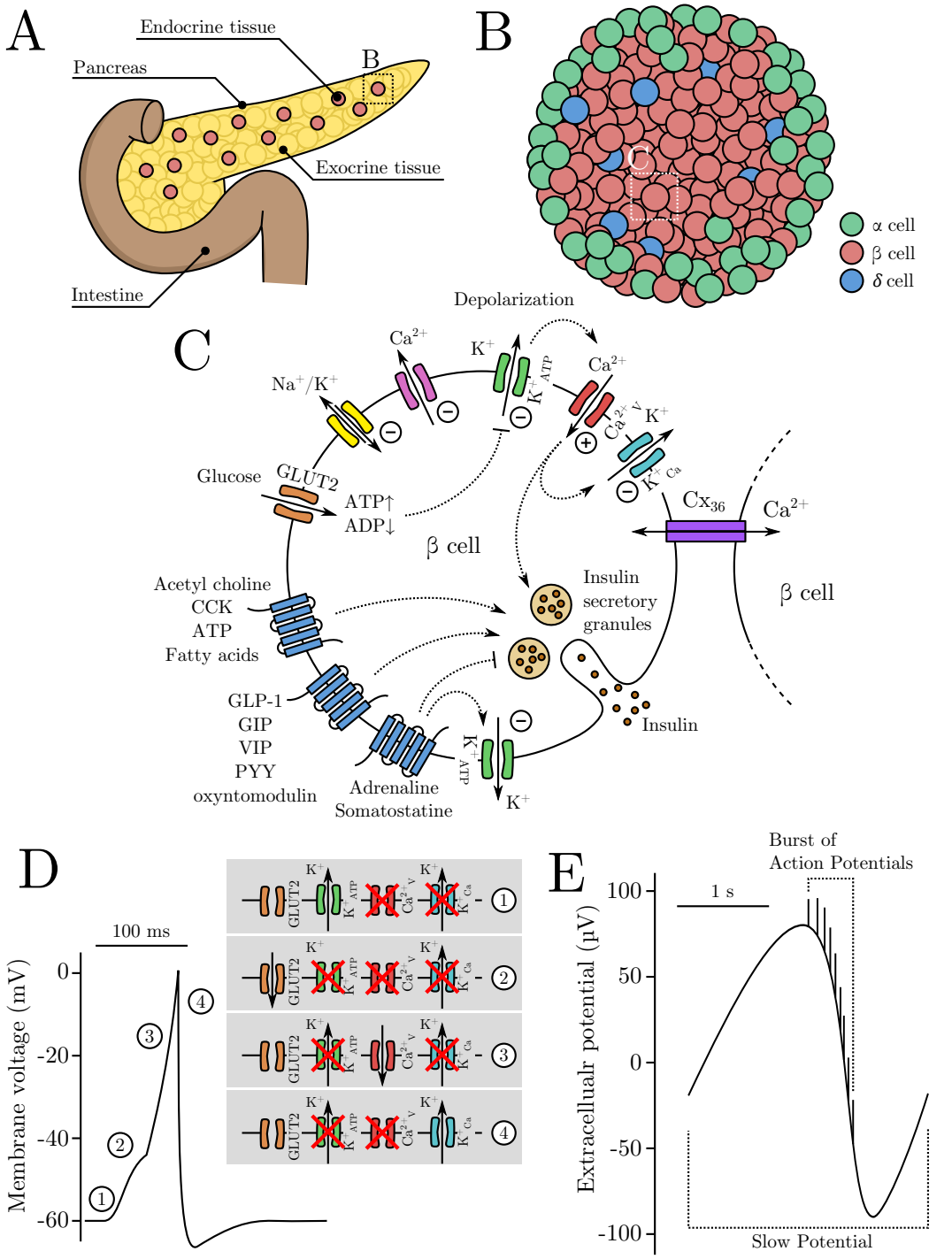

Figure 1.4 – Context and mechanisms of pancreatic β cells. **A**: the pancreas. **B**: An islet of Langerhans. **C**: Mechanisms of the β cell (non-exhaustive). (+) and (-) symbols respectively indicate hyperpolarizing and depolarizing ion fluxes. Plain arrows represent ion fluxes, dotted arrows represent activation relations, dotted flat arrows represent inactivation relations. **D**: An action potential and its constituent stages. (1) The membrane is at its resting potential maintained by the Na/K pump and open K_{ATP} channels. (2) Glucose is metabolized, raising ATP and causing ATP-dependent K^+ channels to close. The membrane depolarizes. (3) Voltage-dependent Ca^{2+} channels open and cause an influx of positive ions that further polarize the membrane and cause exocytosis. (4) Cell membrane is repolarized by the activation of Ca^{2+}-dependent K^+ channels. **E**: Extracellular potential reflects ion fluxes and exhibits bursts of action potentials as well as slow potentials, slow-oscillating signals resulting from complex summations of ion currents.

These techniques require highly controlled experimental conditions and precision, which make them unsuited for multisite recording. In addition to that, they tend to damage cells and prevent chronic or repeated experiments on a single preparation.

Recent topics in cell electrophysiology have widened to include cell network analysis and implantable devices, both incompatible with patch-clamp techniques: the number and density of recording channels required makes it entirely impractical. For that reason, an alternate technique was developed, trading signal-to-noise ratio for simplicity of installation per recording channel: using extracellular microelectrodes in the vicinity of a cell, electrical activity can be measured. To assure electrode coverage and permit multisite recording, electrodes are placed as an array, forming a device called the Microelectrode Array (MEA).

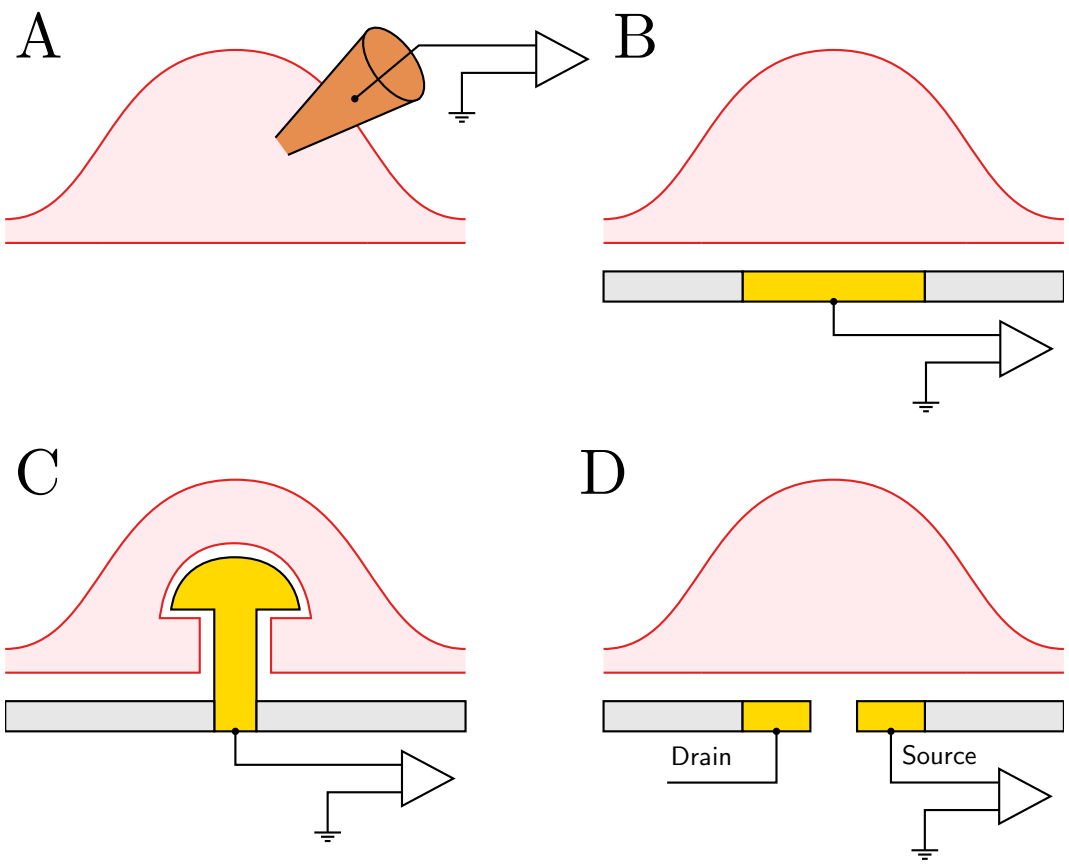

Figure 1.5 – Different techniques for recording cell activity, intra- and extra-cellular. **A**: Sharp-glass intracellular microelectrode. **B**: Substrate-integrated planar microelectrode. **C**: Mushroom-shaped protruding microelectrode. **D**: Field-effect (floating gate) transistor microelectrode.

Extracellular recording: introducing Microelectrode Arrays

An MEA is an arrangement of tens to hundreds (and at present up to thousands [47, 48]) of electrodes designed for multisite recording and stimulation of extracellular activity. A wide variety of terms has been used to describe the different MEA technologies (Fig. 1.5B-D) emphasizing either:

— The type of transducer used (e.g. multi-transistor array, microelectrode array, multielectrode array, micro-nail array, capacitive-coupled array, 3D MEA)
— The shape of the device (needle-type probe, polytrode, neuro dish)

— Electrode density (HD-MEA)
— The application (*in vivo* MEA, *in vitro* MEA)

They can be used for either signal acquisition, stimulation, or both, which essentially changes electrode shape and arrangement.

This study mostly focuses on *in vitro* planar microeletrode arrays utilized for acquisition, therefore it is assumed that any reference to MEAs without further description refers to such devices.

In the case of *in vitro* MEAs, cell preparations are typically cultivated directly on the MEA, which is why materials constituting the insulator, conductor, microeletrode and substrate are carefully chosen with respect to biocompatibility [49, 50]; the materials typically used are transparent glass for the substrate (to allow microscope observation), silicon nitride (SiN) for the insulator and titanium (Ti) or indium tin oxide (ITO) for the conductor. Electrodes use very diverse conductive materials depending on the application, including gold (Au), titanium nitride (TiN), platinum (Pt), stainless steel, aluminium (Al), and iridium oxide (IrOx) [50].

With the small size of electrodes (typically 5 to 50 µm diameter [50]), achieving low impedance with plain conductors only is a challenging feat. The most widespread technique is increasing the effective surface area of the electrode while maintaining its dimensions and apparent area. To achieve this, porous materials are used as coating, such as platinum-black (Pt-black), gold nanostructures, CNTs (carbon nanotubess), and conductive polymers and compounds such as PEDOT (poly(3 4-ethylenedioxythiophene)), PEDOT:PSS (PEDOT-polystyrene sulfonate), or PEDOT-CNT (PEDOT-carbon nanotubes) [50–57].

MEAs detect the changes in the extracellular field caused by the current flows from all ionic processes and transmembrane currents occurring in nearby cells: changes in electric field potential can be detected by conductive electrodes. The magnitude of the resulting signal is influenced by the distance between the current source and the recording site [57, 58].

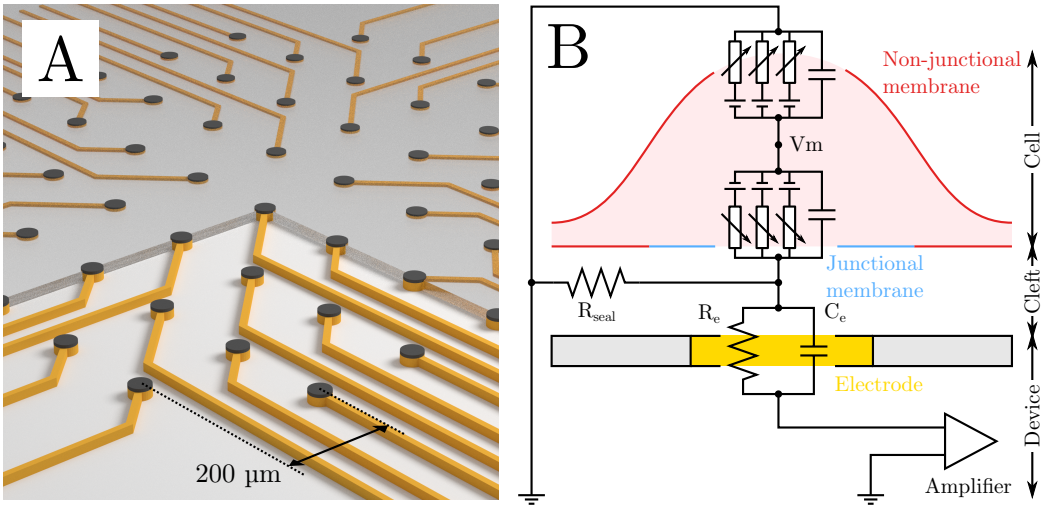

Figure 1.6 – Principle of MEA measurements. **A**: Cut view of a planar MEA. The glass substrate is cut to reveal the conductive tracks (golden) and electrodes (black). **B**: Electrical model of extracellular recording derived from [59]. Membrane-electrolyte interfaces are modelled with a capacitance (membrane capacitance) in parallel with non-linear conductances representing transmembrane ionic fluxes. V_M represents the membrane potential of the cell.

Signals recorded on MEAs generally have a much smaller amplitude than intracellular traces (a few tens to hundreds of microvolts) and are subject to supplementary sources of noise: in addition to device noise and electrode-electrolyte interface noise, a biological noise (also called background noise) resulting from other cells adds a significant amount of unwanted signal that deteriorates acquisition [57]. For these reasons, MEA recordings require careful signal

conditioning, with high-gain, low-noise preamplification applied as closely as possible to the electrodes.

1.4 Biosensors

A biosensor is, by definition, an analytical device that converts a biological response into an electrical signal [60]. Ideally, a biosensor should return a value that reflects the variable of interest, independently from environmental physical parameters (e.g. pH, temperature). Its usual construction includes a sensitive biological element (biological material responsive to the analyte) and a transducer that transforms the resulting signal into a usable electrical signal. The definition is extremely vast and by essence includes enzymatic glucose sensors used daily by diabetic patients. This research however proposes its own biosensor, composed of pancreatic islets as the biological element, and a signal acquisition chain (MEA, signal conditioning and signal processing) as a transducer. The variable measured by this biosensor is complex, as it integrates all signals affecting islet activity. In reality, it reflects exocytose-inducing mechanisms of the cell which, in other terms, is an image of true physiological insulin demand from the body. Even though cell-based biosensors have existed for years [61–63], this one is the first of its kind as β cells have never been utilized to sense insulin demand in the past.

1.4.1 Designing the transducer

In this particular biosensor, it is the electrical activity of cells that needs analysis and conversion. The transducer itself needs several fundamental components:

1. An electrode of some sort, to record variations of cell potential
2. Signal conditioning, to amplify the recorded signal with minimal loss
3. Signal processing, to decode information from the complex biosignals

Among these items, electrodes and signal conditioning equipment are readily available for bench experiments. The electrodes of choice for the biosensor are planar MEAs, that maximize cell coverage, permit multisite recording, provide reasonable cell adhesion, good reusability, and easily controllable culture conditions. A microfluidic topology that ameliorates cell coverage and ease of use in continuously changing media is presented in paragraph 3.1.1. Signal conditioning can also be provided by commercial equipment (see section 2.2.2) with low-noise, high-gain amplification and band-pass filtering. Signal processing, however, requires specific treatment to extract the distinctive features of pancreatic cells.

To complete the biosensor, this last item of the transducer must be designed to extract separate features (action potentials, slow potentials, bursts) of the cell signals, and to integrate relevant information in a time-efficient fashion (real-time), to reduce measurement delays. The consideration of the specificities of β cells and the design of the processing algorithms used in such a system is an integral part of this thesis project and is extensively described in chapter 2.

1.4.2 Applications

The particular design of the described biosensor confers it different measurement paradigms. Indeed, with a replaceable biological element (β cells), it can either measure its intended parameter (i.e. insulin demand), or parameters regarding the biological element itself.

Sensor approach

The first approach is the most obvious, as it is framed within the intended use of the biosensor: a physiological medium is applied to the cell culture, and the biosensor returns an image of the corresponding insulin demand. This approach introduces the concept of using a physiological biosensor as a front-end sensor for glucose regulation in artificial pancreas.

Screening approach

The biosensor can also be utilized in controlled environments, where one wants to characterize the effects of pharmaceutical products such as antidiabetic drugs (sulphonylureas). This process, known as screening, can benefit from this hybrid approach for its scalability and the electrophysiological information it conveys: in controlled environments, it is possible to monitor the separate effects of drugs at a physiological level by observing the modulation of different components of the cell signal (disturbed cell coupling, increased sensitivity to glucose, alteration of activation dynamics, etc.).

Quality control approach

The last approach is less obvious as the biosensor characterizes its own biological element (i.e. β cells). Indeed, in a precisely dosed medium, cells are expected to produce a well-characterized response. Cell lines can be utilized to ensure repeatable results and minimal deviation from target. However, due to pancreatic islets deteriorating with either age or dietetic habits, or even due to interindividual discrepancies [64], response from primary cells can vary dramatically from a preparation to another. For that reason, the biosensor can return valuable information concerning a population of cells if an aliquot is utilized as the biological element of the biosensor. It can assess responsivity to physiological stimuli and help diagnose possible altered cell mechanisms.

1.5 Research context

This thesis was conducted in the Elibio (Electronics Interfacing Biology) team of the bioelectronics group in the IMS (Integration: from Material to Systems) laboratory in Talence (France). This research team specializes in designing electronic systems that interface with biological material, including acquisition and signal processing devices, as well as electrical stimulators. Because of the multidisciplinary nature of its research field, the Elibio team takes part in partnered projects including clinical, biology, microdevice, and neuromorphic engineering partners.

The presented work was conducted in close collaboration with Elibio's historical partner, the CBMN (Institute of Chemistry & Biology of Membranes & Nano-objects) laboratory. CBMN researchers *Cell Biology and Biosensors* team took care of cell culture and biological experiments.

Research subjects

Projects conducted by Elibio all involve some form of interface with biology. It can either be unidirectional, like is the case with acquisition and stimulation, or bidirectional. In the latter case, the whole range of expertise of the team is implicated, from signal acquisition, to electrical stimulation, and through real-time signal processing. The resulting system is referred to as a *closed-loop* system.

Bioelectronic closed-loop systems generally aim at replacing or treating impaired body functions. For instance, a lesion in the hippocampus can be bypassed using neuroprosthetics [65]: neuron AP trains can be recorded on one side of the lesion and stimuli applied accordingly on the other to reinstate communication. Similar approaches can be considered with non-electrical stimulation (like it would be the case with insulin infusion), or non-electrical acquisition (one could regulate respiratory air flow with electrical stimulation of the diaphragm [66]). In any case, Some form of processing electronics is required to act as a controller between the measuring end and the stimulating end of the closed-loop.

Faced with projects that share many paradigms, Elibio opted for designing a pluripotent processing system called *Multimed*. This system takes advantage of a reconfigurable component (Field Programmable Gate Array (FPGA)) to adapt to diverse projects and is extensively described in chapter 2.

The projects that use *Multimed* are described below.

The BRAINBOW [7] project proposes a new approach on cortical prosthesis in which bidirectional communication between a neuron culture recorded on an MEA and a SNN (Silicon Neural Network) is established [67, 68]. It is a collaboration between (1) the IIT (Istituto Italiano di Tecnologia) (Genova, Italy), in charge of biological experiments, (2) the AS2N team of the IMS laboratory, in charge of implementing SNN models, (3) biologists of the university of Tel-Aviv (Israel), and (4) Elibio, in charge of multichannel signal processing of biological neural network activity.

The HYRENE [8] project aims at recovering communication in the spinal cord following injury. Similarly to *Brainbow*, its goal is to record electrical activity on an MEA placed over the lesion, and bridge it to another MEA placed underneath the lesion to provide restored descending commands. The partners involved in the projects are (1) CLINATEC (Grenoble, France), in charge of murine electrophysiology, (2) the AS2N team of the IMS laboratory, in charge of implementing SNN models, (3) ESIEE (Noisy-le-Grand, France), in charge of MEA manufacturing, and (4) Elibio, in charge of multichannel signal processing of *ex vivo* signals.

The CENAVEX [9] project investigates stimulation for a closed-loop ventilatory control system. Using a biomimetic special SNN structure called a Central Pattern Generator (CPG), it proposes to improve ventilatory control for patients with cervical cord injury by stimulating the multiple respiratory muscles with biomimetic electrical stimuli. The partners in the project are (1) the Florida International University (FIU), in charge of biomechanical engineering and *in vivo* experiments on rats, and (2) Elibio, in charge of producing a biomimetic CPG and a multisite stimulation device.

1.5.1 Research projects for diabetes

Aside from punctual interventions in *Brainbow* as a Multimed developer, my personal implication in the team was limited to projects concerning the study of pancreatic cells. These projects cover the different aspects of the biosensor and aim at designing the processing electronics and characterizing the complete biosensor.

Projects related to T1D constitute one of the longest running project lineage of Elibio. Projects *Delivrer* (2007-2010), *HY-BIOPACS* (2011-2013), and *BIODIA* (2012-2014) were all attempts at developing an MEA-based biosensor capable of measuring insulin demand and providing adequate dosage for an insulin pump. These projects lead to the first ever demonstration of extracellular measurements of β cell activity on MEAs, which acquired a patent in 2010 [69]. They characterized electrical signatures of β cells similarly to neurons, especially focusing on the offline analysis of APs as well as the development of effective methods of detecting them [70]. The discovery of Slow Potentials (SPs) [43], reportedly more robust than APs, gave new prospects for this series of projects by providing a novel marker suited for real-time analyses and biosensor approaches.

The ISLET-CHIP [10] project: a new approach for pre-transplant diagnoses

Islet cell transplant is a promising technique to restore insulin-independence for severe cases of T1D [20]. The procedure is however extremely complex and its long-term viability needs improvement. The causes for the progressive loss in islet function probably have multiple origins. One of the causes may originate from the preparation itself. Each pancreas preparation needs to undergo a series of tests which outcomes determines whether the islets are suitable for transplantation. These tests include:

7. European project FP7-ICT-2011-C
8. French ANR 2010-Blan-031601
9. French ANR and USA NIH AN13-NEIC-0001-01
10. ANR 2013-PRTS-0017

1. Visual examination of the pancreas. If the pancreas has no anomalies, the test is passed and the pancreas is dissected for islet isolation.
2. Estimation with imagery analyses of an aliquot coloured with dithizone the number of islets that have been isolated. This test actually yields an *Islet Equivalent (IEQ)*, a measurement method proposed by Ricordi in 1990 [71]. It standardized islet volume measurements by extrapolating an equivalent number of islet based on the calculation that one IEQ corresponds to the tissue volume of a perfectly spherical islet with a diameter of 150 µm. It has been the subject of many refinements [72–74] but remains an approximate method. The test is passed if the measurement is greater or equal than 200,000 IEQ or 3,500 IEQ/kg (relative to the receiver). The preparation can then be purified.
3. Purity of the preparation is evaluated with dithizone colouring of a aliquot and computer-assisted evaluation of endocrine tissue (coloured in red) versus exocrine tissue (uncoloured). Purity must be superior to 30%.
4. Viability of the preparation is estimated with a similar method, with fluorescein diacetate (FDA)/propidium iodide (PI)/trypane blue (TB) colour of an aliquot. Dead cells are coloured in red (FDA/PI) or blue (TB) and their proportion is assessed with computer-assisted imagery. The percentage of dead cells must be inferior to 30% (FDA/PI) or 80% (TB). Only then can the pancreas be labelled as suited for transplantation.

These tests all rely on visual methods that are prone to deviation and do not reflect secretory capabilities of the preparation. A functional test is conducted but does not influence the final decision as results are obtained after the transplant.

ISLET-CHIP proposes to utilize the biosensor as an early indicator of preparation quality, with excitatory tests reflecting secretion. The device (ISLETCHIP) would be able to examine, *in vitro*, a small aliquot ($<$0.1%) of the islet preparation, to conduct a multi-parametric on-line analysis, and to display a diagnostic read-out prior to transplantation.

The project involves two teams from the Bordeaux University (Elibio and the Cell Biology and Biosensors team at CBMN) two clinical groups in France (Grenoble University Hospital and Laboratory of Cell therapy for Diabetes (LCTD, Montpellier University Hospital)) and a third one in neighboring Switzerland (Cell Isolation and Transplantation Centre (Geneva University Hospital)). As a translational research project between research institutes and hospitals, the project is supported both by the ANR (Agence Nationale de Recherche) and by the DGOS (Direction Générale de l'Offre de Soins).

Diaβeta Technologies: Biosensor approaches using β cells

Diaβeta Technologies is a line of products developed by Elibio and its partners in the frame of projects related to T1D. It covers all three biosensor approaches covered by two products:

— the Diaβchip device, the biosensor itself, designed for automated islet screening within the granting period for pre-transplantation quality tests, screening for drug and toxicology tests, and real-time analysis of cell differentiation of stem cells into β cells.
— the Diaβsensor product, a hybrid biosensor capable of sensing insulin demand. Of course, it follows the long-term plan of developing a physiological closed-loop regulation system for T1D patients.

Diaβeta Technologies are currently in a process of technology transfer. They seek industrial partners and clients to mature and industrialize the technology, benefiting from the patent we filed in 2010 on the β cell recording technology [69].

Chapter 2

Multimed, the measuring device

"Each generation wants new symbols, new people, new names. They want to divorce themselves from their predecessors."

- Jim Morrison

2.1 Introduction

Extracellular signals are complex electrical signatures that reflect the internal mechanisms of cells. Contrarily to membrane potential, that ranges from tens to hundreds of millivolts and discernibly reflects endogenous events, signals recorded on Microelectrode Arrays (MEAs) only attain tens to hundreds of microvolts, integrate multiple sources, and have low Signal-to-Noise Ratios (SNRs). Translating them into useable information requires specific signal conditioning and analysis, operated by three principal hardware elements:

— A headstage preamplifier, placed as close to the cells as possible to boost cell signal with a minimal addition of electrical noise.
— Analogue to Digital (A/D) converters, generally an external card performing Data Acquisition (DAQ).
— Processing algorithms, generally implemented as a computer software or dedicated electronics.

Because of their noise sensitivity, headstage preamplifiers are usually built as one separate device, positioned in a noise-free environment. On the contrary, DAQ and signal processing are less noise-sensitive and their build varies depending on the application. Most systems, motivated by and designed for laboratories, promote flexibility and feature separate DAQ and software processing. These notably include commercial products proposed by Multi Channel Systems (MCS), or open-source alternatives like Neurorighter or Open Ephys (see Table 2.1). They propose bench-ready, high-performance material and processing software capable of real-time processing, feedback, and include regular update support.

Moreover, the availability of generic DAQ systems, especially from National Instruments, MCS, or Intan also gave birth to open-source analysis software including MEABench, ArtE, Nspike, and RTXI. These also provide real-time processing tools and promote always-expanding analysis capabilities with limited hardware investment.

Applied research, and particularly closed-loop research cannot however always rely on software processing solutions. Indeed, computation speed is bound by general-purpose Operating System (OS) performance and processing latencies slower than biological delays limit decision-making within physiological windows (e.g. Spike-Timing-Dependent Plasticity (STDP)). Only

RTXI claims to achieve consistent sub-millisecond processing, relying on a real-time Linux kernel. Furthermore, most processing software is too complex for on-chip integration or miniaturization towards implantable devices. Some products answer these issues with a hybrid approach, and take advantage of both software and fast, embeddable, hardware processing: Intan proposes DAQ devices with analogue and digital I/Os (Input/Outputs) and a mounted Field Programmable Gate Array (FPGA) board that can host low-latency material computing, alongside its standard processing software. Müller, Bakkum, and Hierlemann [75] also proposed a hybrid solution using an FPGA to host a reconfigurable low-latency event engine. It is capable of recognizing spatio-temporal spike patterns and delivering sub-millisecond feedback. Further processing is performed in real-time on computer software, with higher processing latencies.

Although these hybrid designs are a step towards complete miniaturization, no fully-hardware biosignal analysis system has been released to date. Specializing in interfaces between biology and microelectronics, the Elibio team required an embeddable solution for biosignal processing. With the wide range of applications covered by the team, such a system should be modular (to avoid duplicate development), be compatible with mainstream acquisition front-ends, be able to recognize various electrical signatures, and have minimal processing latency for closed-loop applications. With a specialty in microelectronics and chip design, the Elibio team has undertaken the design of a fully-hardware DAQ and processing station, Multimed.

Multimed is a generic hardware platform with acquisition and processing capabilities centred on an FPGA. Taking advantage of the reconfigurable logic of FPGAs, it can be reprogrammed, upgrade, and shared between projects with different cellular material (ISLET-CHIP: *in vitro* pancreatic cells, Brain Bow: *in vitro* neurons, Hyrene: *ex-vivo* spinal cord), all the while proposing dedicated hardware processing architectures with very low (sub-millisecond) latency. While the global VHDL (VHSIC Hardware Description Language) architecture (handling both processing and interfacing) is identical between projects, the processing functions and their arrangement are application-specific.

This chapter describes Multimed, its interfaces, processing functions, features, and control environment. Some modules in the system are purely engineering work (drivers, CPU (Central Processing Unit), GPU (Graphical Processing Unit)) and will not be presented in this manuscript, as they provide neither novelty nor understanding of the system.

2.2 Hardware

2.2.1 Architecture

Multimed is a custom electronic system designed specifically to perform acquisition and signal processing on multichannel data. It is composed of three custom boards (all shown in Fig. 2.1):

— An acquisition board ("*Tethys*"), with a secondary stage of amplification and multichannel signal conversion to digital.
— A processing board ("*Titan*") that processes multichannel signal with an FPGA.
— An interface board (""*Dock*"") that provides user interfaces (switches, buttons, USB (Universal Serial Bus) port, Video Graphics Array (VGA) port, digital I/Os, SD (Secure Digital) card slots, JTAG (Joint Test Action Group) connector) and distributes power to other boards.

Tethys: The first board is an acquisition board ("Acquisition Board" in Fig. 2.1), sampling data on 64 parallel channels, at 10 kHz, with 16 b precision. Optimal use of the Analogue-to-Digital Converters (ADCs)' input range is ensured using Programmable Gain Amplifiers (PGAs) with gains ranging from 1 to 100. The board has two SCSI68 connectors, compatible with MCS 60-electrode equipment. All signal pins from the connectors are connected in parallel, which means that Multimed can transparently be inserted in an existing acquisition chain: one connector serves as a signal input and the other as a parallel output. An internal

Table 2.1 – Mainstream electrophysiology DAQ and processing systems.

System	Year	Real-time processing	Includes hardware	Feedback	Processing core	Headstage compatibility	Channels	Sampling Frequency	License
A/D	1990s								Open
DataWave	1990s								Commercial
MEABench	1999	Yes	No	Yes	Linux software	N/A	60	N/A	Open
Neurorighter	2000s	Yes	Yes	Yes	Software		64	1 MHz	Open
Arte	2010s	Yes	No		Software	N/A	N/A	N/A	Open
Open Ephys	2010s	Yes	Yes	Yes	Software[a]	Intan	$\leq$ 512	1-30 kHz	Open
Nspike	2010s	Yes[b]	Yes	No	DSP	Generic	127	30 kHz	Open
UCSD	2010s	No	Yes	No	Software	Intan	$\leq$ 256	20 kHz	Open
RTXI	2010s	Yes	No	Yes[c]	RT Linux	N/A[d]	N/A	N/A	Open
Hierlemann	2012	Yes	Yes	Yes	Mixed[e]	Dedicated	126	20 kHz	Closed
Willow	2015	No	Yes	No	FPGA[f]	Intan	1024	30 kHz	Open
BlackRock-Cerebus	2008	Yes[g]	Yes	Yes		Proprietary[h]	128	30 kHz	Commercial
TDT-PZ2	2008	Yes[g]	Yes	Yes	DSP	Proprietary[h]	256	50 kHz	Commercial

[a] FPGA possible, but not native
[b] Filtering only
[c] Sub-millisecond
[d] Multiple acquisition cards are supported. National Instruments products are recommended.
[e] Software and FPGA
[f] for SATA transfer only
[g] Proprietary external hardware required
[h] Uses Intan

±8 V power supply can be used to power external headstage preamplifiers. Note that the 64 channels are provided for design symmetry reasons; therefore, the four unused inputs with the MCS 60-channel system are accessible via either four SMA (SubMiniature version A) connectors or four standard 2.54 mm pitch square connectors.

Titan: The second board is both a processing board and a control board ("Digital Board" in Fig. 2.1). It has numerous digital I/Os connected throughout the system and to its main component, a Xilinx Spartan-6 FPGA. It can access all digital components and interfaces in the system, meaning it can send configuration instructions to any subsystem in Multimed. It also means that it can read the sampled multichannel data from the first board, process it, and send feedback instructions accordingly, all using reconfigurable architectures. To facilitate communication with high-level interfaces, the FPGA embeds a softcore PIC16F-instruction-compatible processor.

Dock: The third and last board is an interface board ("Dock Board" in Fig. 2.1), that includes multiple Light-Emitting Diodes (LEDs), buttons, and switches, but also generic digital I/Os, a 3.5 mm TRS (Tip Ring Sleeve) jack output, a VGA output, a micro-B USB port, a JTAG connector, and four SD card slots. It also distributes all power supplies throughout the system: both the processing and acquisition board are plugged into and powered by it.

Engineers and graduate students from our group contributed to the design of Multimed: Jean-Baptiste Floderer and Ashwin Mangalore for the hardware, myself for the software, Adam Quotb and myself for VHDL; they were supervised by Gilles N'Kaoua and Yannick Bornat.

2.2.2 Interfaces

MultiChannel Systems equipment

Multimed is merely a part of complete electrophysiology setups. Viable installations include low-noise headstage pre-amplification, temperature control, and multichannel acquisition. With Multimed being primarily a real-time acquisition and signal processing platform, it needs an existing and functional electrophysiology environment to handle specific parts of the acquisition chain. MCS provides such solutions, specifically with its USB-MEA60-Inv-System product line, which is routinely used with Multimed (see chapters 2 and 3). The components of this system are shown in 2.2 and include a headstage pre-amplifier, a data acquisition board, a thermal controller, and a power supply, all described below (note: an actual set-up with detailed connectivity is presented at the end of this chapter, in Fig. 2.12).

The low-noise, high-gain headstage pre-amplifier (Fig. 2.2(a)) is the MEA1060-Inv model. AcpMEA dock in it and electrical contact between the electrodes and the amplifier circuits is ensured by gold spring contacts. Its default version features a 1 Hz – 3 kHz bandwidth, a gain of 1200 on 60 channels, and a built-in heat-plate. Yet MCS also provides customized versions, like the one we specifically use to measure electrical activity of pancreatic islets. This one features a 0.1 Hz – 3 kHz bandwidth.

The temperature of the heat plate is controlled by the STC01 thermal controller, shown in figure 2.2(c). It regulates the preparation temperature at 37 °C.

The commercial acquisition board is the USB-ME64 model(Fig. 2.2(b)), offering acquisition on 60 channels at a sampling rate of 10 kHz and data resolution of 16 bits. Although Multimed performs identical raw data acquisition, this piece of equipment was kept in the acquisition chain to record data in both Multimed and proprietary MCS (`*.mcs` files) format. The double acquisition path was used to validate Multimed acquisition and processing features. It also helped partner physiologists – accustomed to MCS instruments – migrate to the Multimed environment.

Control

Multimed is controled via serial port with the following settings:

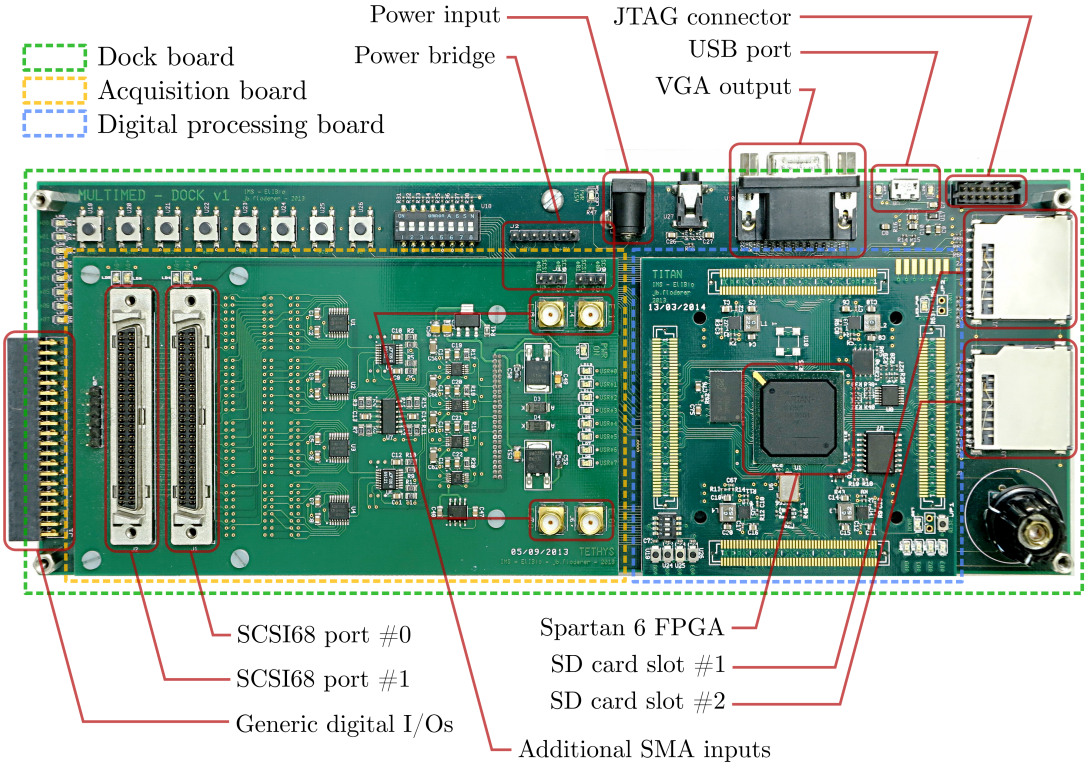

Figure 2.1 – The Multimed hardware and its key components.

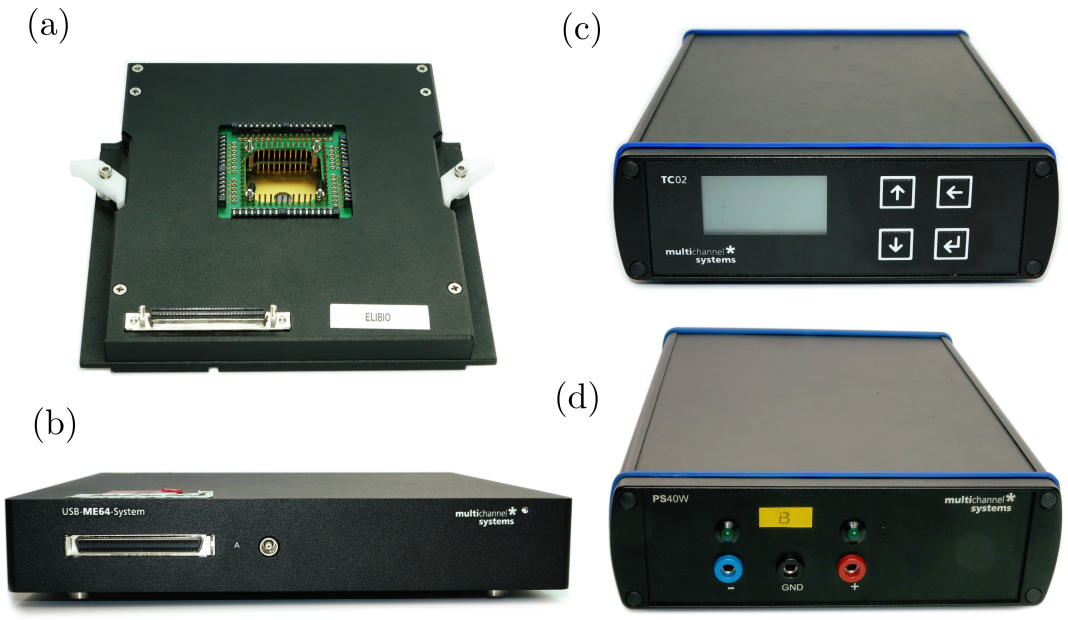

Figure 2.2 – MCS hardware used in conjunction with Multimed. **(a)**: MCS MEA1060-Inv preamplifier. **(b)**: MCS USB-ME64 acquisition device. **(c)**: MCS TC01 thermal controller. **(d)**: MCS PS40W power supply.

— Baudrate: 115200/921600 bauds [1]
— Data bits: 8
— Parity: None
— Stop bits: 1
— Flow control: None

Control includes the possibility to configure processing settings, as well as data display and storage.

Storage

Data are stored on two 32 GB SD cards. One of them stores raw data while the other stores processed data (more detail in section 2.8.1 p. 60). The Multimed specific VHDL SD card driver (not described in this manuscript) has been characterized with SD/SDHC [2] cards only (not SDXC [3]) which is why maximum recording times will be given considering a 32 GB storage capacity.

Display

Display is handled internally, i.e. data are not transferred in real-time to an external display: Multimed has its own VHDL display manager (not described in this manuscript either), including a graphic RAM (Random Access Memory) and VGA protocols. Any screen with a VGA input may therefore be used to visualize data using one of the display modes (temporal waveform display, temporal event display, or spatial event display).

2.3 The FPGA as a core processing unit

The Multimed board is used in multiple projects (ISLET-CHIP: [76], Brain Bow: [77], : [66, 78], Hyrene [79]) that involve different signal signatures and, therefore, different processing requirements. Hosting the processing architecture in an FPGA makes it adaptable, while keeping the exact same hardware. While the same modularity can be achieved with microprocessors or Digital Signal Processor (DSP)s, the FPGA offers better control over processing flows. Data width and number of electrodes can be freely scaled, transfer and processing protocols can be chosen for specific optimizations, and resource uptake can be adjusted. Moreover, such control over the low-level processing architecture eliminates uncertainty on processing latency. While instructions are prioritized and latency is subject to variations in a microprocessor [80], processing time in a VHDL module can be expressed in (or bounded by) a precise number of clock cycles. This is a major advantage in real-time systems with very short processing time windows [75] because it makes any upscale in the number of processing channels more reliable, given the exact limitations (bounded by processing latency and available resources). Finally, it is not uncommon, in multidisciplinary collaborations, to receive requests from partners for improvements or additions to equipment. Once again, the extreme flexibility of the FPGA makes it convenient to update firmware with no modification to hardware.

Due to all these considerations, and taking into account Multimed needs as expressed in section 2.1, an FPGA-based solution is optimal for the Mutimed digital board.

2.4 VHDL architecture

2.4.1 The philosophy behind the architecture

Not all operations have the same level of timing constraint in a real-time system. Signal processing should be fast and consistent, while user interactions do not require precise timing.

1. Depending on board configuration
2. SD High-Capacity
3. SD eXtended-Capacity

These differences in constraint have been exploited in Multimed to facilitate development while ensuring performance: critical real-time operations have dedicated VHDL modules with latency-efficient architectures (parallel computation, pipelines) while other operations (detailed in 2.4.1) are assisted by softcore processors. The VHDL architecture of Multimed is presented in Fig. 2.3

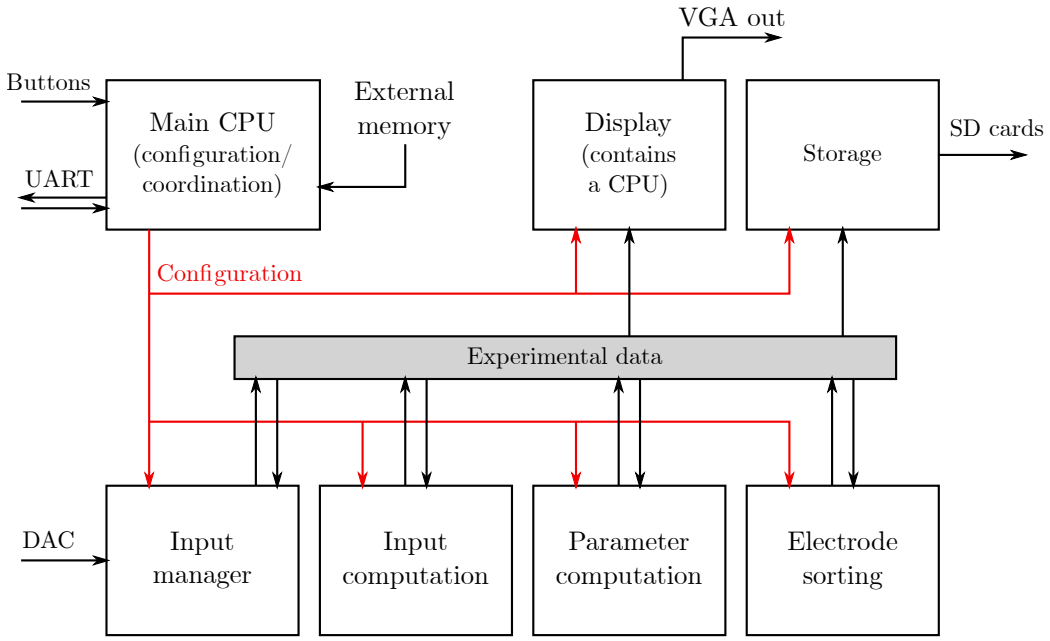

Figure 2.3 – The Multimed VHDL architecture: red lines show configuration signals, black lines indicate data processing flow.

Control through a microcontroller

A microcontroller has obvious benefits in terms of development ease. As opposed to pure VHDL architectures that require synthesis for every modification, programs can be loaded in the processor while in operation. Plus, this facilitates the design flow with C programming, that make communication schemes, user interactions, and high-level instructions more straightforward. As shown in Fig. 2.3, we implemented a softcore processor that acts as an intermediate between the user and the processing modules. It interprets UART and button instructions and writes configuration values in the corresponding module inputs.

A secondary (slave) processor is used to control display on an external screen. Again, it is a machine-user interface that does not necessitate a steady latency. Ultimately, it is only constrained by the screen's refresh rate (60 Hz). Following the scheme described in Fig. D.2, data are retrieved from low-level buffers, shaped, and written accordingly in a graphic RAM. The choice of what and where to display is entirely determined by the program loaded in this slave CPU. Several such programs coexist in memory and may be scrolled through as different display modes.

Note that neither the control, nor the display CPU are ever involved in data processing, as they would bring unwanted latency.

Critical real-time processing

Indeed, real-time processing modules are designed to have a short, well-characterized latency. Therefore, they are fully described in VHDL, which permits a total control over computation procedures. Our strategy is to build a library of processing modules that can interop-

erate while keeping the processing flow fluent, predictable, and latency-efficient. The modules and the associated algorithms are described in 2.5.

Processing chain

To ensure consistent processing, modules have minimal dependencies: ideally, the only condition required to start processing a data frame is to have received it. No handshakes or acknowledgements are required and each module runs independently when it is required to. The main assumption to have such a processing chain working is that the processing latency of each module remains below the sampling period [4]. If it were not, the incriminated modules would still be processing data when new samples arrive, resulting in unwanted skipping and stuttering. While the system would still be running, part of the data would be lost.

2.5 The processing algorithms

Processing algorithms were previously implemented for other projects. They were written and added to the module library by Yannick Bornat and Adam Quotb, and are presented in sections 2.5.1 through 2.5.4. Algorithms developed in this work are described in sections 2.5.5 through 2.5.9.

2.5.1 Wavelet filters

Consistent spike detection relies on good discrimination of Action Potential (AP) waveforms from baseline noise. Though APs may be discerned using only high-pass filtering, a low signal-to-noise ratio will impede detection. To overcome this issue, wavelet filtering is used: this family of filters decomposes signals on an irregular, finite basis rather than the periodic, infinitely long sinusoid basis. They are therefore better at isolating anomalies and other punctual events within the signal, in this case AP waveforms that may otherwise be drowned in noise.

The Discrete Wavelet Transform (DWT) algorithm we use was developed in [70]. It computes d_n^j and a_n^j, the detail and approximation coefficients for detail level j at the n^{th} sample, respectively:

$$d_n^j = \sum_{k=0}^{L} g[k] \times a_{n-2^j k}^{j-1} \tag{2.1a}$$

$$a_n^j = \sum_{k=0}^{L} h[k] \times a_{n-2^j k}^{j-1} \tag{2.1b}$$

Where $g[k]$ and $h[k]$ are the k^{th} coefficient of the high- and low-pass filters, respectively, out of L wavelet coefficients. d_n^j is the useful signal component and a_n^j, the noise component, at detail level j. Its main advantage is to provide an output with an improved signal-to-noise ratio, alongside an other output with low AP contribution quantify noise level on each channel.

2.5.2 IIR filters

To shape the signal and isolate waveforms before more generic processing, classic filters are also used. They are Butterworth Infinite Impulse Response (IIR) filters (first described in [81]) with orders configurable from 1 to 8, configurable as either low-pass, high-pass, or band-pass filters. Typically, Slow Potential (SP) waveforms are isolated using a 3^{rd} order $0.2 - 2$ Hz filter. To anticipate memory optimization and improve configurability, the filter module consists of

4. This is dictated by the ADCs' sampling frequency, but not exclusively: downsampled processing regions from 10 kHz down to 1 Hz exist in the system.

eight first-order, low-pass filters in series, with separately configurable cut-off frequencies, F_c. Each first-order filtering operation is defined by:

$$Y_n = Y_{n-1} \times \left(1 - \frac{1}{2^k}\right) + \frac{X_n}{2^k} \tag{2.2a}$$

$$\frac{1}{F_c} = 2^k(1 - \frac{1}{2^k})2\pi T_s, k \in 0, 17 \tag{2.2b}$$

Where Y_n is the n^{th} output sample and X_n is the n^{th} input sample. The resulting -3dB cutoff frequencies were experimentally measured and summarized in Fig. 2.4. High-pass filtering is also possible by taking the difference between the input signal and the output of one or more low-pass filters. This forms a fully configurable filter unit, up to eight orders. Band-pass filtering is achieved by configuring both high- and low-pass filters within the same filter unit.

2.5.3 Adaptive threshold: standard deviation estimator

APs are detected when the spiking signal exceeds a threshold, chosen to establish a clear distinction between samples that constitute noise and those that belong to an AP. However, in multichannel processing, noise levels may vary between channels and over time [82], thus making it impossible to use a unique, constant detection threshold.

A commonly used solution in electrophysiology consists of setting the detection threshold to a multiple of the standard deviation of individual channel signals [83]. Elegant designs of analogue standard deviation estimators have been proposed [84, 85]. Their design is that of a closed-loop regulator based on noise distribution hypotheses. It estimates a standard deviation value so that a precise proportion of all samples exceeds it [5] (15.9% in the case of a Gaussian noise). Such a design is real-time compatible and was implemented in our group as a digital adaptive threshold module [70]. To accommodate noise-distribution non-idealities, all model parameters have been made accessible for dynamic configuration.

2.5.4 ISI processing: spike cleaning and burst detection

APs detected using simple comparison between the previously described wavelet filters and adaptive threshold require further processing: indeed, simple comparison implies multiple detections of a single event. A minimal duration between two APs , the refractory period, can be defined [66, 86]. It represents the time during which an excitable cell is incapable of firing again to prevent hyperactivity.

2.5.5 Detection of Slow-Potentials

SPs are a low-frequency oscillatory phenomenon. Contrarily to Local Field Potentials (LFPs), their shape is not consistently similar to a low-frequency spike, making the adaptation of AP detection to SP detection impractical and unreliable. Rather than using a threshold detection, SPs are detected on the basis of local maxima and minima in the low-frequency component of input signals: the SP detection module detects local extrema and flags them.

Detection sensitivity may be adjusted with parameter Δ, which defines the minimum amplitude for a cusp point to be considered a local extremum. An illustration of the algorithm is given in Fig. 2.5. Maxima and minima are detected separately and alternately. When the

5. Although such a unit is referenced as a standard-deviation estimator in the literature, it is only used to provide an image of signal amplitude which is immune to cell activity in the measured signal. Deviations from noise distribution hypotheses are therefore acceptable.

module expects a maximum, the detection occurs according to the following criteria:

$$M_0 = X_0 \tag{2.3a}$$

$$M_n = \begin{cases} X_n & \text{if } X_n > M_{n-1} \\ X_n & \text{if } X_n \geq m_{n-1} + \Delta \\ M_{n-1} & \text{otherwise} \end{cases} \tag{2.3b}$$

$$Y_n^M = \begin{cases} 1 & \text{if } X_n \leq M_{n-1} - \Delta \\ 0 & \text{otherwise} \end{cases} \tag{2.3c}$$

Where Y_n^M is the n^{th} output sample of the maximum detection and X_n is the n^{th} input sample. The maximum value of X up to sample n is stored in M_n, and is considered a maximum only when the signal drops below this value by at least Δ, at which point M_n is reset and the module enters a minimum detection mode, which operates similarly:

$$m_0 = X_0 \tag{2.4a}$$

$$m_n = \begin{cases} X_n & \text{if } X_n < m_{n-1} \\ X_n & \text{if } X_n \leq M_{n-1} - \Delta \\ m_{n-1} & \text{otherwise} \end{cases} \tag{2.4b}$$

$$Y_n^m = \begin{cases} 1 & \text{if } X_n \geq m_{n-1} + \Delta \\ 0 & \text{otherwise} \end{cases} \tag{2.4c}$$

Where Y_n^m and m_n are the counterparts for Y_n^M and M_n, respectively, whenever the module expects a minimum.

Experiments showed that non physiological punctual slow oscillations ($<$0.1 Hz) were not getting filtered and were therefore mistakenly detected by the module. A time parameter was therefore added, to blank the first SP detection after a period of inactivity, in case it indeed is an isolated detection. Otherwise, detection resumes as usual.

Validation data on SP signals from *in vitro* pancreatic islets can be seen in appendix A

2.5.6 Amplitude measurements

To measure oscillation (like SP) amplitude, the peak-peak envelope of the signal is recorded. For that matter, a peak detector is used on the positive half of the signal and another on the negative half. The peak detection operations are conducted using a positive (and negative, respectively) value function and a second order IIR low-pass filter. The source signal may be chosen (either raw or filtered signal), and the time constant and order of the peak detector filters may be configured.

2.5.7 Frequency and FOPP measurements

Measuring frequency or Fraction Of Plateau Phase (FOPP) [6] of event data may simply be done by computing windowed averages of event trains (represented by 1s and 0s) or burst envelopes (represented by 1s when in a burst, 0s otherwise). In the case of event frequency, this would yield a reduced frequency, which can be normalized back, knowing the sampling frequency. In the case of FOPP, averaging burst envelopes would immediately yield the plateau fraction, between 0 and 1.

The low-resource solution chosen to achieve such measurements is the use of IIR low-pass filters [7] as windowed-averaging filters, which cutoff frequency may be adjusted to tune

6. FOPP is a figure representing the ratio of active phase (plateau) in a biological recording. Typically, a plateau is defined where a cell or islet is bursting. A cell with no bursts will have a FOPP of 0 (0%), a cell with constant bursting activity will have a FOPP of 1 (100%), and a cell that is bursting half the time will have a FOPP of 0.5 (50%).

7. identical to those described in 2.5.2

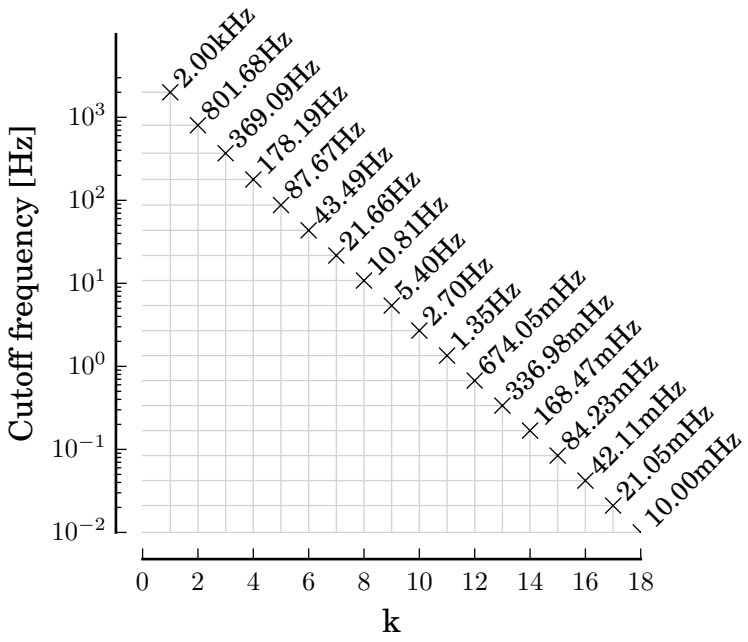

Figure 2.4 – IIR filters cutoff frequencies with respect to k, as defined in eq. 2.2a.

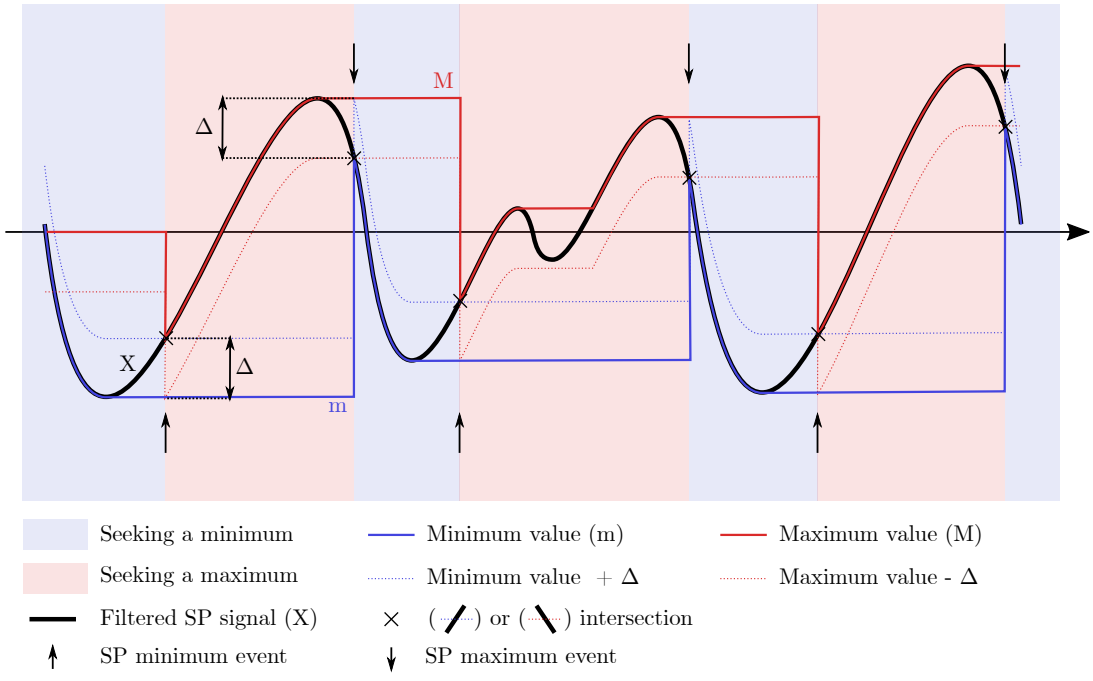

Figure 2.5 – SP detection scheme. Two signals (s_m and s_M) keep track of the current local maximum or minimum value (depending on whether the module is targeting a maximum or a minimum). Whenever $s_m + \Delta = s$ or $s_M - \Delta = s$, an SP maximum or minimum event is fired and the module toggles target.

the window size. Two first-order filters are used in series to reduce oscillations caused by distant events (the module's configuration permits both first- and second-order averaging, but second-order is generally preferred because it offers good measure stability and good response time). Input events are multiplied by $2^{14} = 16\,348$ prior to entering filters, which is equivalent to converting boolean events to a signed 16-bit fixed point representation with 1 sign bit, 1 integer bit, and 14 fractional bits.

Fig. 2.6 illustrates the response time performance of the frequency measurement, depending on parameter k in the IIR low-pass filter (eq. 2.2a).

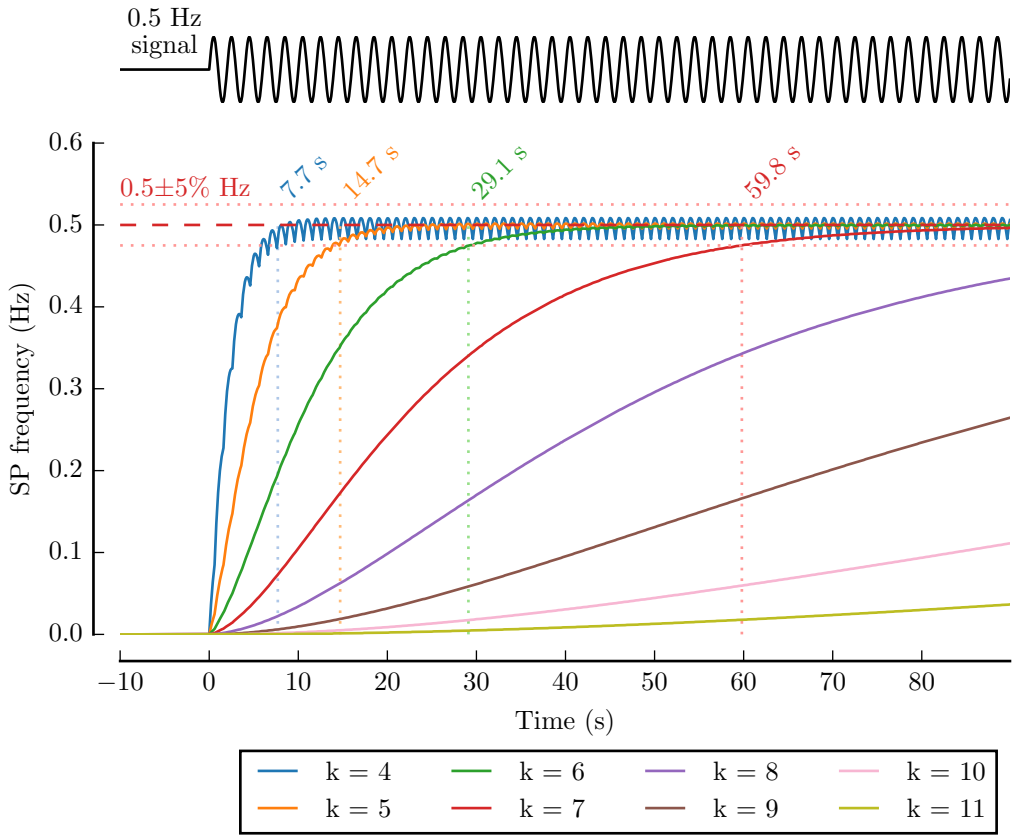

Figure 2.6 – SP frequency measurement performance on a 0.5 Hz sine wave with a second order IIR filter, with different k values. k is as defined in eq. 2.2a. The time required to enter a ±5% interval of confidence from target is indicated when relevant.

2.5.8 Electrode sorting

MEAs are versatile tools, with various uses and applications in electrophysiology. They provide multisite, real- time readouts of cell activity with the potential for network analysis with high time resolution, but generally lack spatial resolution. The chances of having a cell within measuring distance remain slim, considering the small active surface and electrode sparsity (typically, electrode diameter is 10% of electrode spacing). Increasing electrode coverage necessitates an upscale in the number and density of electrodes, cell- guiding techniques [87], or dedicated topologies [88]. Even then, the proportion of covered and exploitable electrodes never reaches 100%. In chronic recordings, the apparition of fibroblasts and scar tissue systematically results in additional electrode loss [89]. Moreover, multiple sources for hardware failure exist in the acquisition chain, from the MEA itself to the multichannel amplifier and the mechanical spring-loaded contacts between them. These issues usually result

in unnecessary processing of uncovered electrodes. To address this important issue, we developed a digital module, inspired from experiments, to sort and automatically constitute a set of normally-behaving electrodes.

The general methodology adopted by electrophysiologists to define a set of valid electrodes is to exclude electrodes that are responsive in inhibitory conditions, and include those that display a physiological response in excitatory conditions. The physiological characteristic of the response is determined by the experimenter and is usually related to both the frequency and amplitude of the measured events (in the context of pancreatic islets, APs and SPs). Finally, electrodes that present an electronic malfunction, such as coupling or saturation are excluded as well.

The electrode sorting module recreates this method and sorts electrodes based on both raw signals and events. The sorting algorithms discriminate electrodes based on any or all of (a) their event frequencies, (b) synchronous activity, and (c) signal amplitude. Event frequency is obtained by counting events over a limited period of time T. An electrode is flagged active if this count exceeds a threshold as described in equation (2.5a) below:

$$a_n^i = \min(a_{n-1}^i + x_n^i, \Delta) \tag{2.5a}$$

$$A^i = \begin{cases} 1 & \text{if } a_N^i = \Delta \\ 0 & \text{if } a_N^i < \Delta \end{cases} \tag{2.5b}$$

Where $n = 1...N$ is the current sample number, a_n^i is the n^{th} value of the event counter of electrode i, x_n^i is the n^{th} input of the event counter of electrode i (either 1 if an event is present or 0 otherwise), Δ is the event threshold, N is the total number of samples over T and A^i is the activity flag for channel i. Detection of synchronization between channels is based on a leaky event counter. For each electrode, incoming events increase a counter s by a step ε_U. Otherwise, the counter decreases by a step ε_D at every T/N. This gives each event a weight that decreases with time. If the sum of all counters exceeds a threshold Q, meaning that a sufficient amount of events were fired in a short time window, a synchronization event S is fired, related to all involved electrodes. This process is summarized in equation (2.6a) below:

$$s_n^i = \begin{cases} 0 & \text{if } \sum_{i' \in I} s_{n-1}^{i'} + x_n^{i'} \times \varepsilon_U \geq Q \\ \max(s_{n-1}^{i'} + x_n^{i'} \times \varepsilon_U - \varepsilon_D, 0) & \text{otherwise} \end{cases} \tag{2.6a}$$

$$A^i = \begin{cases} 1 & \text{if } a_N^i = \Delta \\ 0 & \text{if } a_N^i < \Delta \end{cases} \tag{2.6b}$$

Where n is the current sample number, s_n^i is the n^{th} value of the event counter of electrode i, x_n^i is the n^{th} input of the event counter of electrode i (either 1 if an event is present or 0 otherwise), S_n^i is the n^{th} synchronization event of electrode i, and I is the set of all electrodes. In order to detect repeated synchronization only and avoid false positives, the synchronization events S_n^i are then processed by the algorithm described in (Eqs. 2.5a, 2.5b). Finally, sorting electrodes according to amplitude criteria is simply done by comparing the signal value to a threshold. If the input sample exceeds it, the corresponding electrode is flagged. For more flexibility, the event-based algorithms are duplicated to be used separately for APs and SPs , and the ensemble of all algorithms, forming one sorting cell, is duplicated four times to permit different configurations and intermediary results (see Fig. 2.7). The final sorting result is a definable logic combination of all four intermediary results (intermediary and final results are accessible for readout), representing experimenter-defined inclusion/exclusion rules in a dynamically configurable Lookup Table (LUT).

The complete implementation of the module is given in Fig. 2.7.

The sorting module was tested and used (validation data can be found in appendix B) on three pancreatic islets preparations (Fig. 2.8). The inclusion rule of the module stated that electrodes with more than 10 SPs in 60 s in excitatory conditions were retained. The exclusion

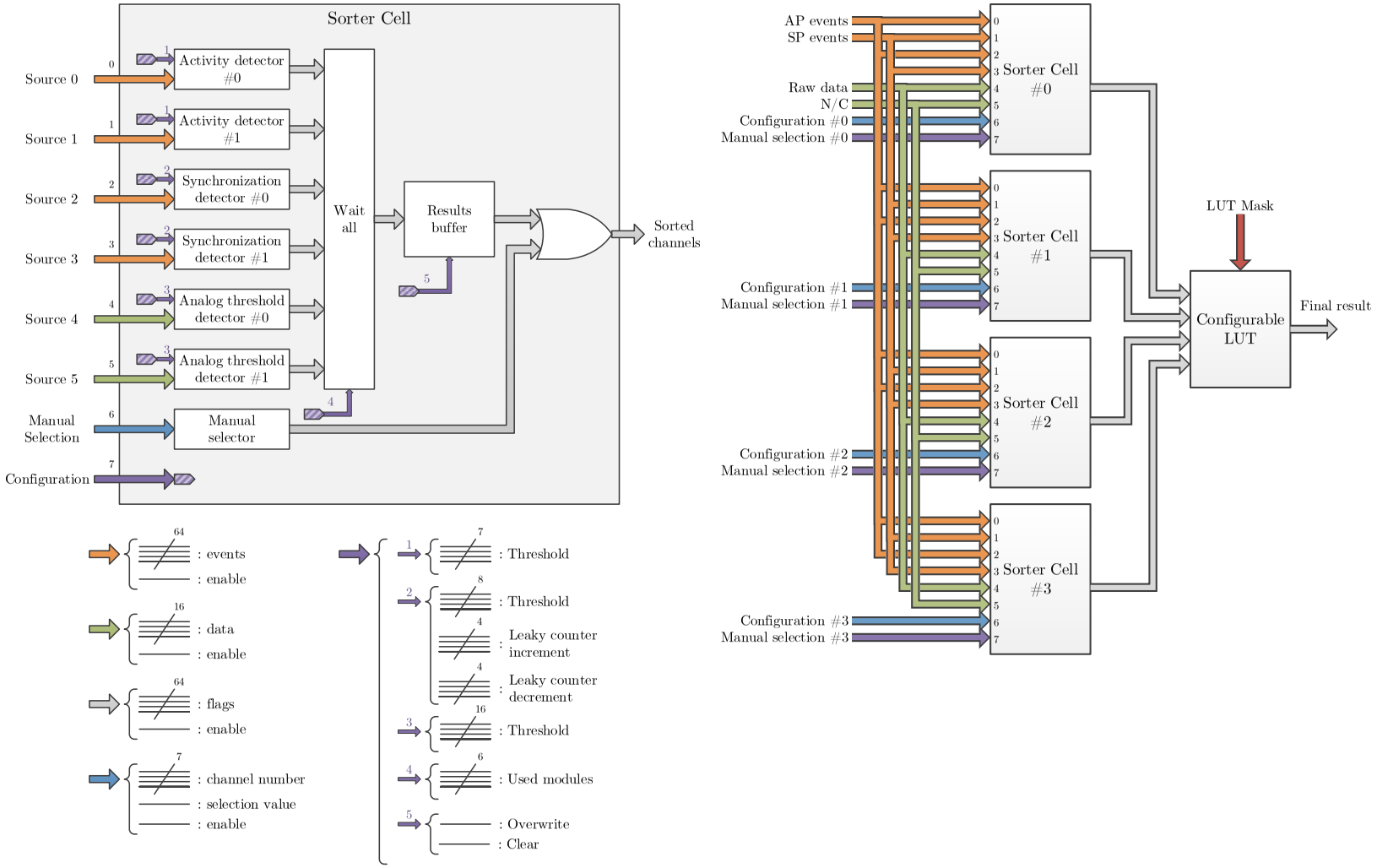

Figure 2.7 – Electrode sorting architecture. Four identical cells, including sorting by activity, synchronization, and amplitude, feed a configurable LUT. Full signal description is given for inputs and internal signals.

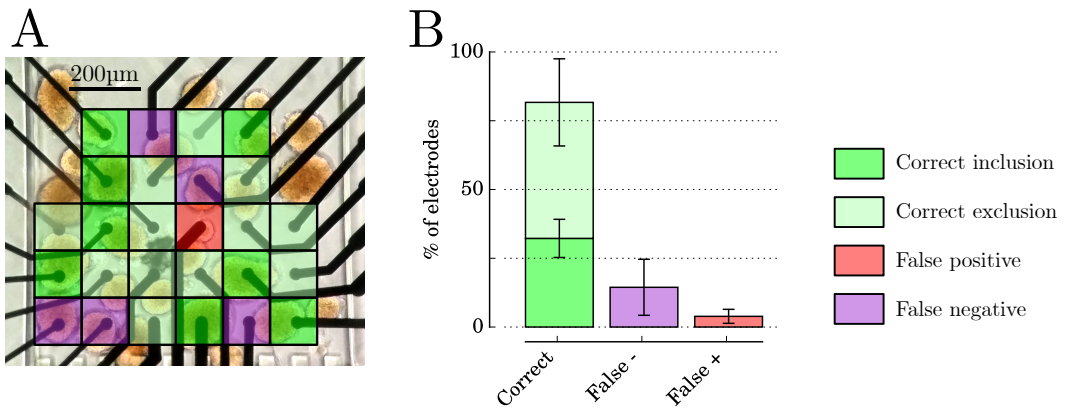

Figure 2.8 – Sorting results on three different experiments. **A**: detection results overlaid with a photography of the preparation. **B**: Repartition of electrode sorting results. On average, the module detected 4% false positives, 14% false negatives, and 82% correct detections.

rule rejected electrodes with either more than 5 SPs in 60 s or a peak amplitude of more than 300 µV in inhibitory conditions. One experimenter manually sorted electrodes, following the routine methodology, while another ran the sorting module, blinded from experimental observations. In Fig. 2.8, we compared both methods, taking manual sorting as a reference. In three experiments, the sorting module detected from 73% to 95% of valid electrodes. False detections leaned towards false negatives rather than false positives. This means that the detected subset of electrodes, though incomplete, is suitable for valid measurements and few (4%) electrodes are disruptive.

2.5.9 Spatial averaging

It is possible to integrate the measurements from several channels by computing their instantaneous mean: the spatial average calculator module averages any combination of N streams into one. The operation is optimized for speed as it is bound to be repeatedly performed at the sampling frequency: the inverse of N is computed once using a Euclidian division, then multiplied to each sample prior to summing. To anticipate more complex modules and free multipliers in the FPGA, a low-resource, pipelined multiplier was written.

Computation consequently occurs as follows: let W be the data width and J be the set of N-channel data to be averaged. The spatial average Y is computed by equations 2.7a and 2.7b below, where a_i is the i^{th} digit of the binary representation of A:

$$A = \frac{2^W}{N} \tag{2.7a}$$

$$Y_n = \sum_{i=0}^{W-1} a_i \times \sum_{j \in J} \frac{X_n^j}{2^{(i+1)}} \tag{2.7b}$$

Where Y_n is the n^{th} output sample and X_n^j is the n^{th} input sample for channel j within a set J of N channels.

2.6 Complete processing architecture

The complete processing architecture is represented in Fig. 2.9. Its organization may be read horizontally, with separate AP and SP processing chains, or vertically, with an identical structure in both AP and SP chains, composed of an *input processing* stage (filtering, event detection) and a *parameter measurement* stage (frequency and FOPP measurement, electrode

sorting). For configuration convenience, all module outputs are available for display, as well as major processing results (raw data, AP detection, SP detection, frequency measurements, FOPP measurements, amplitude measurements, and electrode sorting results).

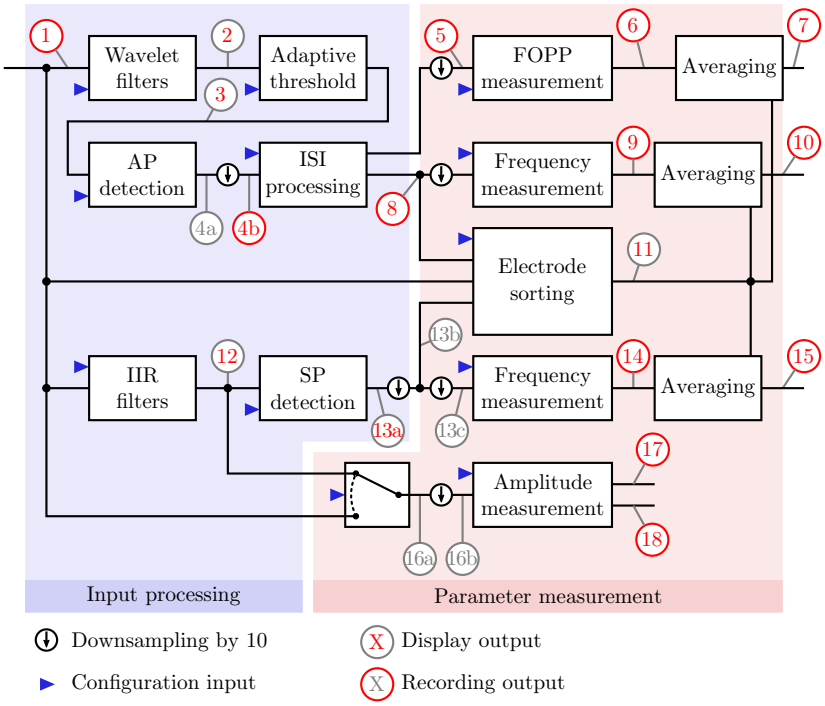

Figure 2.9 – Complete processing architecture. Recording, display, and configuration points are indicated. Signal names and sampling frequencies are as follows: **1**: Raw signals (10 kHz). **2**: Wavelet-filtered signals (AP waveforms) (10 kHz). **3**: Adaptive threshold (10 kHz). **4a**: Raw AP events (10 kHz). **4b**: Raw AP events (1 kHz). **5**: Bursts (1 kHz). **6**: FOPP measurement (100 Hz). **7**: Average FOPP (1 kHz). **8**: Clean AP events (1 kHz). **9**: AP frequency (100 Hz). **10**: Average AP frequency(1 kHz). **11**: List of sorted channels (100 Hz). **12**: Filtered signals (SP waveforms) (10 kHz). **13a**: SP events (1 kHz). **13b**: SP events (100 Hz). **13c**: SP events (10 Hz). **14**: SP frequency (1 kHz). **15**: Averaged SP frequency (1 kHz). **16a**: Envelope base signal (10 kHz). **16b**: Envelope base signal (1 kHz). **17**: Upper envelope (1 kHz). **18**: Lower envelope (1 kHz).

2.7 Hardware implementation

To satisfy the needs expressed for Multimed at the end of section 2.1 (being easily applicable to diverse projects, being easily reconfigurable, recognizing various electrical signatures), design rules were put in place to maximize compatibility between modules as well as performance. This section focuses on some of these design rules, exclusively concerning processing modules (detailed description of their environment and functional modules is given in Appendix D.

2.7.1 Integration and communication

Communication between processing modules is entirely standardized. Multichannel streams [8] are transferred sequentially, with a start bit indicating transmission start (Fig. 2.10A). Modules with pipelined architectures can immediately process these data, while the others buffer them in a local FIFO (First In First Out). Event data, for their part, are transferred in parallel

8. Signals such as raw data, filtered data, frequency and FOPP measurements

alongside an enable bit (Fig. 2.10B). They too are buffered in processing modules. Although these communication scheme sometimes induce duplicated storage in the system, they improve processing latency.

Real-time processing being of the essence, data are transmitted without a handshake signal. Indeed, it is preferable to favour fast and consistent data transmission to data traceability. Plus, in such a controlled environment, where sampling frequency is four orders of magnitude below clock speed [9], it is safe to assume that all transmitted data is processed by the downstream module before the next sample is sent: the longest processing latency in the system is caused by wavelet filtering, with a worst-case processing time of 4160 clock cycles for all 64 channels (or 41.6% of the available processing time between two samples. See table 2.3 for a complete quantification of processing latency). This should however be one of the main cautionary points when considering an upscale in the number of source channels.

2.7.2 Parallelization and serialization of computation

To improve performance, data is transferred between modules in a flow. At the module level, N samples corresponding to N electrodes are serially input and output. Simple modules (and modules that allow it) are fully pipelined [10] and implemented at very little resource and time cost. Other modules need to have data buffered in a local FIFO before processing them at the cost of several clock cycles per electrode. Although this communication scheme induces duplicated storage in the system, it improves processing latency.

2.7.3 Implementation costs and performance

Cost of implementation and processing latencies of all modules are summarized in tables 2.2 and 2.3. Synthesis was run for a Xilinx Spartan-6 FPGA with ISE 14.7 and default synthesis parameters. Since modules are written for a generic number of channels N, table 2.3 gives the processing latency of each module both as a function of N and in the current 64-channel implementation.

9. Clock frequency is 100 MHz, sampling frequency is 10 kHz

10. Pipeline refers to the unbuffered series computing scheme: data are processed as fast as they arrive, at a pace of one electrode per clock cycle. This means that processing latency is constant, equal to the number of processing steps in the pipeline regardless of the number of electrodes to process.

Table 2.2 – Indicative Resource uptake per module. Percentages are device utilization (Xilinx Spartan-6), except for LUT-FF pairs that are a fraction of utilized LUTs. LUT: Lookup Table; FF: Flip-Flop; RAM: Random Access Memory; FIFO: First In First Out.

Module (and submodules)	Registers	LUTs	LUT-FF pairs	Block RAM/FIFO	Others
Input Manager	448 (0.24%)	701 (0.76%)	268 (30%)	1 (0.37%)	
Input Signal Processing	4423 (2.4%)	6604 (7.2%)	4041 (58%)	33 (12%)	
IIR filters	329	1196	285	-	
Wavelet filters	178	371	168	32	1× DSP48A1
Adaptive threshold	206	575	183	1	1× DSP48A1
Burst detection	221	316	219	-	
SP detection	1013	1688	894	-	
Parameter measurements	6153 (3.3%)	5474 (5.9%)	2473 (27%)	4 (1.5%)	2× DSP48A1s
FOPP	505	714	409	1	
AP frequency	505	714	409	1	
SP frequency	505	714	409	1	
Averaging	3830	4804	3486	-	
Electrode sorting	7425 (4.0%)	10019 (10%)	7005 (67%)	-	
Sorting cells (×4)	1930	2347	1868	-	
Output LUT	-	256	-	-	
Display	6298 (3.4%)	8216 (8.9%)	3936 (41%)	18 (6.7%)	
CPU	414	743	349	2	
VGA manager	3187	3839	2376	16	
MEA layout manager	1086	1478	1044	-	
Storage	2260 (1.2%)	3457 (3.8%)	1579 (38%)	97 (36%)	
Event collection	1231	986	643	65	
Data buffer	181	805	154	-	
SD card management	848	1666	782	32	
CPU	643 (0.45%)	1076 (1.2%)	417 (35%)	3	

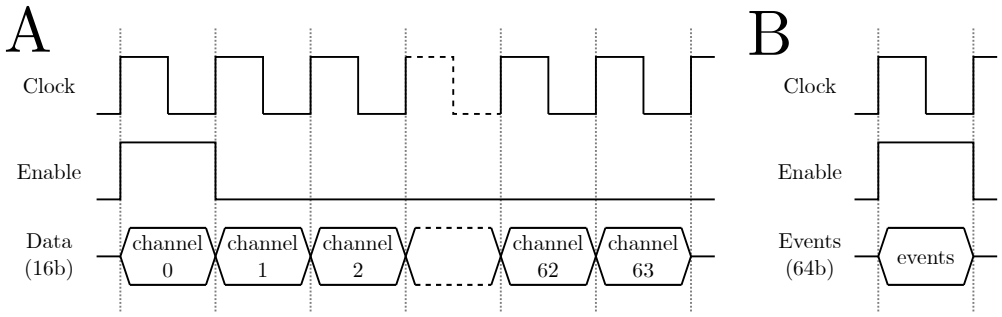

Figure 2.10 – Inter-module communication schemes. **A**: Series data transmission protocol used for stream transfer. **B**: Parallel data transmission protocol used for event transfer.

Table 2.3 – Processing latency of modules and their sub-modules for N channels (generic case) and 64 channels (present case).

Processing module (and submodules)	Latency	
	in clock cycles (N channels)	in µs (64 channels)
AP and burst detection	$17N + 8$ to $75N + 8$	10.96 to 48.08
Wavelet filter	$7N$ to $65N$	4.48 to 41.60
Adaptive threshold	$9N + 4$	5.80
ISI processing	$N + 4$	0.68
SP detection	$23N + 4$	14.76
IIR filters (8 filters)	$16N + 2$	10.26
Extrema detection	$6N + 1$	3.85
SP filtering	$N + 1$	0.65
Frequency/FOPP measurement	9	0.09
Amplitude measurement	9	0.09
Electrode sorting	$9N + 3$	5.79
Averaging	$N + 17$	0.81

2.8 Functional blocks

2.8.1 Recording

Raw and processed data are stored on two separate SD cards: with respect to the notations in Fig. 2.1, raw data are stored in slot #1 and processed data in slot #2. This produces one file containing raw data for verification and archiving purposes, and another one containing detection and measurement results, ready for fast transfer and post-analysis. Processed data include detected events, measurement streams, and configuration information as listed below:

- Events
  - APs
  - Burst starts
  - Burst ends
  - SP maxima
  - SP minima
- Streams
  - AP frequencies
  - SP frequencies
  - FOPPs
  - Signal envelope
  - Averaged AP frequency
  - Averaged SP frequency
  - Averaged FOPP
- Configuration
  - PGA gain

The SD storage driver currently has not file system support, meaning that data must be stored in an unformatted binary format. While this does require dedicated extraction software, the resulting format is very compact and sequential, making it easy to read, convert, or process.

Appendix C provides detailed information regarding raw and processed data formats (C.1 and C.2 resp.), as well as all recorded processed data and their properties (C).

2.9 Graphical User Interface

A Graphical User Interface (GUI) was designed to make system configuration accessible to the uninitiated. It was written in Python 2.7 to permit cross-platform development and convenient releases to partners, taking advantage of it being a free, multi-platform, open-source language. The GUI notably uses the TkInter package to create its graphical handles and the pySerial package to handle serial communication.

2.9.1 Communication layer

A communication and control API (Application Programming Interface) constitutes the bottommost layer of the interface. It is a communication layer that translates user inputs to Multimed command strings (e.g. PGA gain $\times 10$ is translated to command string *i89*, see Appendix E for translation rules). A communication overlay handles serial communication and user interaction. Each configuration input from the user results in a serial instruction to Multimed and a console output. Each configuration instruction indeed has an associated description that is displayed when sent. For traceability, each action on the interface is also logged in a text file created on startup. This log contains all instructions sent to the system, alongside their corresponding descriptions and timestamp. The latter are written to be interpreted by Multimed as comments, meaning that the log file may be sent to Multimed as a command string without modification and restore a previous state for debugging.

2.9.2 Graphical interface layer

The graphical interface layer was designed in collaboration with CBMN (Institute of Chemistry & Biology of Membranes & Nano-objects) to meet their needs during experimental sessions. Exchanges were made between releases to improve accessibility, ease of use, and compatibility (screen size, OS, communication ports). This sections summarizes the decisions that were made to reach the final design.

General structure

The topmost layer of the interface is a TkInter application providing graphical controls over Multimed. It is composed of four main panels (see Fig. 2.11): (1) A panel on the left, providing connection options, hardware information, GUI options (save/recall, log file export), and recording options; (2) A display control panel on the right, to select display modes; (3) A processing configuration panel in the centre, with multiple tabs to configure each module in Multimed; (4) A console at the bottom, to have a readout of all operations and manually enter command strings or comments.

The interface layout is designed to have every essential control immediately available on startup, and still accessible when browsing configuration menus. Only the centre panel can switch tabs, to unravel more in-depth configuration options for every module. They include:

- An input tab, to configure PGAs.
- A SP filter tab, to configure a complete IIR filter block.
- A SP detection tab, to configure both SP detection parameters and SP frequency measurement parameters.
- A SP amplitude measurement tab
- An AP detection tab, to configure the AP detection threshold and AP frequency measurement parameters.
- An AP burst detection tab, to configure burst detection and FOPP computation.
- An AP filter tab, to configure wavelet filters.
- A sorting tab, to configure electrode sorting and read its results.
- A monitoring tab, to read measurement values on any channel in real-time.

User constraints

The system is used in several locations, with different experimenters, on different cells, and for different purposes. The GUI must therefore accommodate various users and situations.

With that in mind, the number of parameters available in the system would make it a particularly dull experience to configure every setting by hand for every experimental scenario. Firstly, it is a very time-consuming and repetitive task; secondly and most importantly, this process is prone to human error. Although it was already possible to send pre-written ASCII (American Standard Code for Information Interchange) configuration strings (see section 2.9.1), a more user-friendly approach of saving and recalling configurations was added. It was integrated in the GUI, meaning that Multimed does not save or recall a given state, the interface does, setting both its own and Multimed's states. This gives more complex possibilities in terms of instruction parsing and generates configuration files that are both legible and editable. The configuration file format adopted is structured with opening and closing tags [11] that define a configuration region for each module, permitting partial configuration files (e.g. a configuration file may only configure SP filters).

This feature also facilitates system utilization for users with little training, as it provides presets, making navigating advanced configuration tabs virtually unnecessary.

11. inspired by Extensible Markup Language (XML)

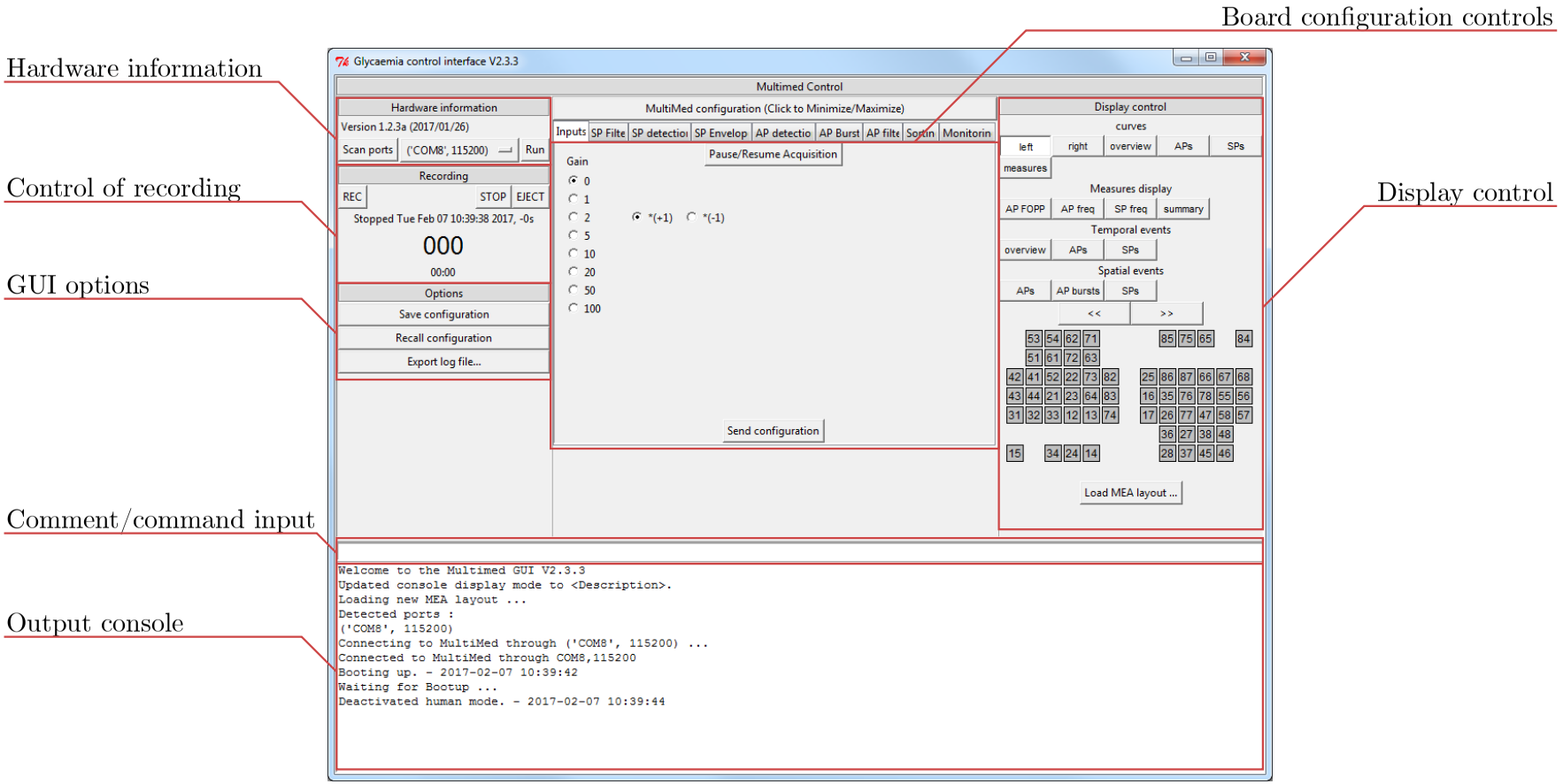

Figure 2.11 – GUI layout.

2.10 Hardware support

2.10.1 Complete setup

A complete electrophysiology setup including Multimed has many interacting parts, and connections must be thoroughly respected to avoid malfunctions and hardware damage. Figure 2.12 shows the connection diagram of a setup for pancreatic cell measurements (ISLET-CHIP project). It is composed of (1) a Multimed board, (2) a MCS preamplifier and (3) its thermal controller, (4) a computer for controlling Multimed, (5) a VGA monitor for displaying real-time data, (6) a MCS acquisition board (optional), (7) a MCS filter module (optional), all on (8) a single power strip (recommended). For detailed material setup instructions and safety precautions, see appendix F.

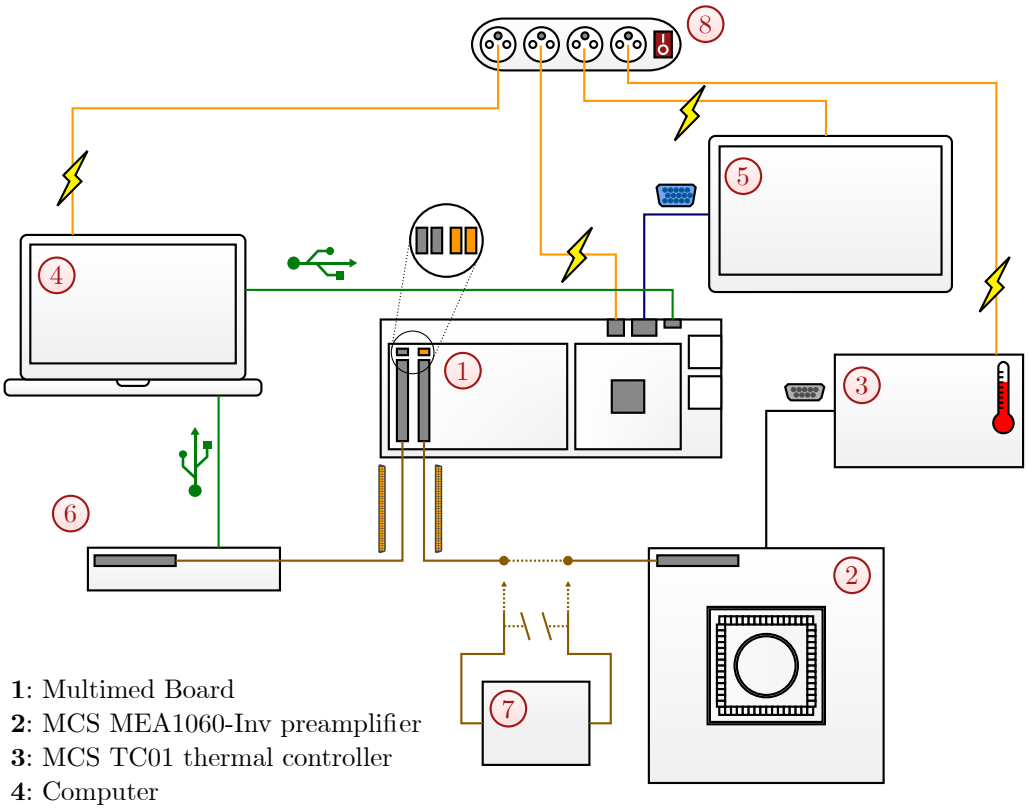

1: Multimed Board
2: MCS MEA1060-Inv preamplifier
3: MCS TC01 thermal controller
4: Computer
5: VGA monitor
6: MCS USB-ME64 acquisition board (optional)
7: Optional filters

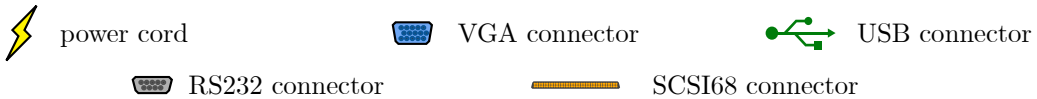

Figure 2.12 – Complete measurement setup scheme

2.11 Modularity and Evolutivity

2.11.1 Macro-module aspect

Processing modules in Multimed are written to facilitate rearrangement and share hardware between projects. Even though the presented architecture is optimized for pancreatic cells, it

is easy to reorganize modules and adapt to other projects' specifications. While the interface part of the architecture remains the same (Main CPU, display management etc.), the whole processing chain may be redesigned, making each version of Multimed an application-specific arrangement of the same macro-modules. Data manipulation protocols between processing units are standardized to ensure compatibility.

The motivation behind such a design is twofold: it facilitates both new collaborations with a pre-built adaptable system, and prototyping for processing ASICs (Application-Specific Integrated Circuits). Architectural choices can indeed be explored prior to using digital synthesis tools to generate chip designs.

New needs in terms of processing capabilities are constantly being expressed, leading to regular updates of the digital library of modules. In parallel, hardware developments are ongoing, in an effort to improve the interfaces with a custom high-voltage stimulation ASIC [90] and facilitate the prototyping of fully-customized, autonomous System-In-Package (SIP) solutions.

2.11.2 Technology transfer

Multimed setups have been installed in multiple sites and are being used by partner laboratories in collaborative projects, always aiming for closed-loop experiments (Brain Bow, Cenavex, ISLET-CHIP). In the case of ISLET-CHIP, that involved clinical associates, partnership agreements included the installation of measurement setups in different sites. A first setup was installed at CBMN (Fig. 2.13A), the geographically closest partner, to test it in lab conditions, verify that uninitiated personnel could be trained to use it independently, and conduct quality control measurements on human islets sent by the isolation centres in Geneva, Switzerland and Montpellier, France. The underwhelming success rate of these experiments motivated a second installation directly in the Geneva Cell Isolation and Transplantation Centre (Geneva University Hospital, Switzerland, Fig. 2.13B) to bypass long-distance cell transportation. In both sites, resident personnel was trained to handle not only Multimed, but the complete measurement chain of Fig. 2.12, multiplying independent islet quality control sites.

At the same time, the biosensor technology developed is being promoted by Aquitaine Science Transfert (AST), a technology transfer firm, to find entrepreneurs and possible collaborators and clients to continue research and development of the technology in a start-up company.

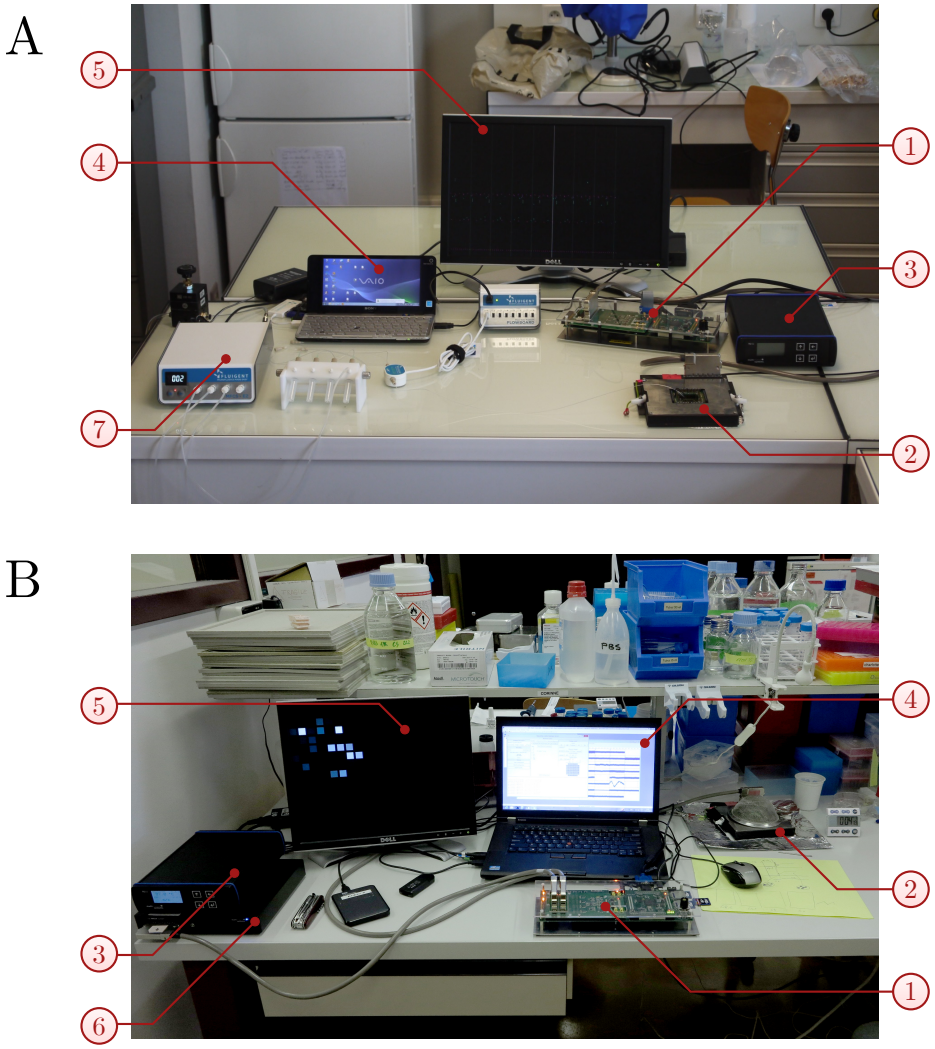

1: Multimed Board
2: MCS MEA1060-Inv preamplifier
3: MCS TC01 thermal controller
4: Computer
5: VGA monitor
6: MCS USB-ME64 acquisition board (optional)
7: Microfluidic pump

Figure 2.13 – Pictures of two different measurement setups. **A**: System set up at CBMN , Pessac, France. **B**: System set up in Geneva, Switzerland.

Chapter 3

Experiments and results: a peek inside extracellular electrophysiology

If you try and take a cat apart to see how it works, the first thing you have on your hands is a non-working cat.

- Douglas Adams, *The Salmon of Doubt: Hitchhiking the Galaxy One Last Time*

The development of Multimed's processing architecture for the study of signals as specific as pancreatic islets' has been an opportunity to explore many experiments: from writing algorithms to testing the processing electronics, involvement in experiments with our biology partners was key. The constant exchange to better the system led to fruitful collaborations not only towards ISLET-CHIP's goal of measuring islet quality, but also towards characterizing and understanding the underlying mechanisms of pancreatic islets.

This chapter describes the experiments that were conducted using Multimed (online analysis) or its prototype algorithms (offline analysis), as well as post-analyses and their interpretations. The primary objective of these measurements was to characterize the response of various cell preparations with the developed electronics (forming the complete biosensor setup). The extracted data serve as a reference for islet quality measurements in ISLET-CHIP, but also help extract models to simulate the biosensor in a closed-loop configuration.

3.1 Materials and methods

This section describes the materials used for the experiments (electrophysiology material and biological material), as well as the general experimental protocols adopted and analysis methods. With one exception, all the presented experiments took place at CBMN (Institute of Chemistry & Biology of Membranes & Nano-objects) (Pessac, France). Biological protocols [1] were applied by either Fanny Lebreton, Eleonore Bertin, Manon Jaffredo, Julien Gaitan, Romain Perrier, or Matthieu Raoux. The experiment presented in 3.5.2 took place in the Geneva University Hospital (Geneva, Switzerland). In this case, biological protocols were applied by Fanny Lebreton.

1. Including preparation and experimentation

3.1.1 Electrophysiology material

Gold standard MEAs

The reference Microelectrode Array (MEA) used was the MEA200/30-Ti-gr (see Fig. 3.1A-B) from MCS [Multi Channel Systems, Reutlingen, Germany]. It featured 59 30 µm-diameter Titanium Nitride (TiN) recording electrodes with 200 µm spacing and an announced impedance of <100 kΩ at 1 kHz. A 60^{th} electrode, bigger in surface than the others, is grounded and used as an electrical reference (electrode #15). Note that it is not included in the 8×8 layout of Fig. 3.1B. It can be seen on the left side of the well (Fig. 3.1A), a 6 mm-high glass cylinder, used as a culture chamber. These MEAs are widely used in extracellular electrophysiology and were the first choice to measure pancreatic cells prior to ISLET-CHIP. In our studies, they defined the gold standard in terms of electrode distribution, impedance, noise, and bandwidth.

HD MEAs

HD-MEAs (High-Definition MEAs), also provided by MCS (60HexaMEA40/10iR-ITO-gr), have a higher electrode density and have dimensions that permit multisite recording on single islets. Their culture chamber contain 59 circular Titanium Nitride (TiN) recording electrodes, each 10 µm across and with 40 µm spacing. Their announced impedance is $250 - 400$ kΩ at 1 kHz. The 60^{th} electrode is a reference electrode, again significantly bigger than recording electrodes.

Microfluidic MEAs

To study continuous variations in cell activity, MEAs with microfluidic channels were used. The motivations for replacing the well culture chamber with a microfluidic-compatible one were multiple: having fluidic inlets and outlets permits to automatically change the medium with pumps [2], instead of manually pipetting it, thus reducing the risk of detaching cells. More importantly, it permits continuous recording with no perturbation of the cells by the experimenter during changes. It is also more physiologically accurate, as it continuously and progressively changes the culture medium and washes away the secreted insulin and glucagon. Finally, it is a necessity for the long-term plans for the biosensor that require a contained solution for interstitial fluid perfusion (see 1.5.1).

These μ-MEAs (see Fig. 3.1C-D) were custom-made and supplied by Qwane Biosciences company [Qwane Biosciences SA, Lausanne, Switzerland]. They feature two symmetrical microfluidic chambers (6.2 mm × 1 mm × 0.4 mm) formed by a single cast SU-8 epoxy structure. Each chamber has a perforated comb (50 µm) to maintain cells on the recording electrodes. On the input side of the comb are 26 30 µm diameter electrodes (seen in Fig. 3.1D) with 150 µm spacing. On the output side of the comb, 3 control [3] electrodes and 1 bigger reference electrode (1 mm × 0.5 mm) amount to a total of 30 Platinum-black electrodes per chamber. Recording electrodes have an announced impedance of $20 - 30$ kΩ at 1 kHz. The two chambers are closed by a cast PDMS block [91] in which two holes (diameter 800 µm) give access to each chamber and connection to a microfluidic pump.

PEDOT-CNT MEAs

PEDOT (Poly(3 4-ethylenedioxythiophene)) is a conducting polymer widely used as a coating material on recording electrodes for its electrical properties and its good biocompatibility. It has been reported to improve electric properties of electrodes (reduced impedance) and favor charge transfer properties of the electrolyte-electrolyte interface. This is partly due to its porous structure, that increases the surface area of contact with electrolyte solution and enhances the transport of ions [92, 93]. Its low mechanical stability can be compensated by CNTs (carbon nanotubess), which also showed favourable biocompatibility properties [94, 95]

2. This is also feasable in well culture chambers, but the topography of these microfluidic-specific chambers favors medium replacement and facilitates fluidic connections.
3. as in they should not be covered by cells and provide flat readings

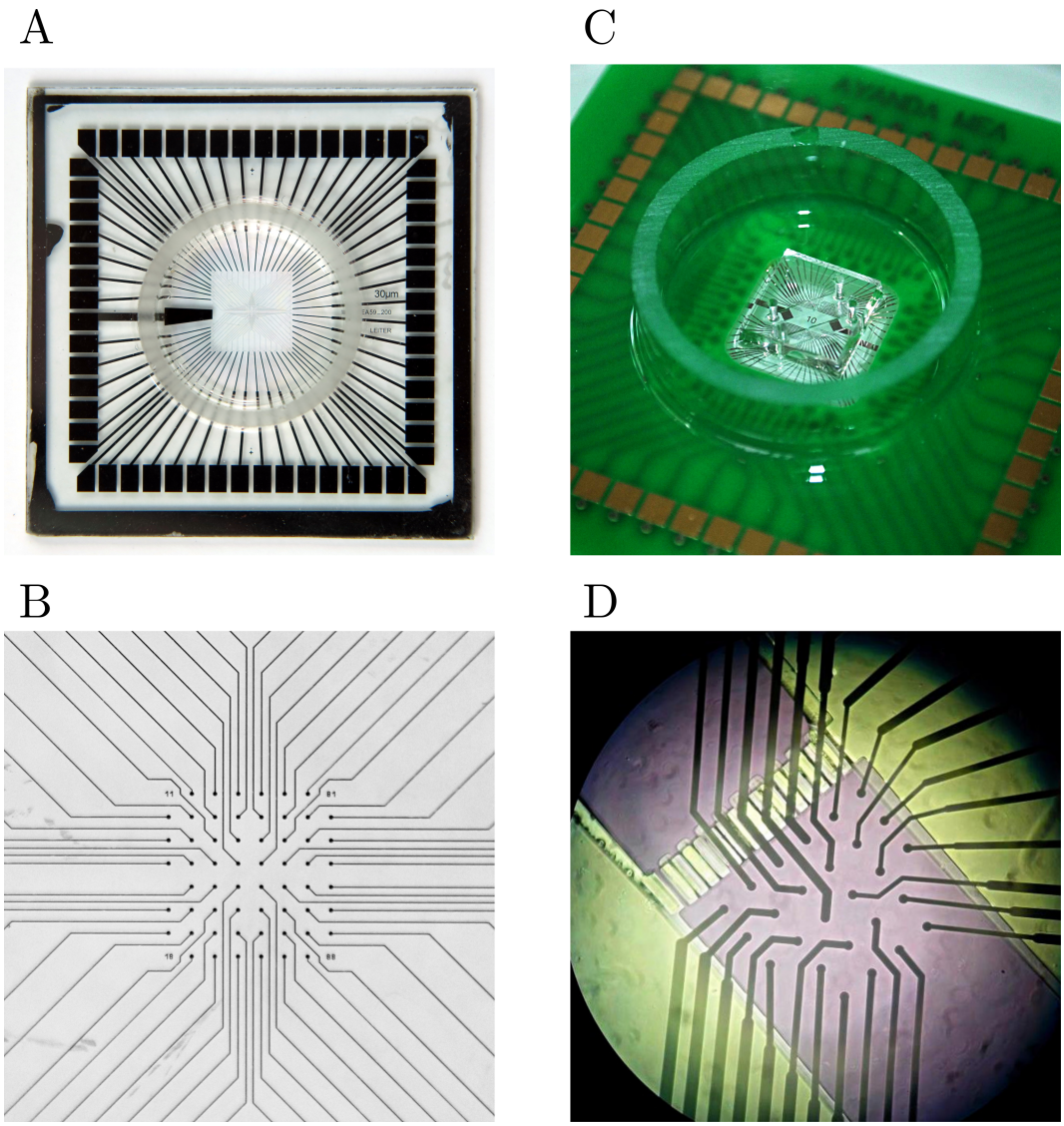

Figure 3.1 – Two planar MEAs used in ISLET-CHIP . **A**: A MCS 60MEA200/30iR-Ti-gr MEA . **B**: Microscope photograph of the 60MEA200/30iR-Ti-gr MEA . **C**: A custom 60-electrode MEA by Qwane with a PDMS microfluidic mask. **D**: Microscope photograph of the Qwane μ-MEA

and better electrochemical sensing [96, 97]. This composite PEDOT-CNT (PEDOT-carbon nanotubes) coating is used by MCS on MEAs identical to the gold standard MEAs , except their electrodes are PEDOT-CNT-plated Gold (Au) instead of Titanium Nitride (TiN), with a subsequent announced impedance of <20 kΩ at 1 kHz. These MEAs (60PedotMEA200/30iR-Au-gr) were used to improve Action Potential (AP) visibility: early experiments showed that PEDOT-CNT-coated electrodes improved AP visibility and generally achieved higher Signal-to-Noise Ratios (SNRs) in their frequency range, to the detriment of Slow Potentials (SPs) (unpublished data, corroborated by [98]). This trade-off was however acceptable, due to the robustness of SPs, contrasting with that of APs .

Acquisition material and electronics

When the *Delivrer* project first started in 2007, planar MEAs had never been used to measure activity on pancreatic islets and β cells . Although it has been known for decades that these cells had measurable electrical activities, only patch-clamp measurements had been conducted. The techniques and tools used at the time were that of neuroscience, that had been well established. Using these materials and methods for pancreatic cells helped set a reference as to which activity patterns should be detected, especially on planar MEAs, where features such as APs are harder to detect.

Early experiments exclusively used equipment from MCS, as described in 2.2.2:

— MEA1060-Inv preamplifier with a 0.1 Hz – 3 kHz bandwidth and a gain of 1200.
— USB-ME64 60-channel, 10 kHz, 16-bit
— STC01 thermal controller acquisition board
— PS40W power supply

These permitted 60-channel recording at 10 kHz directly on a computer and post-processing with its dedicated software MC_Rack. The setup could detect APs as intended, but also SPs by adapting AP detection parameters to lower frequencies.

However, using neuron-specific techniques and equipment on pancreatic cells has its limits. Signal processing provides limited flexibility to adapt to the specificities of the cells, and closed-loop capabilities are limited to punctual electrical stimuli, unusable on β cells. As described in the previous chapter, Multimed was the solution to these issues by design. It was inserted in the acquisition chain (Fig. 2.12), between the preamaplifers and the MCS acquisition board. The two Data Acquisition (DAQ) devices were used in parallel to store validation data, and did not deteriorate signal quality and had no noticeable effect on one another.

3.1.2 Biological materials

Cell cultures

Murine pancreatic islets were obtained by enzymatic digestion and handpicking, and were cultured by CBMN directly on MEAs as described in [43, 99]: 100-200 islets per mouse were cultured for 2-7 days on MEAs as whole islets or partially dissociated islet cell clusters (>10 cells per cluster).

Human islets were provided by the GRAGIL [4]. They were isolated from cadaveric non-diabetic donors at the Cell Isolation and Transplantation Centre (Geneva University Hospital) [100] or the Laboratory of Cell therapy for Diabetes (LCTD, Montpellier University Hospital, France). After transport, the human islets were maintained in suspension for recovery (25 °C, 95% O_2, >90% relative humidity) in CMRL-1066 medium (Invitrogen, Carlsbad, CA, USA) containing 5.6 mmol/l glucose, supplemented with FBS (10% vol./vol.; Eurobio, Courtaboeuf, France), penicillin-streptomycin (1% vol./vol.; Invitrogen, Saint Aubin, France) and L-glutamine (1% vol./vol.; Invitrogen). The islets were subsequently cultured on MEAs in this medium for 5–13 days using the same procedure as for mouse islets. Culture media

4. The GRAGIL (Geneva-Rhine-Rhone-Alps Group for the transplantion of Islets of Langerhans) consortium is a network of several transplantation centres from France (Grenoble, Lyon) and Switzerland (Geneva University Hospital) that act as a central islet production structure.

were renewed every 2–3 days. The use of human islets was approved by the ethics committee of Geneva University Hospital (Geneva, Switzerland).

Within the context of the STABILOT study, a sample of around 1000 Islet Equivalents (IEQs) were retrieved from islet preparations accepted for transplantation (Fig. 3.2). Their quality was then evaluated using Multimed. The STABILOT study proposes to prospectively assess the economic impact of islet transplantation by analysing the evolution of the patients' insulin-independence and comparing it to the current best medical treatment (SAP, or sensor-augmented pump) [101].

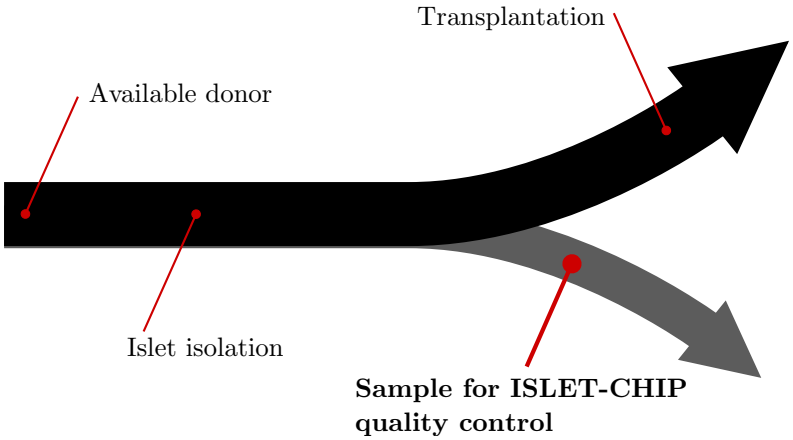

Figure 3.2 – Human islets are sampled from preparations destined for transplantation. After isolation, an average of 1000 IEQ are reserved for quality control with ISLET-CHIP. For scale, up to 11000 IEQ/kg are required for a transplantation.

Biological markers

All chemicals were obtained by CBMN from Sigma-Aldrich (St. Louis, MO, USA) except for GLP-1 (BachemBioscience, King of Prussia, PA, USA). Nifedipine and glibenclamide were solubilised in dimethyl sulfoxide, and adrenaline was solubilised in ascorbic acid. Solvents (final concentrations $\leq$0.1%, vol./vol.) were without effect on SPs and APs .

3.1.3 Routine setups and protocols

Static experiments on classic MEAs Static experiments refer to the study of cell behaviour in a stationary state. Between two conditions, the preparation medium is changed entirely using pipettes and cell activity is only measured after 5 or 10 minutes of waiting for the culture to settle. It is simple to set up as it requires no equipment other than the recording equipment and the usual glassware but has the disadvantage of losing 5 to 10 minutes of activity after each medium change.

Perfused experiments on classic MEAs Perfused experiments were put in place to reduce disturbance to the cells when changing medium. Instead of pipetting the liquid, a two-channel peristaltic pump drained it with one channel while the other refilled it with the new medium.

In both cases, the main drawback of the technique is the risk of detaching cells from the electrodes. The risk is obvious when pipetting the liquid, and still exists with perfused experiments, where pipe placement is manual and risks scrubbing cells away. Plus, these techniques are not applicable in a context other than bench experiments: a different way to condition cells is therefore proposed to permit an embedded device approach.

Perfused μ-MEAs: The complete biosensor setup μ-MEAs were designed by CBMN and manufactured by Qwane Biosciences to improve conditions of perfused experiments and investigate embeddable solutions. They supply easier pump connections and a more robust culture chamber in which cell adhesion is improved even with fluid displacement. Only one pump channel [5] is needed to use this device: different solutions are pumped inside the microfluidic channel that simply spills out the excess liquid. The measuring device including this MEA constitutes a prototype of an entire biosensor capable of measuring glucose concentrations in a flowing medium. With fluidic switches, this permits continuous variations in the medium and analyses of the activity that ensues.

3.1.4 Analysis methods

Online measurements

Data analysed and recorded using Multimed will be referred to as "online measurements" or "real-time measurements" [6]. These data were generated without post-processing, and only with the processing electronics described in the previous chapter (2).

Offline measurements

Post-processing will be referred to as "offline measurements" [7]. These were performed in MATLAB using custom functions, that are either parts of Multimed's algorithms [8], optimized for vector computation, or external tools, not included in Multimed's function library.

Event correlation

Correlation between events detected on couples of electrodes was computed following a method inspired from [102], originally used to compute synchronization between trains of neuron spikes. This method, yielding time-dependent correlation, consists in convoluting each train of events with a Gaussian function and computing the cross-correlation between the resulting waveforms. The Gaussian functions spread and weight each event in time into a continuous waveform, permitting the computation of continuous correlation from discrete events. The standard deviation of the Gaussians (expressed in seconds) may be adjusted to control the spreading of each event, hence the timescale of the measurement. In this instance, the standard deviation was set at 1 s (to match the order of magnitude of SP frequency). Cross-correlation measurements were performed in a 60 s moving window, by steps of 2 s. See appendix G for an illustration of this method.

Statistics

Statistics results are presented as means and SEM (Standard Error of the Mean) of n electrodes. One-way ANOVA (Analysis Of Variance) with Bonferoni post hoc correction is used to compare different conditions in a single group. Two-way ANOVA with Bonferoni post hoc correction was used for comparisons between more than two groups. P values < 0.05 are considered statistically significant.

3.2 Glucose dose-response

To characterize the biosensor, its response to glucose was first measured. These experiments helped determine whether it could indeed be substituted for a classic glucose sensor. The studied outputs include AP frequency, SP frequency, SP frequency reversibility, all measured in static experiments. Dynamic responses are characterized in section 3.4.2.

5. as opposed to perfused experiments in a culture well that require an inlet and outlet pump
6. and more generally recordings, processing, etc. will be referred to as "online" or "real-time".
7. and "offline" recordings, processing, etc.
8. see sections 2.5.1 through 2.5.9 for algorithmic description

3.2.1 Action Potential frequency dependence

Detection of APs in β cells with intracellular techniques has extensively been done in the past [38, 103, 104]. Activated by glucose, they appear in a typical burst pattern [38, 105, 106] which, like those of neurons, can be measured with extracellular techniques. Figure 3.3 shows the difference in AP activity between low (G3) and post-prandial (G8.2) glucose concentrations. As expected, APs fire at G8.2, in burst-like patterns (Fig. 3.3A). In the zoomed portion of Fig. 3.3A, they appear to be condensed in the falling phase of SPs, which is confirmed in section 3.4.1.

The low SNR of AP signal makes it very difficult to detect APs with 100% accuracy, and in many cases even makes it difficult to visually assert their presence in the recorded waveforms. The wavelet transform method used in the system [70] was a first tentative to achieve reliable AP detection in extracellular recordings of β cells. Additional efforts were made on electrode design to favour it: PEDOT-CNT- and PEDOT-PSS-coated electrodes were investigated and tended to improve AP visibility and detection rate (unpublished data, corroborated by [98]). APs were nonetheless mostly disregarded (and consequently Fraction Of Plateau Phase (FOPP)) to favour SPs, which are easier to detect, more robust, and show similar tendencies.

3.2.2 Slow-Potential frequency dependence

While APs are signatures that had been characterized before in intra-cellular recordings, electrical measurement of SPs is unique to extra-cellular recording and has only been characterized by the Cell Biology and Biosensors team at CBMN . Early experiments showed that these oscillatory signatures are modulated by glucose (Fig. 3.4a, 3.5), marked by the near-absence of activity in low glucose concentrations ($<$5 mmol/l) and an increase in frequency with raising glucose levels (Fig. 3.5b).

3.2.3 Asymmetry in glucose dose-responses

Glucose dose-responses were characterized both in increasing and decreasing glucose concentrations, and it was noted that islet response was not symmetrical: for an equal glucose concentration, islet activity was higher with increasing steps of glucose than decreasing steps. Figures 3.6A-B show this tendency, illustrated by SP frequency. The measured hysteresis suggests that an endogenous algorithm is naturally present in islets to protect against hypoglycaemia: a drop in sugar levels would cause a quick extinction of islet activity, stopping insulin secretion and preventing from further lowering blood glucose.

3.3 Hormone dose-response

Within a biosensor approach, in most cases, the biological part of the device is sensitive to multiple substances which may be considered – and relevant – depending on the biosensor application. While the primary interest in using pancreatic islets as a biosensor was glucose evaluation, their sensitivity extends to various hormones and substances present in the human body. characterization of islet response to these markers not only strengthens the pre-transplant quality control proposed by ISLET-CHIP, but also brings us closer to a hormone-sensitive artificial pancreas: hormonal signals translate the general body status and strongly influence insulin secretion depending on activity. Secretion is also naturally modulated through hormones (like incretins) during the circadian cycle [32].

3.3.1 Adrenaline

Adrenaline (epinephrine) is a hormone produced by the adrenal glands in situations of stress or physical activity, and playing an important role in acute stress response. Aside from its most-known effects of increasing heart output and blood flow, it also increases blood sugar

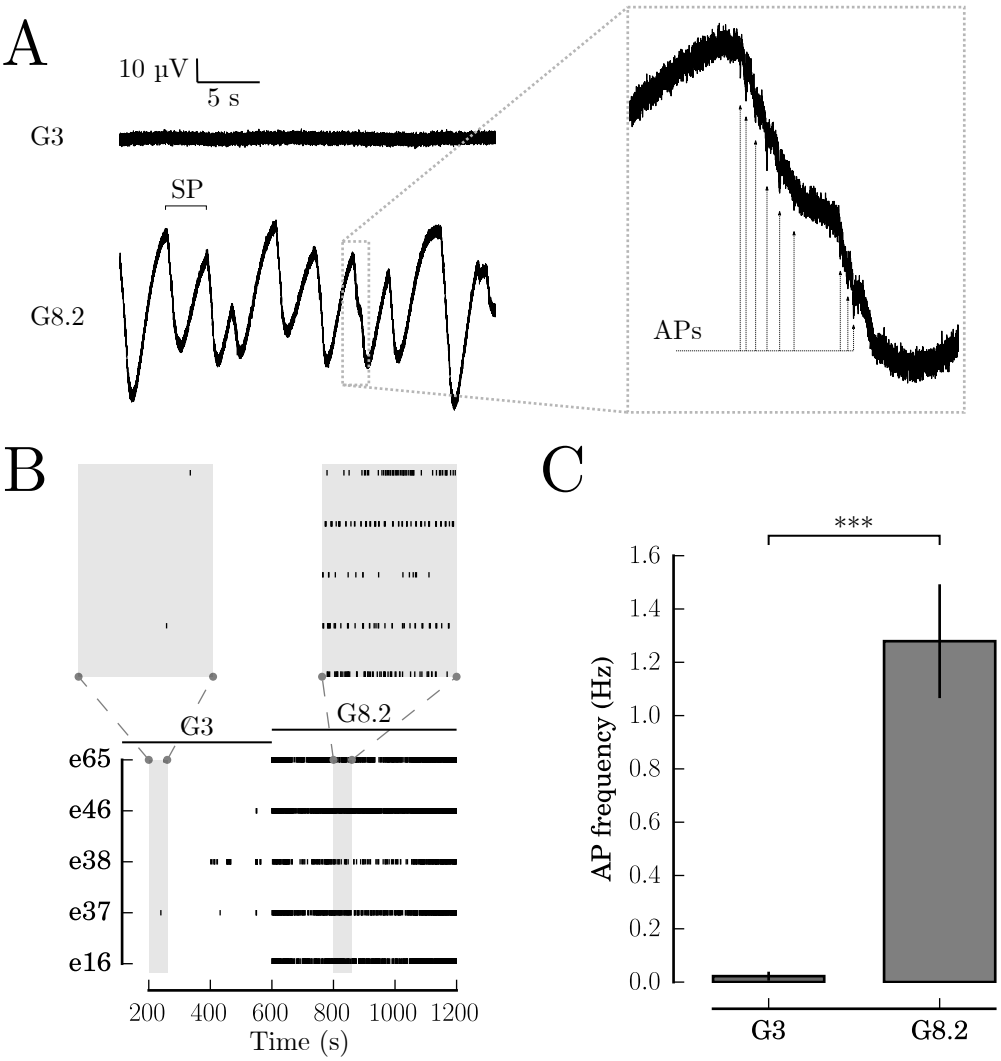

Figure 3.3 – APs activate at post-prandial glucose levels in mouse islets. **A**: Difference in electrical activity between G3 and G8.2. Cell activity at G8.2 exhibits SPs as well as APs, as shown in the zoomed portion. **B**: AP frequency measurements, averaged from real-time measurements on $n = 5$ electrodes. $^{***}p<0.001$. **C**: Raster plot of real-time AP detections on five active electrodes during G3 and G8.2 conditions.

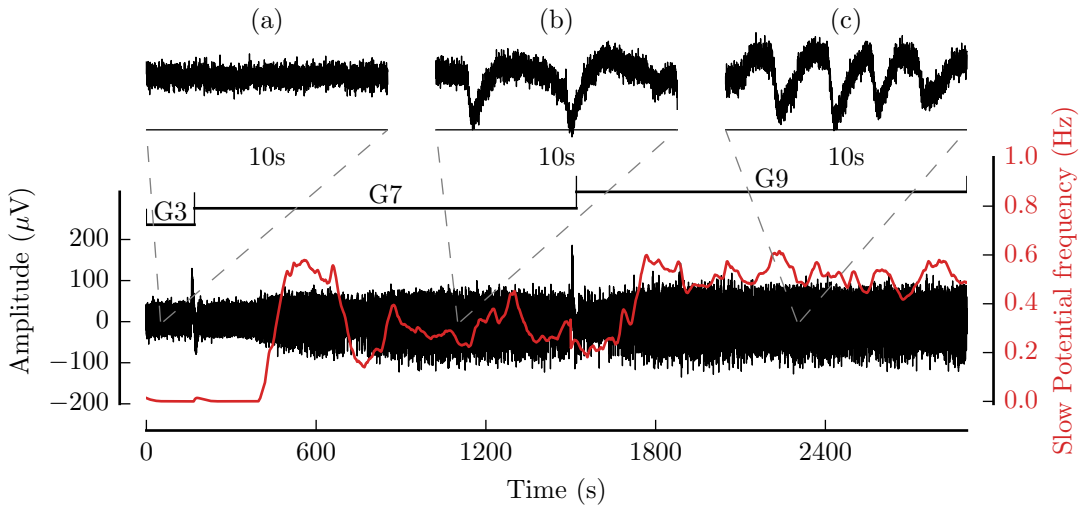

Figure 3.4 – Electrical activity recorded on mouse islets and real-time SP frequency measurement, showing SPs modulated by glucose concentration. No SP can be seen at G3 (a), while some appear at G7 (b) and increase frequency at G9 (c). Signals were recorded on μ-MEAs and processing (filtering, SP detection, and frequency measurement) was performed online with Multimed.

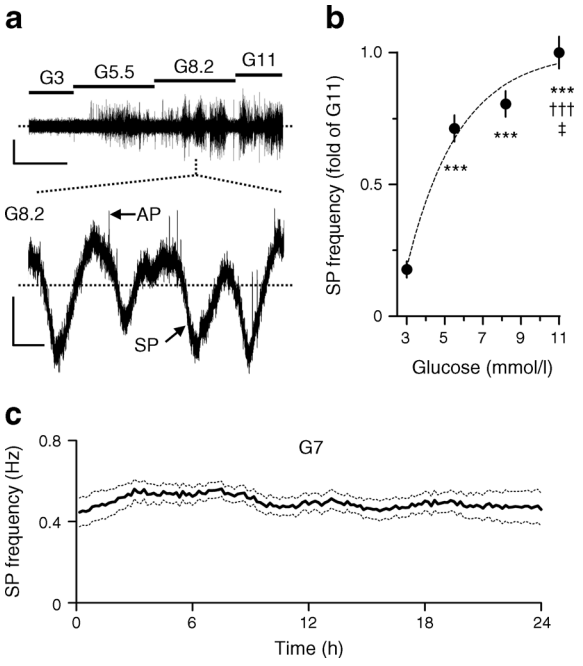

Figure 3.5 – Human islets show glucose-dependent SPs. **(a)** Representative electrical response of human islet cells to increasing glucose concentrations (upper trace).Higher temporal resolution shows the presence of both APs and SPs at 8.2 mmol/l glucose (G8.2, lower trace). Scale bars: horizontal 10 min (upper trace), 0.5 s (lower trace); vertical 50 µV (upper trace), 25 µV (lower trace). **(b)** Glucose concentration-dependent frequencies of SPs in human islet cells (offline analysis with MC_Rack). Statistics on data pooled from three donors: n=65; $^{***}p<0.001$ compared with the value obtained in the presence of 3 mmol/l glucose (G3) or $^{\dagger\dagger\dagger}p<0.001$ compared with the value obtained in the presence of 5.5 mmol/l glucose (G5.5), $^{\ddagger}p<0.05$ compared with the value obtained in the presence of G8.2 (Bonferroni post hoc test). **(c)** A 24 h long recording shows the stability of SP frequency evoked by 7 mmol/l glucose (G7). Solid line: mean SP frequency, dotted lines: SEM (n=12).
Source: Lebreton, Pirog, Belouah, Bosco, Berney, Meda, Bornat, Catargi, Renaud, Raoux, and Lang [43]

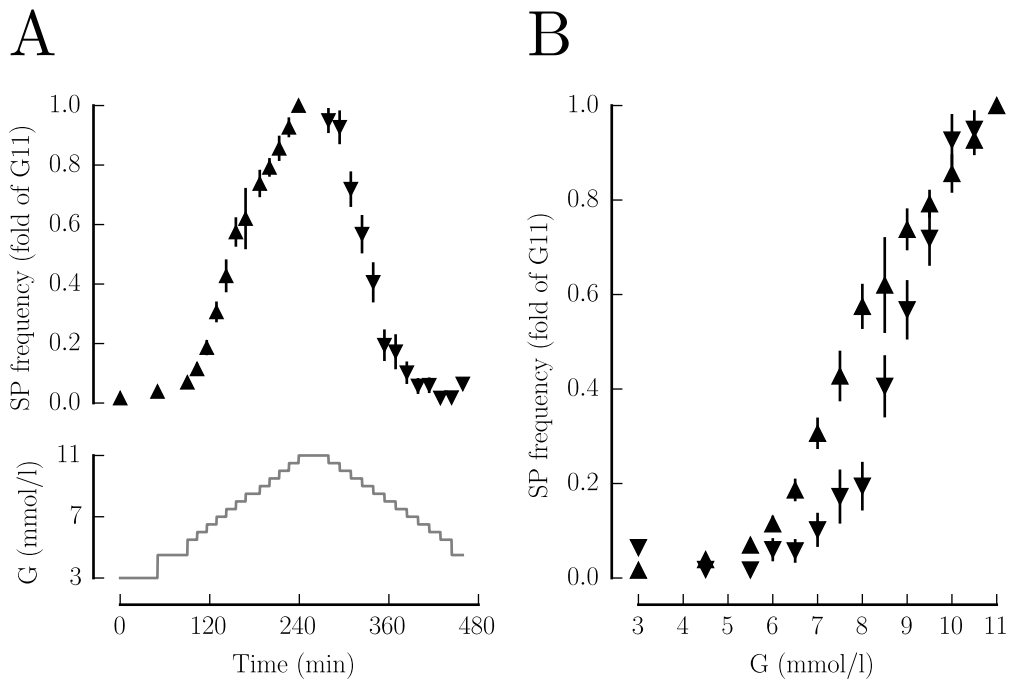

Figure 3.6 – Asymmetrical response of SP frequency to small glucose steps in the physiological range (3-11 mmol/l). Upward triangles (▲) indicate an increase in glucose concentration and downward triangles (▼) indicate a decrease. **A**: Time-dependent variations in SP frequency superimposed with the glucose steps protocol. **B**: Glucose-dependent representation of the same experiment, showing a hysteretic response with a quicker fall response. Data were sampled from 21 electrodes from two different experiments.

by inhibiting insulin release [107]. Physical or emotional stress increases adrenaline, signals a lesser demand in insulin and decreases insulin secretion from islets [33]. More specifically, adrenaline is an inhibitor of β cells and an activator of α cells [108]. Islet measurements on MEAs showed that SPs induced by glucose were reversibly inhibited by adrenaline (Fig. 3.7a). However, adrenaline did not affect the APs , presumably due to α cells being recorded together with β cells on MEA electrodes (Fig. 3.7b).

3.3.2 GLP-1

Glucagon-like peptide-1 (GLP-1) is an intestinal hormone, or incretin, secreted in response to food intake. It increases insulin secretion, increases glucose sensitivity of β cells and decreases glucagon secretion. We recorded islet activity exhibiting GLP-1 dependency (Fig. 3.8): SPs were potentiated by GLP-1, and a 0.5 pmol/l concentration increased their frequency, with a maximal effect at 50 pmol/l (high physiological range).

Of course, other hormones (as well as nutrients and neurotransmitters) would be of interest: as described in section 1.3.2, many molecules (naturally produced by the body) modulate of β cell activity. These can be summed up into three categories: nutrients, hormones, and neurotransmitters.

Many hormone sources in the body influence islet activity and insulin secretion. Because experiments require investment and many iterations to produce relevant data, hormones of interest have been prioritized. Those released by pancreatic islet (glucagon, somatostatine) for instance have not been characterized because they are considered endogenous to the biosensor and are *de facto* transparently taken into account. Other hormones, such as ghreline or leptine have lesser effects and have been ignored to prioritize those with more potency. Incretins for instance are the principal hormone regulation path. Among them, GLP-1 is the most

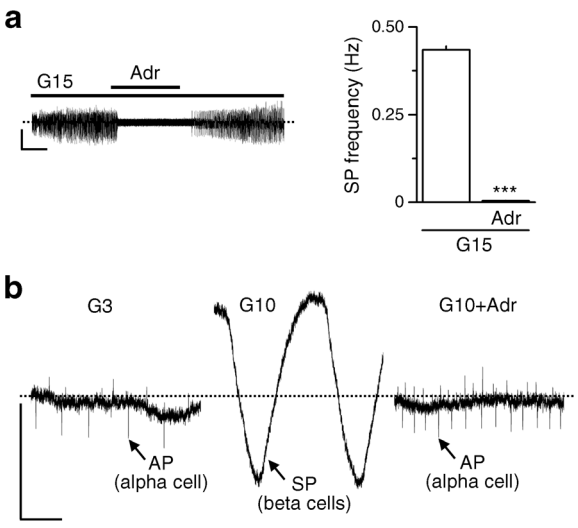

Figure 3.7 – SPs of mouse islet cells are inhibited by Adrenaline. **(a)** Glucose-induced SPs were abolished by 25 µmol/L of nifedipine (Nif) or 5 µmol/L adrenaline (Adr). Representative traces and statistics are shown (n=53–140). $^{***}p<0.001$ (Bonferroni post hoc test). **(b)** α cells and β cells in islets can be recorded by the same electrode. APs are activated by low glucose (G3: 3 mmol/l) or adrenaline (G10+Adr: 10 mmol/l glucose with 5 µmol/l adrenaline) and are attributed to alpha cells. SPs activated by high glucose (G10: 10 mmol/l) and inhibited by adrenaline represent an electrical signature of beta cell activity. **Scale bars:** horizontal (a) 3 min, (b) 0.5 s; vertical 100 µV **Source:** Lebreton, Pirog, Belouah, Bosco, Berney, Meda, Bornat, Catargi, Renaud, Raoux, and Lang [43]

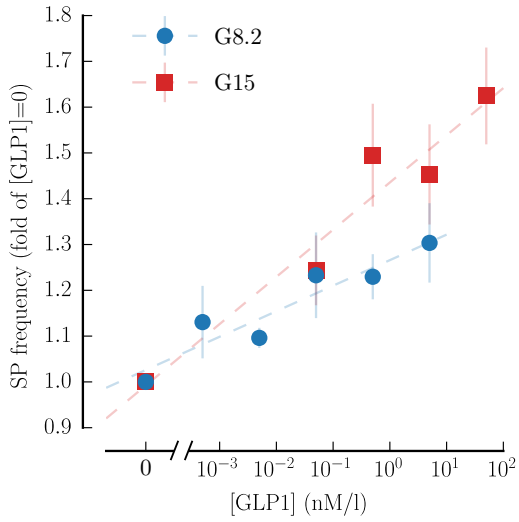

Figure 3.8 – SPs of mouse islets are excited by GLP-1. Tenfold steps of GLP-1 concentration were applied in the physiological range at G8.2 and G15. Measurements are normalized to conditions of G8.2 and G15 respectively.

potent, but GIP also attracts interest and will be characterized in future works. Adrenaline is the principal inhibitor of β cell activity with powerful and fast effects, which is why it was characterized early on. One last hormone of interest is melatonine, which regulate insulin secretion during the circadian cycle. Its effects have been investigated in the past but no change in electrical activity was detected (unpublished data).

Regarding nutrients other than glucose, characterizing effects of lipids and amino-acids would provide valuable information. Again, they need to be prioritized for future characterization.

Neurotransmitters such as acetylcholine and noradrenaline have significant effects on β cell activity. They have however not been characterized because the biosensor in closed-loop configurations will not be innerved and will not be subject to neurotransmitter effects.

3.4 A general analysis of pancreatic signals

Tendencies beyond static dependency were observed during experiments, and were further investigated to either provide supplementary criteria for islet quality, gather information

regarding endogenous islet algorithms, or further refine biosensor models. The observed behaviours notably included synchronization between SPs and APs from the same electrode, synchronization between SPs between neighbouring electrodes, and time-dependent variations of activity during experimental changes. The current section describes the dedicated experiments and processing functions that were developed to study these behaviours.

3.4.1 Correlation between Action Potentials and Slow Potentials

As mentioned in section 3.2.1, it appeared that APs were generally fired during the falling phase of SPs, as supported by Fig. 3.9A that shows clearly discernable APs and SPs on an unprocessed signal recorded on a human islet. Data from four different experiments, selected for the presence of both signatures, were used to investigate this phenomenon. APs and SPs were isolated offline using Stationary Wavelet Transform (SWT) filtering and zero-phase filtering respectively, ensuring no time displacement of the events. Each AP was attributed an angular position on its associated SP , ranging from 0°at SP minimum, through 180°at SP maximum and to 360°back to SP minimum. The results are shown in Fig. 3.9B, indicating that APs are indeed mainly present on the falling phase of SPs: 70.47% of all detected APs were concentrated in the falling phase $(180 - 360°)$ and 48.27% in the third quadrant alone $(180 - 270°)$.

One hypothesis would explain this phenomenon by drawing a parallel with Local Field Potentials (LFPs), that are generated in neuron cultures by a complex summation of many synchronized ionic fluxes. Indeed, SPs and APs are observed simultaneously at elevated glucose levels only if the measured β cells are coupled via connexins [43]. By contrast, only APs are recorded at excitatory glucose concentrations when coupling is disrupted, suggesting that SPs reflect the electrical activity and coupling of β cells. SPs could therefore result from the summation of synchronized ionic fluxes of coupled groups of spiking β cells.

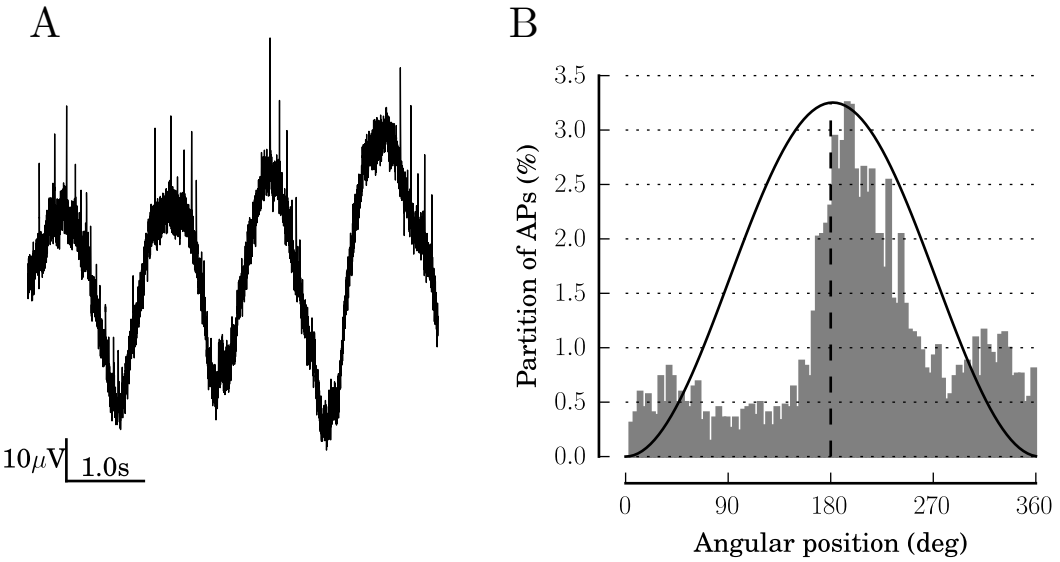

Figure 3.9 – Tendency of APs recorded on mouse islets to fire during the falling phase of SPs. **A**: Signal recorded on human islets, showing a tendency of APs to fire during the falling phase of SPs . **B**: Temporal correlation between APs and SPs showing that APs are mainly present during the falling phase of SPs (four independent experiments). The black curve represents the position on an SP at a given angular position.

3.4.2 Biphasic activity

Continuous recordings were conducted to establish the transient response of cells subjected to a physiological step of glucose. Murine islets were cultured on MEAs with PEDOT:PSS-coated electrodes, and maintained at 3 mmol/l of glucose, then an excitatory solution was perfused in the culture chamber. The used solutions were three glucose solutions at 5.5 mmol/l (G5.5, at the activation threshold), 6 mmol/l (G6, immediately above the activation threshold), and 8.2 mmol/l (G8.2, close to post-prandial sugar levels). Figure 3.10 shows a two-phase response in SP frequency, SP amplitude, (Fig. 3.10A,C-D) and AP frequency (Fig. 3.10B), much like biphasic insulin secretion patterns [109–112]. During 1st phase, which lasted on average 8.40 ± 1.18 min (n=7), SPs had high frequency and low amplitude, and APs had high frequency. After a drop of global activity (Nadir, (N)), electrical activity entered a 2nd phase, SP and AP frequencies were reduced, and SP amplitude was increased. After a moment of sustained activity, APs and SPs in the 2nd phase become pulsatile, with regular cycles in frequency and amplitude (period 3.28 ± 0.41 min).

A second set of experiments was conducted to investigate the effects of the glucose step size. Instead of a unique G3→G8.2 step, electrical activity was measured with G3→G5.5, G3→G6, and G3→G8.2 steps. Biphasic responses were observed in all three cases, with a scaling effect causing signal amplitude and event frequency to decrease with glucose (Fig. 3.10B-D).

These experiments show that and electric two-phase activation pattern exists at physiological glucose level, similar to documented biphasic insulin secretion profiles [109–112], and that it can be recorded in real-time using our processing electronics.

3.4.3 Correlation between Slow Potentials

Changes in dynamics between 1st and 2nd phase raise questions as to what mechanisms are involved. The slow increase in amplitude and the first spike in frequency suggest that activity between islets may be desynchronized in the first place, and progressively synchronize. To verify this hypothesis, correlation between islets was investigated using SP detection, representative of islet activity (as opposed to single cell activity). Time-dependent correlation was quantified using an event-correlation method used in [102], for neuron APs and applied to SP events (see section 3.1.4 and appendix G). Correlation ranges between +1 (synchronized events) and −1 (out-of-phase events). A null correlation (0) indicates uncorrelated events. Electrical signals were recorded using HD-MEAs, to visualize multisite activity from single islets. Correlation between couples of electrodes from the same islet (intra-islet) and from separate islets (inter-islets) (see Fig. 3.11A) was computed offline over 60 s every 2 s and between all electrode couples for the total duration of the experiment. As can be seen in Fig. 3.11A, activity recorded on separate electrodes from the same islet (islet 1) is similar, whereas activity recorded on a different islet is different. A quantification of this observation is given in Fig. 3.11B. It represents correlation matrices taken at different instants in time and shows that inter-islet correlation is quasi-null at G8.2 for all couples (Fig. 3.11B) and oscillates erratically around 0 (Fig. 3.11C). More importantly, Figs. 3.11B-D show the evolution of event correlation between the 1st and 2nd phase. It is moderate in 1st phase (0.25 ± 0.07) and significantly higher in 2nd phase (0.64 ± 0.06) (Fig. 3.11D).

This suggests that internal behaviour of pancreatic islets evolve during stimuli: a functional model of islet activity is given in Fig. 3.11E, proposing that small groups of cells (functional units) first activate independently causing the faster 1st phase, then all units synchronize and cause the slower, bigger, syncytial behaviour of the 2nd phase.

3.5 Functional experiments

With the biosensor extensively characterized, experiments have been conducted to verify its function as both a front-end sensor for insulin demand and a tool for determining islet quality. A blind experiment proves that islet activity is sufficiently changing to discern different glucose concentrations (3.5.1), and a full islet quality control protocol is described (3.5.2).

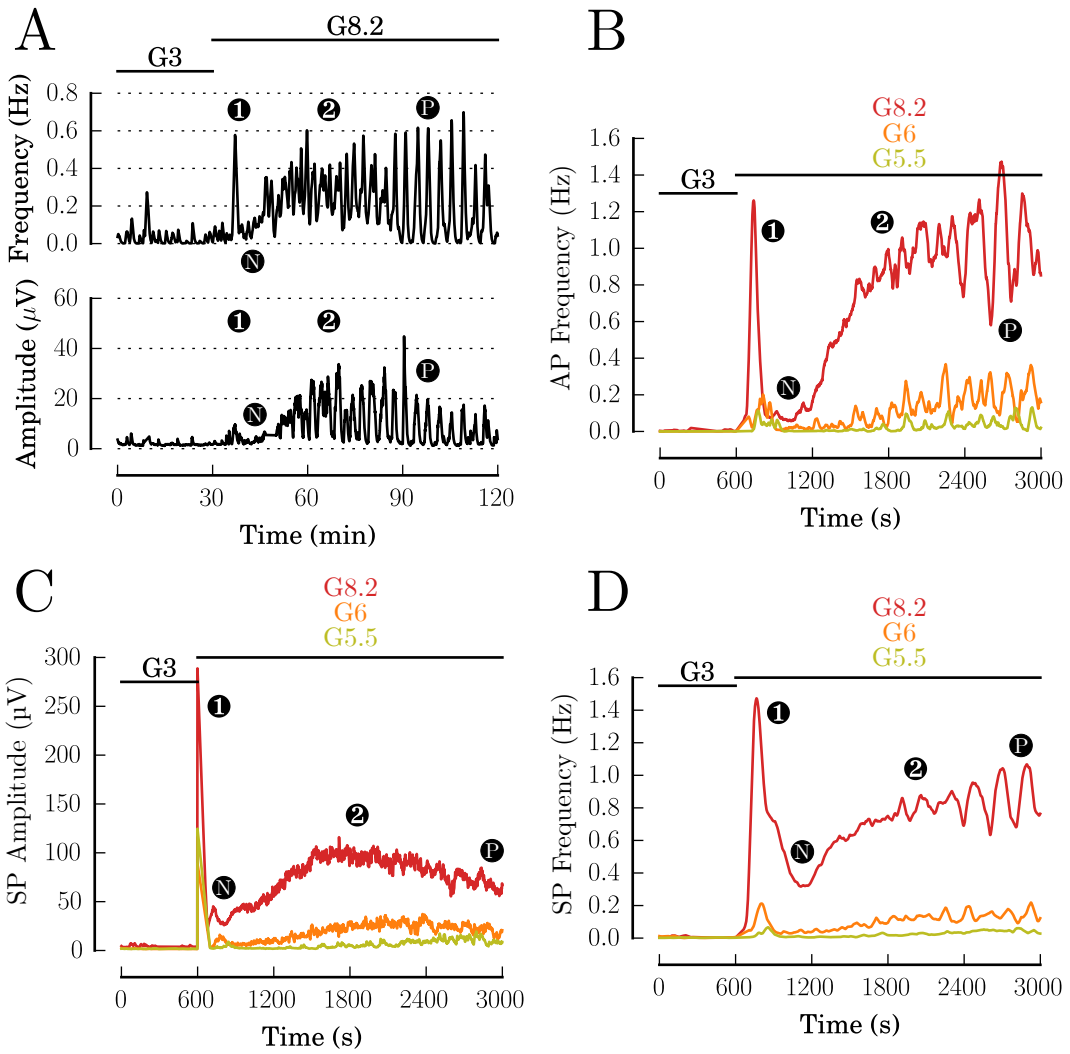

Figure 3.10 – Signals recorded on murine islets show a two-phase activity when stimulated by a glucose step. **A**: SPs have a biphasic response in both frequency and amplitude when stimulated by a glucose step. The first phase (❶) consists of a low-amplitude, fast oscillating burst of SPs , and the second phase consists of high-amplitude, slower, and pulsating SPs . The two phases are separated by a moment of very low activity, the Nadir (N), and the second phase starts by a sustained activity followed by pulsating SPs (P). **B-D**: Differences in AP frequency (**B**), SP amplitude (**C**), and SP frequency (**D**) biphasic response when applying different glucose level steps (G3 to G5.5, G3 to G6, and G3 to G8.2). All signal processing was performed in real-time using Multimed.

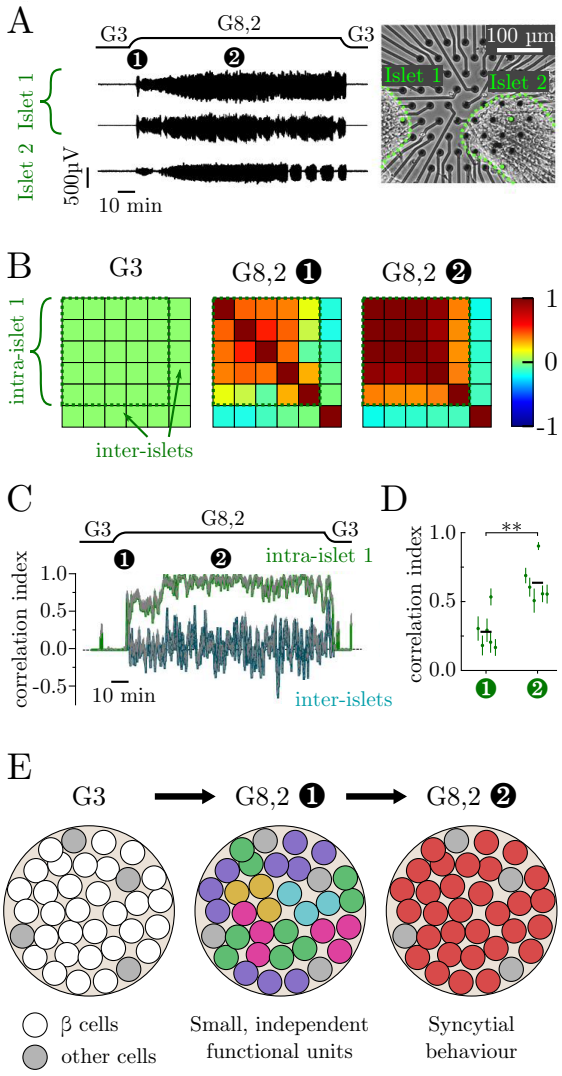

Figure 3.11 – Changes in electrical coupling in pancreatic islets during Glucose-induced biphasic response. **A**: Representative signals (left panel) recorded on three electrodes (right panel, green dots): two were chosen from the same islet (islet 1) and one from an other (islet 2). **B**: Correlation matrices extracted at different times during the experiment presented in **A**. Each square, depending on its x/y coordinates, indicates the correlation between a couple of electrodes. A total of 6 electrodes are shown: 5 are from islet 1 and 1 is from islet 2. The submatrix representing correlation within islet 1 is designated as "intra-islet 1", and the remainder of the matrix, representing correlation between electrodes from islet 1 and islet 2 is designated as "inter-islets". **C**: Evolution of the average correlation index between electrodes from islet 1 (78 couples from intra-islet 1) and between electrodes from both islets (5 randomly chosen couples from inter-islets). **D**: Statistical comparison of intra-islet correlation indexes between first and second phase (indicated by ❶ and ❷ in **A**,**B**, and **C**) on six different islets (36-78 couples of electrodes per islet). Each symbol represents the average ±SEM correlation index within an islet, and black horizontal bars represent the average correlation for all islets. $^{**}p<0.01$. **E**: Functional model of islet activation and biphasic electrical response. Colours indicate groups of activity. With courtesy of Eleonore Bertin, CBMN

3.5.1 Blind experiments

With the observation of noticeable changes in cell activity between conditions, and with the objective of producing a biosensor, we must investigate the ability of the prototype to distinguish between and detect changes in media. Double-blind experiments were therefore conducted to determine whether Multimed could correctly discern and match different glucose concentrations. Four solutions were prepared at 3 mmol/l, 5 mmol/l, 7 mmol/l, and 9 mmol/l. The 3 mmol/l reference[9] solution was labeled "G3" and the three others were shuffled and labelled "S1" ("solution 1"), "S2" ("solution 2"), and "S3" ("solution 3"), with no other indication and only a person exterior to the experiment knowing the correspondence. The experiment started with 300 s of G3, followed by the application of 5 solutions, picked randomly.

The matching of the solutions was based on real-time SP frequency measurements, shown in Fig. 3.12. Each condition has a clearly discernible frequency step, leading to the conclusion that, concentration-wise: Condition 3 < Condition 1 < Condition 2 = Condition 4, i.e. $[S3] < [S1] < [S2]$ (results are summarized in table 3.1). This drew the correct conclusion that $[S1] = 7$ mmol/l, $[S2] = 9$ mmol/l, and $[S3] = 5$ mmol/l.

9. It was necessary to confirm that cells responded to inhibitory conditions.

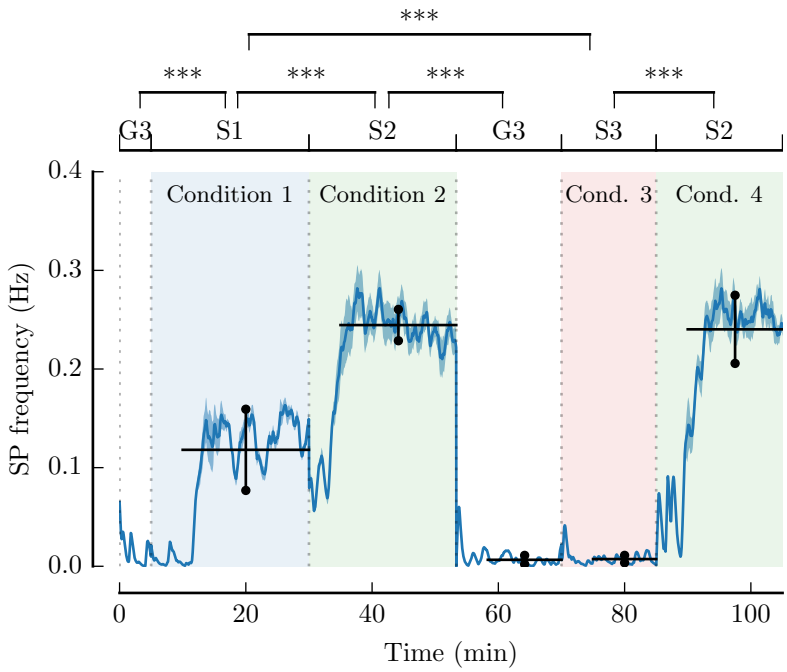

Figure 3.12 – Blind experiment. SP frequency was measured online on a μ-MEA, in response to 3 different unknown glucose concentrations (solutions S1, S2, and S3); only G3 is known by the experimenter. Statistical analysis of slow potentials frequency from the last five minutes of each condition is overlaid. *** $p<0.001$, one-way ANOVA (Bonferoni post-hoc test).

Table 3.1 – Summary of the blind experiment. Each column refers to the conditions shown in Fig. 3.12, with the corresponding solution between parentheses. Average frequency was computed in post based on real-time measurements. Ranking gives the highest to the lowest frequencies measured, hence the highest to the lowest concentrations. "Matched concentration" gives the experimenter's decision as to what solution was used in which condition.

	Condition 1 (S1)	Condition 2 (S2)	Condition 3 (S3)	Condition 4 (S2)
Average frequency (mHz)	118 ± 41.2	245 ± 15.9	7.31 ± 3.77	240 ± 34.6
Ranking	2	1	3	1
Matched concentration	7 mmol/l	9 mmol/l	5 mmol/l	9 mmol/l

This result is proof that the biosensor can discern different glucose concentrations, distributed in both inhibitory and excitatory conditions. It is therefore capable of recognizing the absence or presence of glucose, and recognizing an increase or decrease in glucose levels. Although this blind experiment was conducted for only three separate concentrations, stability of SP frequency for the given conditions suggests that higher glucose level resolutions can be achieved.

3.5.2 Quality control of pancreatic islets

One objective of the ISLET-CHIP project, in the context of islet transplantation, is to provide a quantitative indication of islet response to physiological stimuli to reflect islet preparation quality. A protocol (Fig. 3.13) was defined with our biologist partners to assess various responses and indicate, based on response consistency with inhibitory and excitatory stimuli, levels of preparation quality.

The following paragraphs explain the decision-making and different outcomes of the protocol. For a better understanding, it is important to remember that, among the drugs and molecules used:

— **Glucose (G)** is the main molecule of interest, usually excitatory above levels of 5.5 mmol/l.
— **Adrenaline (Adre)** is a β cell inhibitor and α cell activator.
— **Nifedipine (Nife)**, as a calcium channel blocker, is a strong inhibitor for both β- and α-cells.
— **Glucagon-like peptide-1 (GLP-1)** is a β cell activator, as it increases their glucose sensitivity.
— **Glibenclamide (Glib)** is a strong β cell activator, indirectly increasing intracellular calcium.

Following the decision tree of the protocol, a total of 10 scenarios may occur. A description of each scenario is given, preceded by its unique identifier referring to the different +/- paths taken in Fig. 3.13 and starting at G1 (e.g. **(+++)** refers to the leftmost path "G1, Adre 5 μM, Nife 25 μM"):

1. **(+ + +)** : Detection of activity at G1, despite the addition of Adrenaline and Nifedipine, indicates that there is an electrical problem in the setup, because all physiological, calcium-driven activity should be extinguished. Nothing can be deduced about the culture, electrical problems must be fixed (generally by physically grounding faulty electrodes) and the experiment must be re-run.
2. **(+ + −)** : Detection of activity at G1, maintained by Adrenaline but extinguished by Nifedipine indicates that the observed activity results from α cells . Islets are of poor quality, as activity mainly consists of α cell activity.
3. **(+ −)** : Detection of activity at G1 extinguished by Adrenaline suggests that activity results from β cells , and not from α cells , which should be activated by Adrenaline. Islets are of moderate activity, as it suggests β cell hypersensitivity to glucose.
4. **(− + + +)** : The preparation is inactive at low glucose (G1), activates at high glucose (G15), shows physiological response to dose-responses and hormones (G1, G3, G5.5, G8.2, G11, G11+GLP1, G11+GLP1+Adre), and has biphasic response to a G1-G7 step. Islets are of excellent quality.
5. **(− + + −)** : The preparation is inactive at low glucose (G1), activates at high glucose (G15), shows physiological response to dose-responses and hormones (G1, G3, G5.5, G8.2, G11, G11+GLP1, G11+GLP1+Adre), but has no biphasic response. Islets are nevertheless of very good quality.
6. **(− + −)** : The preparation is inactive at low glucose (G1), activates at high glucose (G15), and shows poor or partial response to dose-responses and hormones (G1, G3, G5.5, G8.2, G11, G11+GLP1, G11+GLP1+Adre). Islets have bad sensitivity but are nevertheless responsive to stimuli: they are therefore of good quality.

7. $(- - + +)$: The preparation is inactive at low glucose (G1), remains inactive at high glucose (G15), but activates in presence of GLP-1 and remains active with Adrenaline. Islets can neither reliably indicate elevated sugar levels (need for insulin) nor detect Adrenaline (need for glucagon): they are of poor quality.
8. $(- - + -)$: The preparation is inactive at low glucose (G1), remains inactive at high glucose (G15), but activates in presence of GLP-1 and inactivates with Adrenaline. Islets have only a normal response with GLP-1 raising their sensitivity. They have poor glucose sensitivity in a physiological medium and are therefore of moderate quality.
9. $(- - - +)$: The preparation can only be activated by Glibenclamide (inactive with G1, G15, and G15+GLP-1). Islets are only sensitive to antidiabetic drugs (sulphonylureas) and are of poor quality.
10. $(- - - -)$: The preparation can never be activated (inactive with G1, G15, G15+GLP-1, and G15+GLP-1+Glib). No detectable activity occurs, the islets are of very poor quality.

The quality control protocol was thoroughly applied to every human islet sample sent by partner clinics. Initially experiments were conducted at CBMN, and most of them were unfruitful, as the measured quality was far inferior to that announced by clinics. This led to believe that transportation of islets between distant sites (from the harvesting centre in Geneva or Montpellier to the analysis site in Bordeaux) might be a source for cell stress and deterioration. To improve experimental conditions, a series of experiments was programmed to measure, on-site, freshly harvested pancreatic islets (Days In Vitro (DIV) 4) intended for transplant. Measurements were conducted at the Geneva University Hospital, where islets are harvested from human donors. The protocol was also revised after the experimental session reported in Fig. 3.14 and is described in Appendix H

The presented experiment (Fig. 3.14) was conducted on whole human islets. Activation of the islets was verified with a G1-G15 step, revealing good glucose sensitivity and a low electrode coverage (5% or 3/60 electrodes). After this successful experiment, a dose-response was conducted with small steps of glucose between G1 and G11, ending with the administration of 50 pM of GLP-1. The culture responded with step increments of SP frequency, coherent with the protocol. Note the long extinction delay in condition G1. Finally, a dynamic recording of a G1-G7 step was conducted, showing a pronounced two-phase activity in SP frequency. The path followed by this protocol according to notations in Fig. 3.13is $(- + + -)$, indicating islets of very good quality.

The results of quality control protocols will be included in the STABILOT protocol to study the correlation between (a) islet quality measured with Multimed, (b) islet secretion tests, (c) visual assessment of islet preparation purity, and (d) long-term viability of the transplanted pancreas. Islet quality measurements had no influence on the final decision to conduct the transplant.

3.6 Discussion

3.6.1 Introducing Glucose-equivalents

Measurements showed (Sec. 3.3) that pancreatic islets were not only sensitive to glucose, but also to hormones naturally present in the human body. These hormones have a significant role in physiological glucose regulation, and yet self-monitoring devices used for insulin therapy only measure glucose levels. Of course, charts exist, that indicate recommended insulin doses not only depending on sugar intake, but also fat intake and exercise. Nevertheless no process to date has entirely automated such decision-making and even smart insulin pumps rely on user input.

A biosensor such as the one presented may permit such automation because of its multi-hormone sensitivity. It could constitute a richer front-end self-monitoring device. However, mainstream insulin delivery systems and charts provide glucose-insulin correspondence rules, that are not immediately compatible with the multiparametric output of islet activity. To

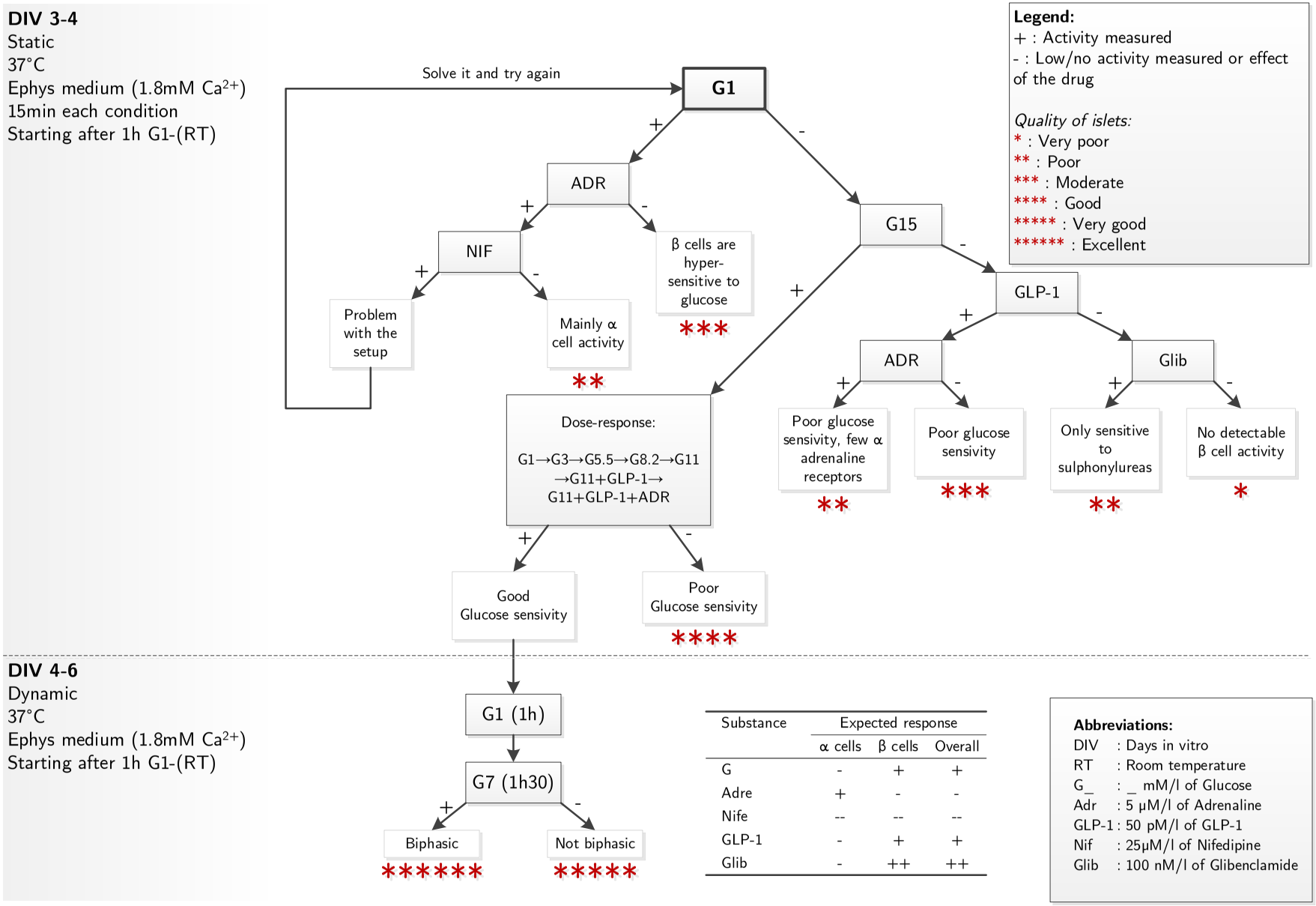

Figure 3.13 – Islet quality control protocol.

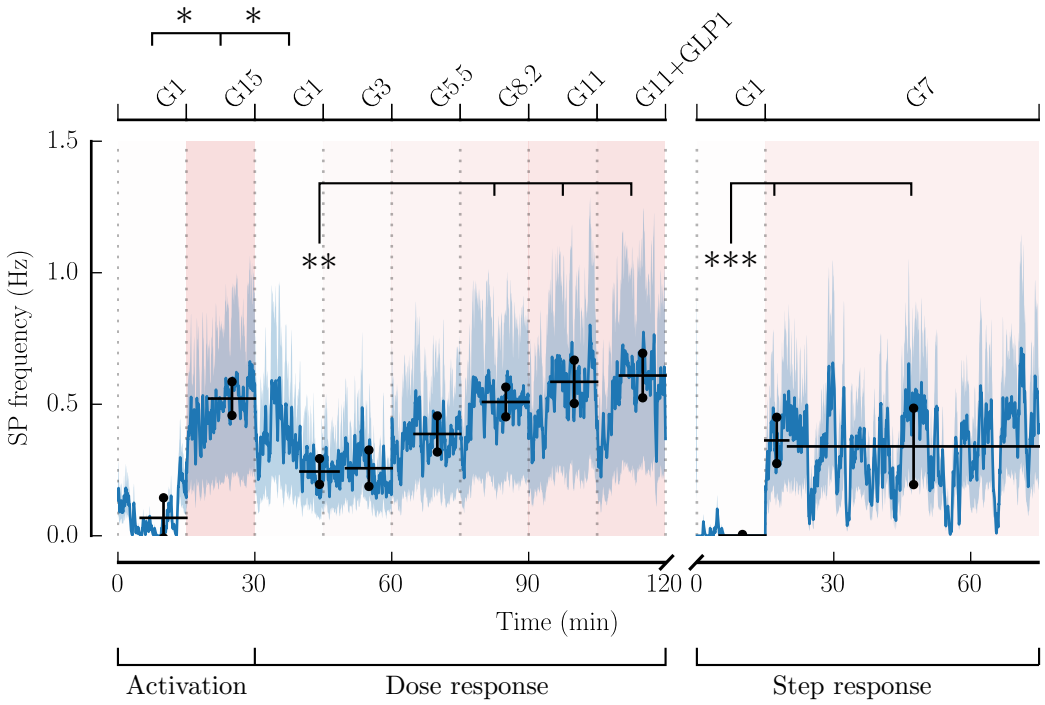

Figure 3.14 – SP frequency measured in real-time during a quality control experiment on whole human islets at the Geneva University Hospital. Activation of the islets was validated with a G1-G15 step. Then, the dose-response was verified with small steps of glucose between G1 and G11, ending with the administration of 50 pM of GLP-1. Finally, a dynamic recording of a G1-G7 step validated the preparation's biphasic response. Following the notations of the decision tree in Fig. 3.13, this is the $(- + + -)$ path, indicating islets of very good quality. $^{*}p<0.1$, $^{**}p<0.05$, $^{***}p<0.001$.

ensure compatibility, a unique output measurement must be defined. The measurement proposed expresses a glucose concentration at which islet activity, with all other markers at basal concentrations, would be measured in identical proportions as in the actual medium: a solution with glucose and GLP-1 would yield a glucose equivalent higher than the actual glucose concentration, while a solution with glucose and adrenaline would yield a glucose equivalent lower than the actual glucose concentration.

This measurement and the process to produce it are further studied in the next chapter.

3.6.2 Towards a data-based biosensor model

Static and dynamic characterizations of the biosensor were given (sections 3.2.1 through 3.3.2 and 3.4.2) and its ability to discern between glucose concentrations was verified (section 3.5.1). Separate actions of glucose, the potentiating effect of the GLP-1 hormone, the inhibiting effect of adrenaline, as well as biphasic response profiles were measured with sufficient resolution and repeatability to be exploited in a modelling approach.

With the investment required for experiments, especially in closed-loop configurations, models of the biosensor must be established. These will permit *in silico* development of contextual use of the biosensor. First, they will provide a reference for the expected behaviour of the biosensor. Deviation from this reference will yield information regarding islet quality (in the ISLET-CHIP context), drug effects (in a drug screening context), or cell development (in a cell screening or stem cell differentiation context). Second, it will help develop algorithms and controllers for closed-loop glucose regulation. Indeed, sensitivity to hormones makes this biosensor

unlike existing devices, and it ideally requires its own specific controller. Alongside further experimental characterization, electronic development (conception and proof-of-concepts) will henceforth be assisted by *in silico* tools.

Chapter 4

Towards the artificial pancreas

> *"Evelyn, a dog, having undergone further modification pondered the significance of short-person behavior in pedal-depressed panchromatic resonance and other highly ambient domains... Arf she said."*
>
> - Frank Zappa, *Evelyn, a Modified Dog (One Size Fits All)*

Artificial Pancreas Devices (APDs) have been conceived to automate the process of insulin therapy for persons with Type 1 Diabetes Mellitus (T1D), involving information collection, decision-making, and insulin management. The main sources to take into account in this process are meals (ingestion of sugar, but also all carbohydrates that are later transformed into glucose), physical activity, sleep, and stress.

APDs have three main components: sensors, a controller, and insulin infusion mechanisms. While significant progress towards full automation has been made in all three parts since the first clinical experiments of APDs in 1974 [113], APD sensors are still only sensitive to glucose, limiting automation to meal compensation, and ignoring exercise, sleep, and stress. While biometric variables such as heart rate, can be monitored to collect information regarding patient physiological state, the most reliable sources of information are hormones, secreted in response to activity [114].

The APD component we propose to alter is the sensor, which we substitute for our hybrid biosensor. Taking advantage of β cell response, it is by design sensitive to all variables that affect glycaemia. Because of the endogenous islet algorithms it relies on, it also overlaps with part of the controller with naturally occurring proportionate and derivative responses. This however does not exempt the biosensor from having a dedicated controller, as regulation dynamics in an APD needs to account for measurement and infusion delays and guarantee robustness and minimized error within the closed-loop.

This chapter describes the data-based modelling of the complete biosensor (cells and processing electronics) and its simulation within closed-loop regulation contexts. It does not provide a complete or robust solution for APDs, but rather produces a contextualization and proof of concept of the biosensor within a closed-loop environment. Controllers and regulation algorithms are discussed, as they constitute an essential part of any robust and efficient closed-loop system, but their in-depth study and application is only put into perspective for future works.

4.1 Simulation environment

To evaluate the biosensor's potential for glycaemia regulation, a simulation environment that mimics the body's reaction to glucose intake, insulin injection, and hormonal response has been implemented. Fortunately, the difficulty of animal experiments prior to clinical tests has motivated the development of many simulation environments, facilitating research for algorithms, sensors, and any piece of technology meant for *in-* or *ex-vivo* use on diabetic patients.

4.1.1 Models for whole-body glucose-insulin dynamics

The mathematical modelling of glucose-insulin dynamics, diabetic condition, and therapeutic routes of treatment has been rapidly growing and has brought both insight into the physiological mechanisms and improvements into automated insulin therapy. Over the five past decades, many approaches to putting whole-body glucose-insulin interactions into equations have been explored, including Artificial Neural Networks (ANNs), Delay Differential Equations (DDEs), Integrodifferential Equations (IDEs), Partial Differential Equations (PDEs), Stochastic Differential Equations (SDEs), and Ordinary Differential Equations (ODEs) [115].

The models developed in the literature have different purposes and focus on different mechanisms: some are dedicated to direct clinical tests for diagnostics [115–127] and control ([115, 127–134]), to better treatments and account for insulin delivery routes, while others focus on precise mechanisms at different physiological scales from whole-body through to organ, cellular and subcellular levels [134–141].

In our case, a whole-body model must be chosen to constitute a simulation environment and investigate the practicality of the biosensor in a closed-loop. The candidate models take into account any or all of: insulin injection routes, glucose ingestion routes, glucose measurement routes glucose utilization, liver contribution, and pancreas contribution [133, 134, 142–147].

The model adopted for our study was developed by Dalla Man, Rizza, and Cobelli [133] (the UVA/Padova simulator, or T1DMS) to describe scenarios on individual *in silico* patients. It as chosen because of its readily available equations and parameters, and because it is now an Food and Drug Administration (FDA)-approved substitute for pre-clinical animal trials [148] for APDs: as opposed to "average" models [1], that do not provide enough insight regarding algorithm safety, this simulator proposes a set of defined patients (adults, adolescents, and children), that will help assess robustness in future controller design. It features insulin injection routes, glucose measurement routes, insulin pump models, regulation algorithms, daily scenarios, and patient models. T1DMS is a commercial product (T1DMS, The Epsilon Group) now used by many researchers as an alternative to animal testing of T1D control strategies [149–157].

4.1.2 Python integration of the T1DMS model

Before the Matlab/Simulink UVA/Padova simulator was bought by Elibio, development was made using a Python implementation of the *in silico* model. This gave total control over internal signals of the model and permitted the addition of mechanisms missing from the original model. This section describes the port of this simulation environment to Python 2.7 . Model equations and parameters were retrieved from [133, 147, 158, 159].

Original model

The Python 2.7 port of the UVA/Padova simulator is a collection of several published models: the Glucose-Insulin system equations and normal patient parameters are accessible in [133, 147], oral glucose absorption and gastro-intestinal tract equations and parameters in [158], and additional gastro-intestinal equations and parameters in [159]. A more complete set

1. Models that only recreate average behaviour, but not interindividual variability

of equations describing Glucose-Insulin-Glucagon interactions was proposed in [160], but this one was not included in the Python 2.7 port for a lack of published model parameters.

The original model simulated glucose-insulin [147] interactions in a healthy human (Fig. 4.1). The "virtual patient" was then made diabetic in the T1DM simulator [147] by removing its β cell system, mimicking the self-immune destruction of β cells. In the Python 2.7 port, the β cell system was not removed, but instead was made insensitive to glucose [2], making pancreatic ISR null. This facilitated patient model swapping (e.g. simulating a non-diabetic patient and a T1D patient with the same set of equations) with no change in the outcomes of the scenarios. Figure 4.2 presents the model simulation for a non-diabetic person over a 24 h cycle.

Additions to the model

The UVA/Padova original model only represent interactions in the glucose-insulin system, but does not support realistic insulin injection routes. To accommodate that and anticipate closed-loop regulation simulations, intravenous (IV) and subcutaneous (SC) delivery routes were added.

SC injection model equations were retrieved from [147] and [159]: they represent the dissociation of insulin from non-monomeric to monomeric in the subcutaneous space and its appearance in plasma:

$$\begin{cases} \dfrac{dI_{sc1}}{dt}(t) = -(k_d + k_{a1}) \times I_{sc1}(t) + IIR(t) & \text{(4.1a)} \\ \dfrac{dI_{sc2}}{dt}(t) = k_d \times I_{sc1}(t) - k_{a2} \times I_{sc2}(t) & \text{(4.1b)} \\ R_i(t) = k_{a1} \times I_{sc1}(t) + k_{a2} \times I_{sc2}(t) & \text{(4.1c)} \end{cases}$$

Where R_i is the rate of appearance of insulin in plasma, I_{sc1} the amount of non-monomeric insulin in the subcutaneous space, I_{sc2} the amount of monomeric insulin in the subcutaneous space, $IIR(t)$ (pmol/kg/min) the exogenous insulin infusion rate, and k_d, k_{a1}, k_{a2} are rate constants (min^{-1}).

IV insulin was added as an insulin rate of appearance in the liver, parallel to portal insulin.

2. by setting pancreatic response to glucose, glucose rate of change, and basal Insulin Secretion Rate (ISR) to 0

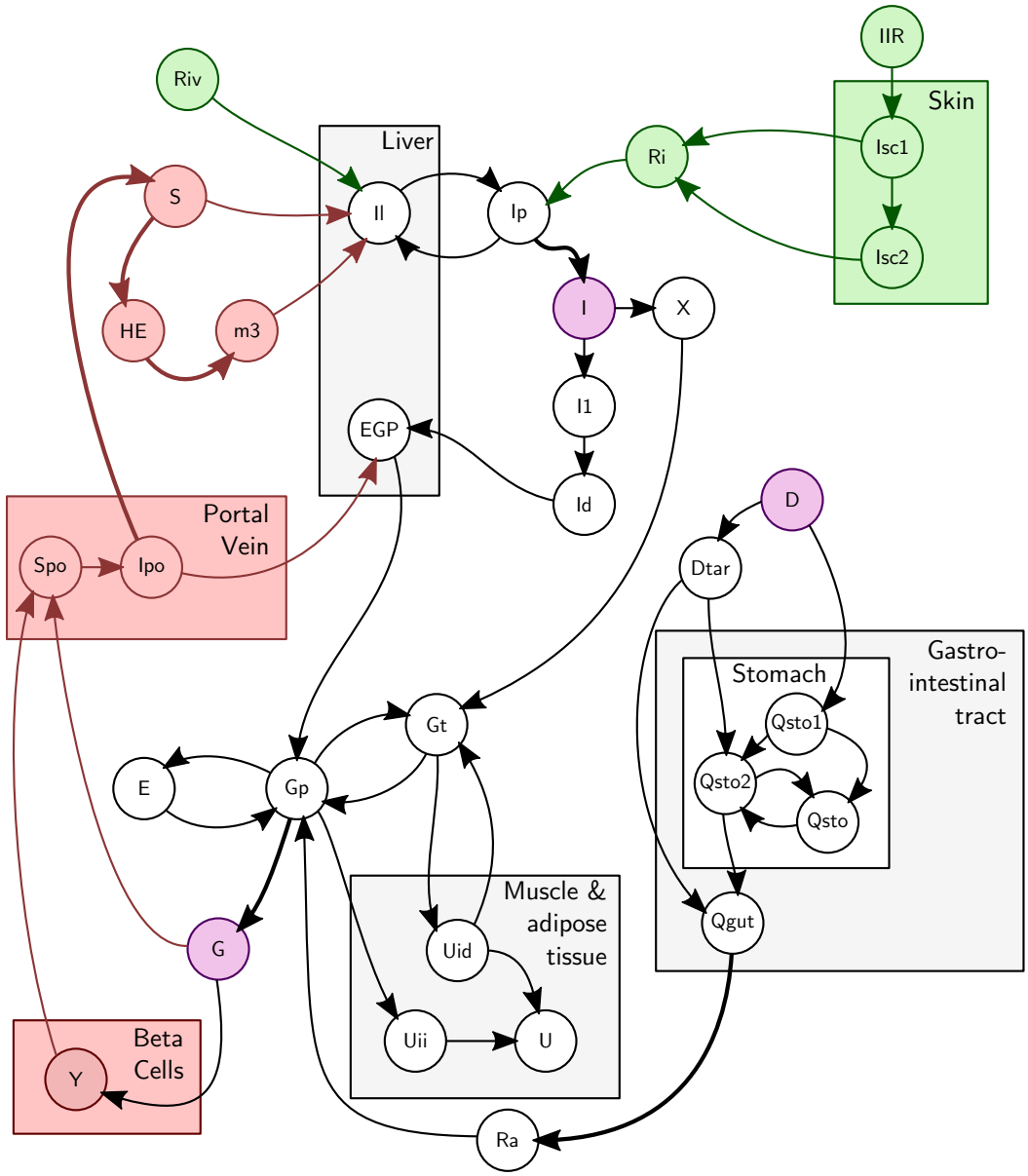

Figure 4.1 – Whole body model used as a simulation environment. Insulin injection routes are represented in green, purple indicates the main signals of interest (inputs and outputs: D is the sugar intake input signal, I is plasma insulin level, G is plasma glucose level). Red highlights the model elements affected by T1D. **Liver**; Il: insulin in liver; EGP: Endogenous Glucose Production. **Portal vein**; Spo: Insulin secretion in portal vein; Ipo: Quantity of insulin in portal vein. **Beta cells**; Y: Insulin secretion rate. **Muscle & adipose tissue**; Uid: Insulin-dependent glucose utilization; Uii Insulin-independent glucose utilization; U: Glucose utilization. **Stomach and Gastro-intestinal tract**; Qgut: quantity of glucose in the gut; Qsto: amount of glucose in the stomach (Qsto1: solid phase; Qsto2: liquid phase); **Skin**; Isc1: quantity of non-monomeric insulin; Isc2: quantity of monomeric insulin. **Others**: Ip: plasma insulin; X: remote insulin signal; I1: delayed plasma insulin; Id: delayed plasma insulin; Dtar: target ingested glucose; Gp: Plasma glucose; Gt: Glucose in rapidly-equilibrating tissues; E: renal excretion; Ra: Glucose rate of appearance in plasma; Riv: Intravenous insulin rate of appearance; S: insulin secretion; HE: Hepatic extraction; m3: modulated model parameter.

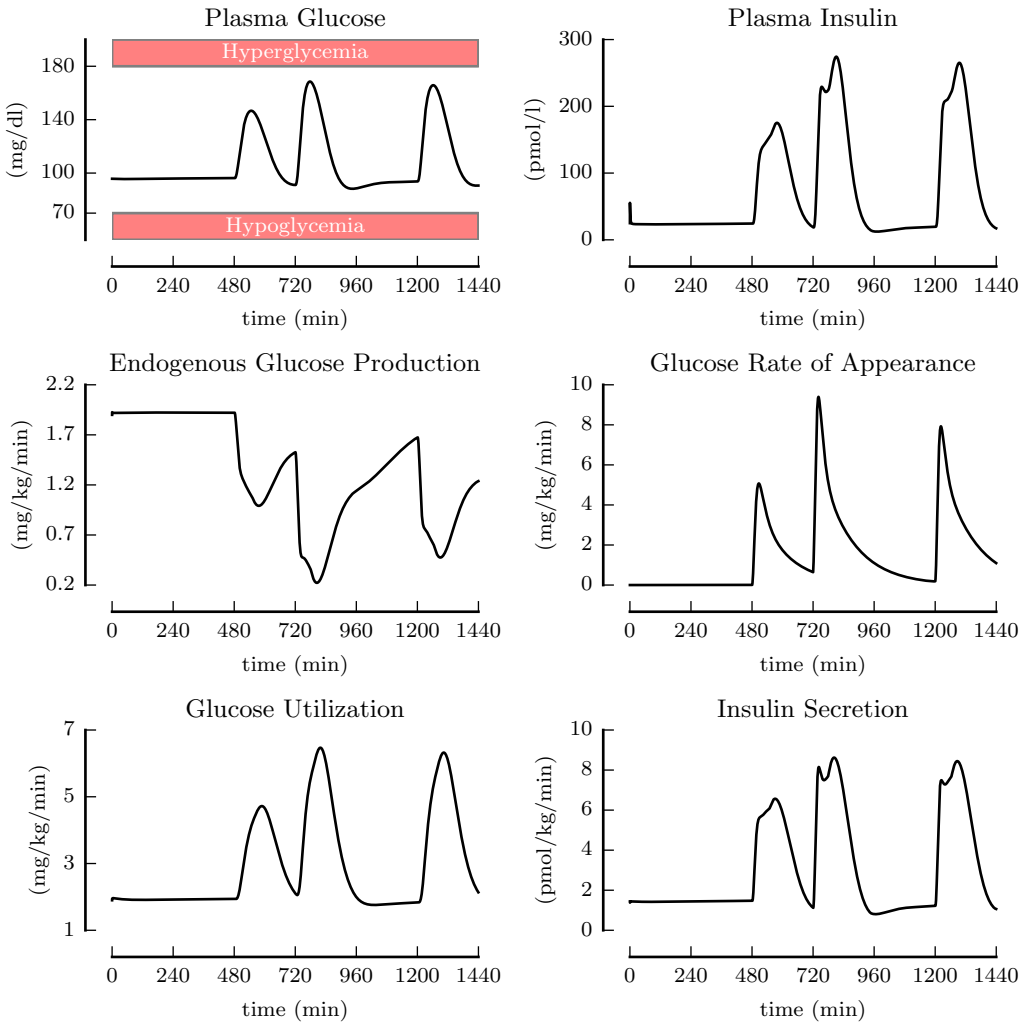

Figure 4.2 – Original Glucose-Insulin model ported to Python 2.7 for a non-diabetic person. It is simulated over a 1440 min (24 h) cycle starting at midnight at basal conditions and shows plasma glucose, plasma insulin, EGP, glucose rate of appearance, glucose utilization by the brain and muscles, and insulin secretion; simulation recreated one of the results in [133] for a non-diabetic person.

4.2 Integrating the biosensor

In silico models were specifically written to validate the whole acquisition and processing chain including Multimed. Therefore, the biosensor model is simulated as the whole acquisition chain, including cell signal generation and signal processing rather than a single glucose-Slow Potential (SP) frequency relation. Due to their higher robustness, SPs constitute the signal of interest in this model, meaning that it in fact includes SP waveform generation, SP detection, and SP frequency measurement.

This section describes the different steps involved in modelling the biosensor, and produces a proof of concept for a closed-loop configuration. It firstly focuses on the glucose response of the biosensor, then proposes a solution to account for hormone effects. The modelling of processing electronics will not be discussed as it is a software integration of the algorithms embedded on Multimed (all described in chapter 2), respective real-time constraint (causal implementation) and data format (fixed point representation). One processing channel is simulated, generating the signal recorded on one electrode. It is assumed that the data modeled on this unique channel is representative of the average results of active recording channels of a whole Microelectrode Array (MEA). All model equations and identified parameters are given in appendix I

4.2.1 SP generation

To generate synthetic, frequency-modulable, SP waveforms, the average shape of SPs was computed and made into a periodic function using Fourier series. After a $0.2 - 2$ Hz, 5^{th} order filtering, SPs from three different experiments were recorded. Their individual shapes were linearly interpolated, normalized, and made periodic to compute their average. Finally, the first ten Fourier coefficients of this average waveform were computed. The resulting average waveform is represented in Fig. 4.3. In this approach, only SP frequency is taken into account. SP shape generation is therefore normalized in amplitude.

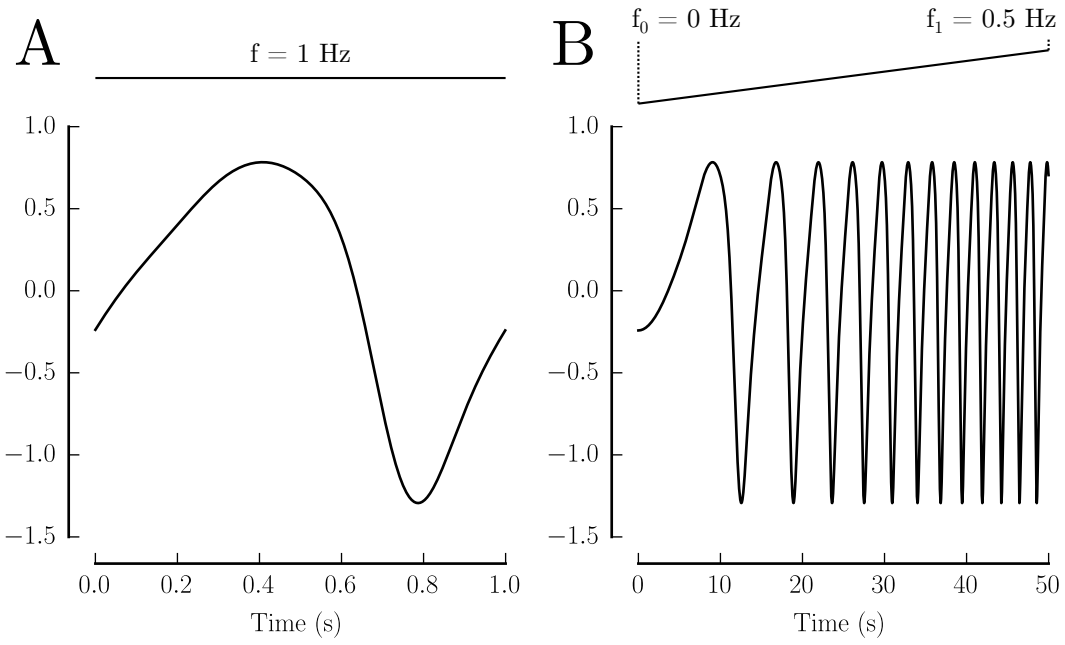

Figure 4.3 – Model of average and normalized SPs. **A**: One period of the modeled SP at 1 Hz. **B**: 0-0.5 Hz ramp of SPs.

4.2.2 SP response static model

The fitting equation of the SP frequency response to glucose was inspired by Stamper and Wang [161], where Insulin Secretory Granule (ISG) docking, priming, and fusion are modulated by a glucose-dependent function. This function, further referred to as $\mathscr{A}$, the *activation function*, follows a Hill equation [162, 163] widely utilized to model biological processes. It is bounded between 0 and 1 and defined by a half-activity constant G_{50} and the Hill coefficient, n. The only modification from classical Hill equations is the addition of an activation threshold G_0 under which $\mathscr{A}$ is null (Fig. 4.4A). The resulting equation is defined as follows:

$$\mathscr{A}(G) = \begin{cases} \dfrac{[G - G_0]^n}{[G_{50} - G_0]^n + [G - G_0]^n} & \text{if } G \geq G_0 \\ 0 & \text{otherwise} \end{cases} \tag{4.2}$$

This equation was de-normalized using a scalar f_M, the maximum SP frequency attainable by the model. The resulting equation, $f_M \times \mathscr{A}$ was fitted to SP frequency response to small steps of glucose. The fitting result is shown in Fig. 4.4.

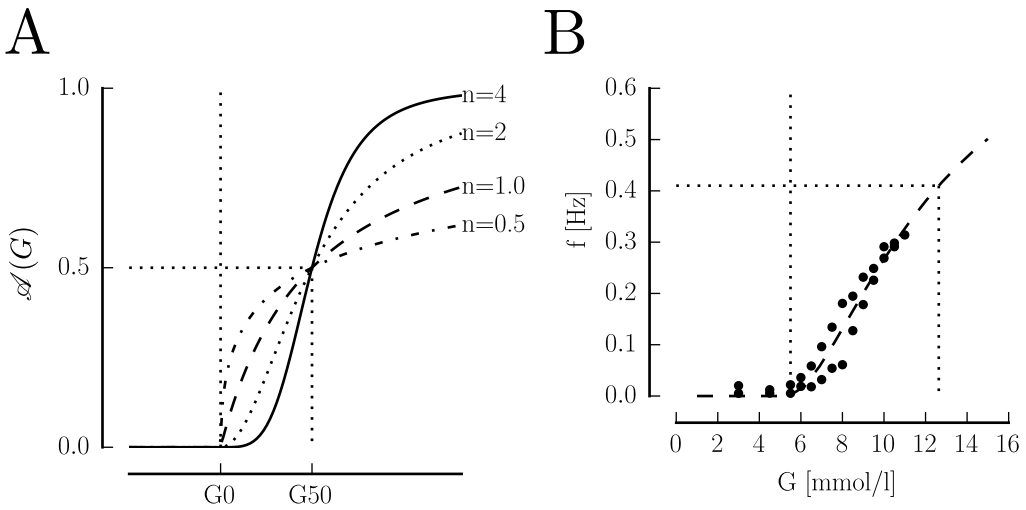

Figure 4.4 – Static model of SP response to glucose. **A**: Hill-inspired activation function with an activation threshold G_0, a half-activity constant G_{50}, and a Hill constant n for different values of n. **B**: Fitted $f_M \times \mathscr{A}(G)$ model on small steps of glucose.

4.2.3 Hysteresis model

As seen in section 3.2.3, changes in static SP frequency occur at different rates when glucose concentration is either increasing or decreasing. This further demonstrates that β cells not only respond to glucose levels, but also to glucose rate of change. To model this behaviour, the resulting hysteresis was fitted to a Preisach model of hysteresis.

The Preisach model [164] is a widely accepted model that decomposes a hysteresis loop into a summation of discrete hysteretic elements, the relay hysterons. Hysteretic experimental data from Fig. 3.6 was first separated into increasing and decreasing glucose and each half was fitted to an activation function. The region within the two intersections of the resulting curves (approximately between G3 and G11, Fig. 4.5A) was utilized to generate the Preisach matrix. Results are shown in Fig. 4.5.

4.2.4 Dynamic model

Biphasic insulin release is a well-known secretory mechanism that has been extensively modeled [112, 139, 161, 165, 166]. The earliest mathematical model was that of Grodsky

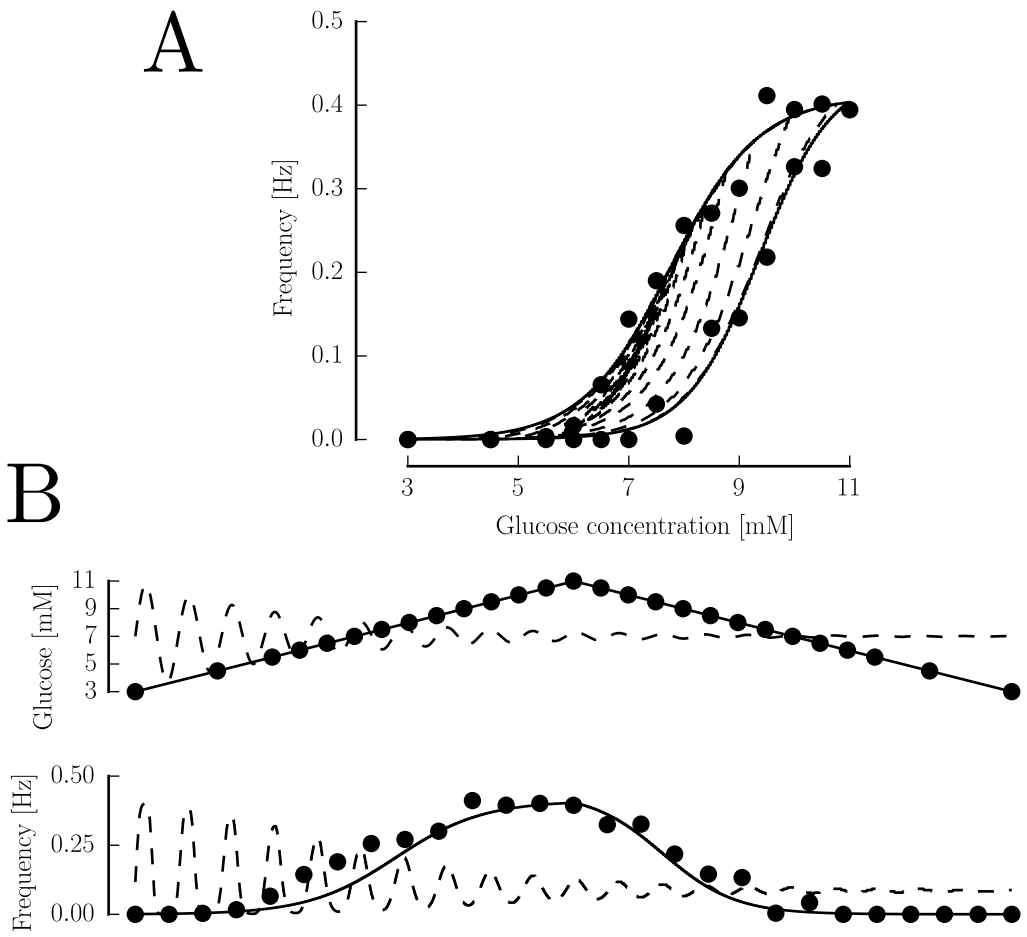

Figure 4.5 – Preisach hysteresis model fitted to SP frequency response to small steps of glucose. Dots represent experimental data. Plain lines represent the continuous G3→G11→G3 path, yielding the exterior bounds of the hysteresis. Doted lines represent oscillations of decreasing amplitude around G7, showing interior paths of the hysteresis. **A**: Hysteresis representation of the fit. **B**: Time-dependent representation of the fit.

[139], pioneering an ODE-base multiple pool concept, later revisited by Pedersen, Corradin, Toffolo, and Cobelli [166] and Stamper and Wang [161]. These models describe ISG trafficking as a set of communicating pools with glucose-dependent transfer rates. A Readily Releasable Pool (RRP) of granules is emptied rapidly, forming the first phase, followed by a lower, more steady flow of ISGs.

Let aside ISGs, an empirical model for biphasic SP frequency can be drawn following a similar set of equations. Biphasic responses from 17 recordings were decomposed into the sum of two exponentials (one falling for first phase and one increasing for second phase). From this decomposition, four parameters were identified and used in the model: the peak frequency of 1^{st} phase f_1, the plateau frequency of 2^{nd} phase f_2, and the falling and rising rates of 1^{st}

and 2nd phase, respectively τ_1 and τ_2. The model is defined by the following set of equations:

$$\begin{cases} \dfrac{dY_0}{dt}(t) = -\lambda_4 \times Y_0(t) + \hat{\lambda_3}(G) \times R & \text{(4.3a)} \\ \dfrac{dY_1}{dt}(t) = -\hat{\lambda_5}(G) \times Y_1(t) + \lambda_4(t) \times Y_0(t) & \text{(4.3b)} \\ \dfrac{dF}{dt}(t) = -\lambda_2 \times F(t) + \hat{\lambda_5}(G) \times Y_1(t) & \text{(4.3c)} \\ \mathscr{F}(t) = \dfrac{\lambda_1}{\lambda_3} \times \dfrac{\lambda_3 \times \lambda_4}{\lambda_3 + \lambda_4} \times F(t) & \text{(4.3d)} \\ \mathscr{N} = \dfrac{\mathscr{A}}{\lambda_3} & \text{(4.3e)} \end{cases}$$

Y_1 acts as a RRP, a pre-filled reservoir with a high transfer rate λ_5 towards the fused signal F permitting the high-rate frequency increase of 1st phase. F then decreases at a λ_2 rate to form the complete 1st phase. The 2nd phase is formed by Y_0 that empties into Y_1 at a $\lambda_4 = \tau_2$ rate. The limit value of 2nd phase is determined by λ_3. The transfer chain $Y_0 \to Y_1 \to F$ is limited by the lowest transfer rate λ_4, ensuring the accuracy of 2nd phase. F is finally scaled by a factor $\frac{\lambda_1}{\lambda_3} \times \frac{\lambda_3 \times \lambda_4}{\lambda_3 + \lambda_4}$ to obtain the frequency signal $\mathscr{F}$, necessarily setting the remaining transfer rate $\lambda_2 = f_1 \times (\frac{\lambda_3}{\lambda_4} + \frac{\lambda_3}{\lambda_5})^{-1}$. $\mathscr{N}$ is the normalized biphasic response. All $\lambda_.$ values are constants, and $\hat{\lambda_.}(G) = \mathscr{A}(G) \times \lambda_.$.

More data is required to establish whether SPs satisfy the staircase experiment (i.e. a two-phase profile is not generated between two excitatory conditions since Y_1 is entirely depleted), therefore this model implementation does not satisfy it. As a consequence, in regulation terms, the derivative contribution of islet activation only occurs at glucose appearance in the body. All further contributions until basal levels are restored are proportional.

4.2.5 Glucose-equivalents

Exploiting β cell electrical response as a biosensor not only makes it sensitive to glucose, but also to hormones present in the bloodstream, as was demonstrated in sections 3.3.1 and 3.3.2. Therefore, when exposed to a physiological medium, the biosensor does not return a direct image of glucose concentration, unlike classic glucose sensors. Instead, it returns a composite image resulting from multiple sensitivities. As a direct image of cell activity, it reflects glucose- and hormone-dependent insulin secretion.

To ensure compatibility with current glucose regulation techniques and algorithms, the unique measurement returned by the biosensor must be converted to a classic glucose measurement. The returned value is a glucose concentration at which, in a glucose-only medium, cell activity is equivalent to that of the actual measured cells, hence the term *glucose equivalent*; for example, at equal glucose levels, adrenaline will lower glucose equivalents (resulting in a lower insulin demand), while GLP-1 will raise them (resulting in a higher insulin demand).

The proposed method to calibrate *glucose equivalents* consists in identifying separate hormone effects and model them as SP frequency modulation parameters (Fig. 4.6A). Let $f(G)$ be the glucose-dependent SP frequency, $\alpha([Adr])$ the normalized (fold of [Adr]=0) Adrenaline effect on SP frequency, and $\gamma([GLP1])$ the normalized (fold of [GLP1]=0) GLP-1 effect on SP frequency. Modulated SP frequency is therefore $f_m(G, [Adr], [GLP1]) = f(G) \times \alpha([Adr]) \times \gamma([GLP1])$. Therefore, computing $f^{-1} \circ f_m(G, [Adr], [GLP1])$ yields the glucose equivalent concentration.

Like glucose-induced activation, normalized hormone effects were modeled using the Hill-inspired activation function $\mathscr{A}$ of eq. 4.2. Fitting results are shown in figure Fig. 4.6B-D. Because of apparent glucose-dependency in GLP-1 effect (Fig. 4.6C), fitting coefficients were

extrapolated assuming linear dependency to glucose (see non-linear effect on Fig. 4.7B).

$$f(G) = \begin{cases} f_M \times \dfrac{[G-G_0]^n}{[G_{50}-G_0]^n + [G-G_0]^n} & \text{if } G \geq G_0 \\ 0 & \text{otherwise} \end{cases} \tag{4.4a}$$

$$\gamma(X^\Gamma) = \begin{cases} 1 + \dfrac{[X^\Gamma - X_0^\Gamma]^{n^\Gamma}}{[X_{50}^\Gamma - X_0^\Gamma]^{n^\Gamma} + [X^\Gamma - X_0^\Gamma]^{n^\Gamma}} & \text{if } X^\Gamma \geq X_0^\Gamma \\ 1 & \text{otherwise} \end{cases} \tag{4.4b}$$

$$\alpha(X^A) = \begin{cases} 1 - \dfrac{[X^A - X_0^A]^{n^A}}{[X_{50}^A - X_0^A]^{n^A} + [X^A - X_0^A]^{n^A}} & \text{if } X^A \geq X_0^A \\ 1 & \text{otherwise} \end{cases} \tag{4.4c}$$

$$X^\Gamma = \log_{10}([\text{GLP1}]) \tag{4.4d}$$

$$X^A = \log_{10}([\text{Adr}]) \tag{4.4e}$$

Model simulations are shown in Fig. 4.7. Note the behaviour of glucose equivalent values below G5.5: since $\mathscr{A}$ is not a bijective function (it returns 0 for all glucose levels below G_0), f^{-1} is not defined for sub-threshold glucose levels. An exception is made for these values, defined by $G_{eq} = G$ if $G < G_0$. This is acceptable within the biosensor model since all signal generation is null in these conditions and all sub-threshold glucose levels are treated identically.

This approach of glucose equivalents unfortunately suffers from two major limitations:

— the model itself assumes that hormone effects can be separated (i.e. the effect of one hormone is independent from other hormones).
— the whole-body model does not take into account hormone effects.

Even though effects of glucose on GLP-1 modulation of SPs have been taken into account, combined effects of hormones have not been experimentally characterised: the currently available data only permits a derived glucose equivalent of the form $G_{eq} = f^{-1}(f([G]) \times \alpha([Adr]) \times \gamma([GLP1], [G]))$ when the safest assumption would be $G_{eq} = f^{-1}(f([G]) \times H([G], [Adr], [GLP1]))$ where H is a multivariate function taking into account combined hormone and glucose effects. Section 4.3.1 puts into perspective more robust identification methods suited for such an intricate behaviour.

On top of that, hormone action is not limited to the pancreas, and the absence of hormone-dependent activity of other organs in the whole-body model is a source for severe inaccuracies. However, no model to date recreates the complex interactions of the glucose-insulin system with both glucose and hormone dependencies. Future identification and characterization of these properties is vital for further development of the biosensor in a closed-loop environment.

4.2.6 Simulation results

Successive versions of the biosensor model were simulated in a closed-loop environment (Fig. 4.8A). Simulations aimed at verifying that SP frequency could indeed control insulin infusion and mimic insulin secretion using the most direct measurement and injection routes (IV glucose, IV insulin). While impractical, these methods of measurement and infusion seem fair in the absence of a dedicated regulation controller (calibrating the regulation is achieved by adjusting a scalar K normalizing SP frequency (Fig. 4.8A), equivalent to a proportionate controller). The Glucose-to-Insulin conversion rule (*synthetic islets* inFig. 4.8A) was defined by *in silico* islet models described in [161]. This model yields insulin secretion for a single islet, which was then scaled up to 80,000 active islets.

Simulation results are shown in Fig. 4.8. Like in the original 24 h cycle simulation of Dalla Man, Rizza, and Cobelli [133], meals were planned at $T_{breakfast}$=480 min (45 g of glucose), T_{meal}=720 min (70 g of glucose), and T_{dinner}=1200 min (70 g of glucose). For comparison, glucose variations are represented for a T1D patient manually injecting insulin

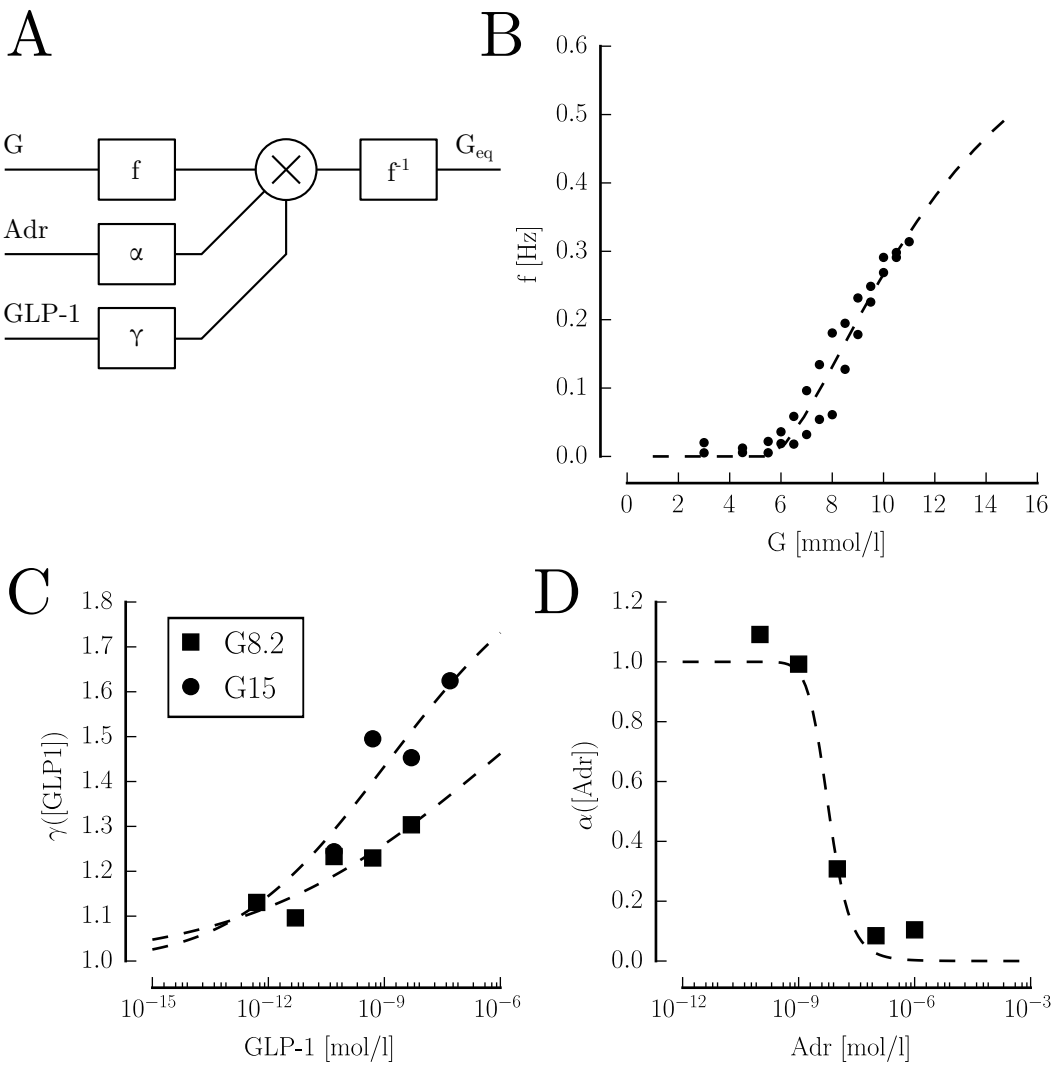

Figure 4.6 – Glucose equivalent principle and identification. **A**: Glucose equivalent data flow. f converts glucose concentration into SP frequency. α converts adrenaline concentration into a scalar between 0 and 1 (inhibitory effect) and γ converts GLP-1 concentration into a scalar superior to 1 (excitatory function). SP frequency is modulated by these two scalars and the result is converted back into a glucose concentration by f^{-1}, the reciprocal of f. **B**: Identification of f on experimental data from Fig. 3.6. **C**: Identification of γ on experimental data from Fig. 3.8 at two different glucose concentrations (G8.2 and G15). **D**: Identification of α on experimental data from one experiment ($n = 24$ electrodes) at G15.

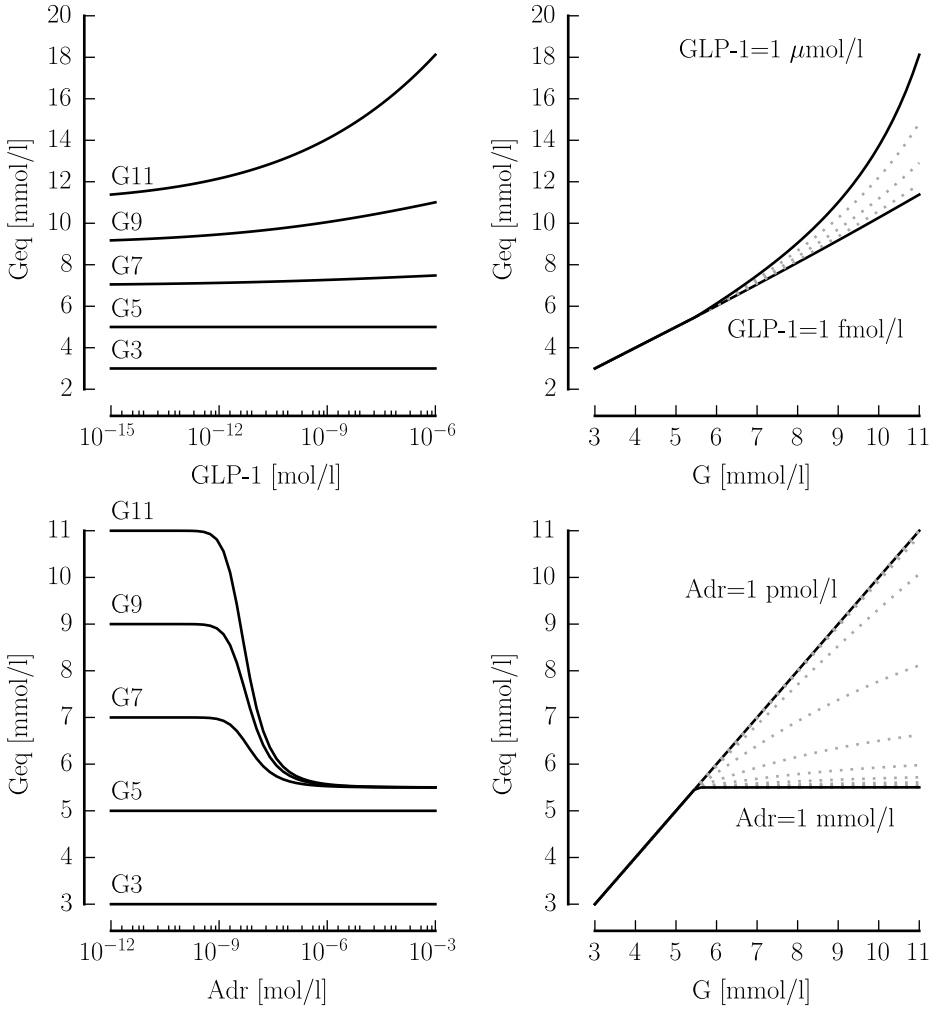

Figure 4.7 – Derived glucose equivalent models. **A** and **B**: GLP-1-dependent glucose equivalents. **C** and **D**: Adrenaline-dependent glucose equivalents.

(subcutaneous). Manual injections of insulin were made 15 min before meals, at 1 U of insulin per 10 g of glucose ingested (1 U = 6945 pmol).

Each iteration of the simulation highlights the role of endogenous islet algorithms: with the static model as a reference, adding a biphasic response makes insulin delivery slightly faster and achieves similar glucose regulation with lower insulin delivery. The hysteresis model, on another note, makes insulin delivery extremely brief and, as expected, blocks insulin delivery rapidly after glucose levels drop. The subsequent glucose levels after noon are the highest of the three tested models, although the glucose concentration drops obtained remain a high hypoglycaemia risk. Among the three models, the biphasic one (red) seems to make the best use of insulin, with the lowest peak levels and comparable performance in glucose regulation. The model including both biphasic and hysteretic actions (green), however, has the highest insulin release peaks, which compensate for its early stop in insulin release; of course few conclusions can be drawn in the absence of a dedicated controller, but such an early interruption in islet activity must be anticipated in controller design, as it drastically affects performance. Indeed, this endogenous mechanism of preventing hypoglycaemia is tuned for *in corpore* dynamics and its *extra corpore* behaviour must be interpreted differently.

While the simulated closed-loops successfully limit hyperglycaemia, they tend to overshoot and cause hypoglycaemic events between noon and dinner. This can be explained with cell activity ceasing completely at the glycaemic target and below (the regulation target is a null SP frequency). No information is therefore returned by the biosensor in hypoglycaemic conditions. This absence of information currently originates from the lack of Action Potential (AP) data, as α cells signal low glucose levels with AP firing. The resulting electrical signal, with α cell-only APs and inhibited β cell SPs and APs could be interpreted as the body's glucagon demand. The current state of the processing electronics and the low Signal-to-Noise Ratio (SNR) of APs (and especially α-generated APs) unfortunately prevents this approach.

On that note, one of the limitations of the simulated regulation loop is that of single-hormone artificial pancreas: with insulin-only injections, the command can decrease glucose levels but has no automated way of increasing blood sugar. A sane pancreas would automatically counteract hypoglycaemia with glucagon secretion, consequently raising EGP. Dual-hormone APDs have both insulin and glucagon pumps to decrease and increase blood glucose. In the proposed simulations, raising blood glucose would require glucose intake or manual glucose injections.

The main limiting factors of APDs, not addressed in the closed-loop model we investigated, are the measurement and feedback delays introduced by subcutaneous interfaces. Indeed, subcutaneous Continuous Glucose Monitors (CGMs) do not measure glucose in blood vessels, but rather in the interstitium. While interstitial glucose and venous plasma glucose are almost identical in steady-state [167, 168], they take from 10 to 20 minutes to equalize [169] and can be considerably different during rapidly changing conditions [148, 170–172] (e.g. in the post-prandial state or during a hypoglycaemic event). Moreover, subcutaneous insulin delivery (in contrast to physiological portal release) can partially abnegate oscillatory delivery but recent progress in ultra-fast insulin may allow obtaining some variations in blood levels [173]. Likewise, Continuous Subcutaneous Insulin Injection (CSII) introduces a problematic delay causing insulin peaks up to 2 h after injection [174]. On the measuring side, sensors have an integration time that further delays loop response. Even in the favourable conditions of the presented simulations, measurement delay effects can be seen: insulin delivery starts approximately 5 min after glucose variations (caused by integration time in SP frequency measurement). Of course, we do not claim with these simulation to seek optimal regulation, but rather to produce proof that from extracellular measurement's perspective, a hybrid biosensor approach is feasible. These issues will be addressed in further projects, where dedicated controller design is a main topic: It is indeed control algorithms that undertake delay compensation and state prediction.

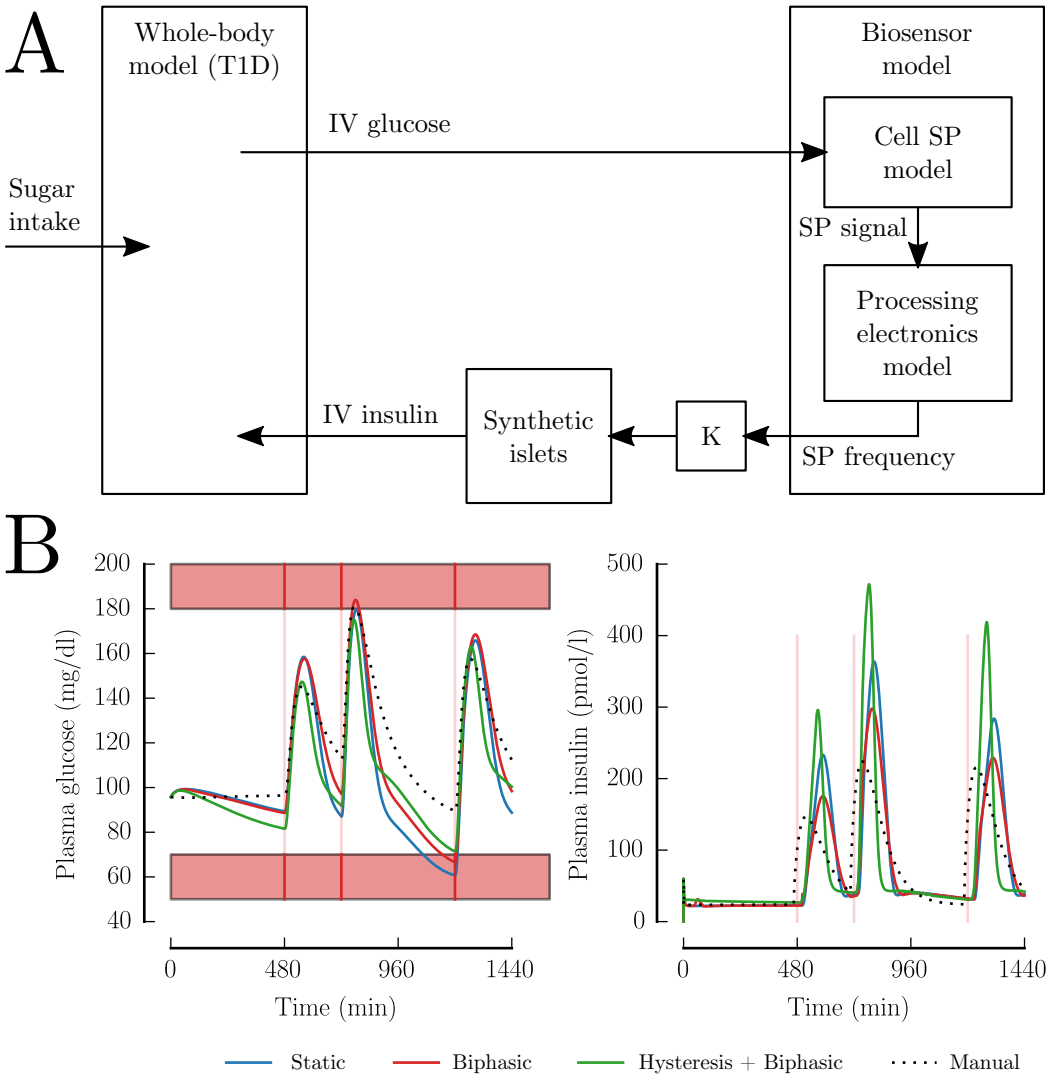

Figure 4.8 – Simulations of *in silico* T1D patients. **A**: simulation scheme, including a whole-body model (section 4.1.2) and the biosensor model. **B**: Simulation results for different versions of the biosensor model showing plasma glucose and plasma insulin. For reference, evolution of glucose and insulin levels are shown for manual, subcutaneous injections. Meals are indicated by vertical red lines.

4.3 Perspectives

4.3.1 Robust controllers and model identification

Diffusion delays and the different kinetics required to compensate for either hypo- or hyperglycaemia are historically widespread issues in the development of artificial pancreas [148, 175, 176]. Classic control theory solutions, such as Proportionate Derivative (PD), Proportionate Integrative (PI), or Proportionate Integrative Derivative (PID) do not have efficient solutions to these problems. For that reason, more advanced controllers have been investigated in the literature with promising results. Model Predictive Control (MPC) for instance has been tested in 17 clinical studies out of 37 between 2010 and 2013 only [177]. It has produces promising results in reducing hyper- and hypoglycaemic events [175, 178–180] by constantly reassessing the effects of its control with model-based predictions. Less popular but nonetheless notable methods based on optimal $\mathcal{H}_\infty$ controllers [181] and Fuzzy Logic [182] have also been investigated.

With a data-based proof of concept of a working closed-loop using the biosensor, future projects welcoming a new partner in control theory have been proposed. This new partnership should improve model identification and permit the design of a robust $\mathcal{H}_\infty$ controller, more performing than the classical controllers mentioned earlier.

While previous work focused on identifying the dynamics of the human insulin/glucose system based on SISO (Single Input Single Output) approaches (insulin injection and blood glucose respectively), the new approach proposes a more advantageous MIMO (Multiple Inputs Multiple Outputs) class of parametric identification techniques. Its major advantages compared to previous approaches are:

— identification will proceed by the identification of a dynamical model transducing a number of important hormonal and nutritional signals (Multiple Inputs) and the different electrical activities of the islets (Multiple Outputs), taking into account the coupling between the different islet signals.
— it is robust with respect to some signal non-stationarities [183–185].
— it performs prediction into the unseen future using an optimal predictor.

To implement the biosensor in the T1DM simulator the body model will be firstly improved to be sensitive to insulin secretion during mainly non-glucose nutritional stimuli and (non-insulin) hormonal regulation based on the works published in [186–190]. Next, a MISO (Multiple Inputs Single Output) controller will be designed in the non-smooth $\mathcal{H}_\infty$ setting by considering the action and SP signals of islet-based biosensor as controller inputs. Compared to the SISO solutions [191–193], the non-smooth $\mathcal{H}_\infty$ controller design is advantageous since:

— it can deal with time delays (physiological and measurements delay),
— it can achieve robust performance against modelling errors such as the CGM errors,
— it can achieve robust performance against a large variability of patient conditions,
— it deals with MIMO systems and objectives, leading the possibility to address e.g. bihormonal (insulin and glucagon) control, and more generally multi-physiological control.
— it is possible to derive a low order controller to make the closed loop implementation feasible in a device.

The new control loop Fig. 4.9 will be finally assessed in a test population and compare to the state-of-the art based on the classical glucose sensor. This *in silico* model, when used with constant and basal (non-insulin) hormone concentrations, will validate the described closed-loop paradigm with standard, glucose-only approaches, but will also, when these are applied, demonstrate its sensitivity to (non-insulin) hormonal stimuli.

4.3.2 Supervised closed-loop on mice

To test the function of the controller in a realistic scenario including diffusion delays and biological noise, we have planned to test the applicability of our sensor in a controllable open-loop *in-vivo* setting. Experiments will be run in anesthetized mice bearing a subcutaneous

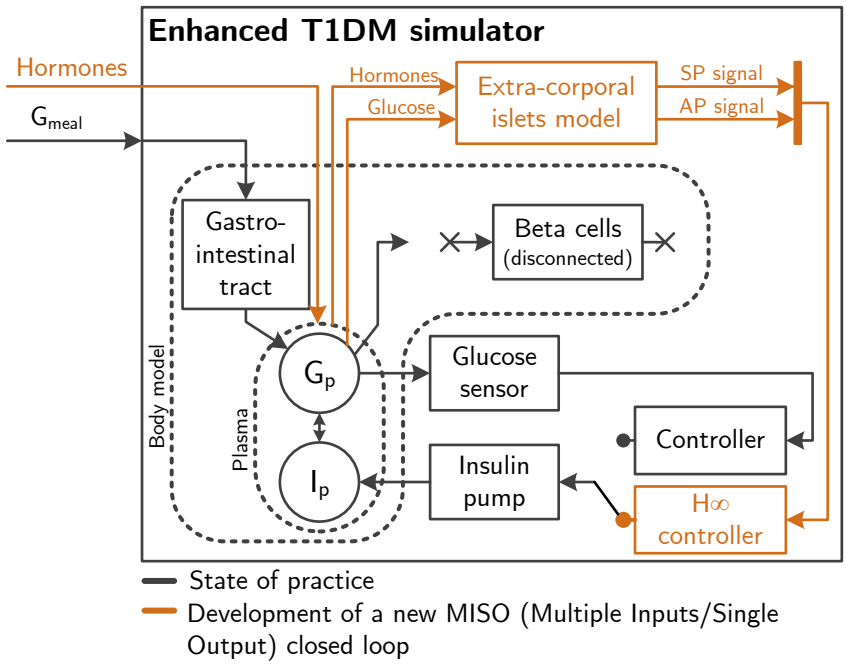

Figure 4.9 – Integration of a Glucose- and Hormone-sensitive regulation scheme including the biosensor model and a $\mathcal{H}_\infty$ controller in the T1DM simulator. This will constitute an *in silico* validation of closed-loop experiments on standardized patients and scenarios. The G_{meal} input represents the quantity of glucose ingested during a meal, and the "Hormones" input is a multiple input (non-insulin hormones such as adrenalin, GLP-1), representing the hormonal adaptation to non-nutritional clues, such as physical activity.

microdialysis device without sample dilution linked to our sensor containing also a CGM electrode. Glucose will be given in IV or intraperitoneal (IP), healthy animals will be used for algorithms calibration purposes, then rendered diabetic (streptozotocin) (Fig. 4.10). Regular interstitial fluid samples will be utilized to stimulate the islets. The measured glucose equivalent for this activity will be help manually determine the insulin dose necessary to maintain blood glucose homeostasis. We will assess the performances of the biosensor by comparing its glucose equivalent output with actual measured glycaemia. We will then test our algorithms and device *extra corpore* in man via subcutaneous microdialysis in healthy volunteers.

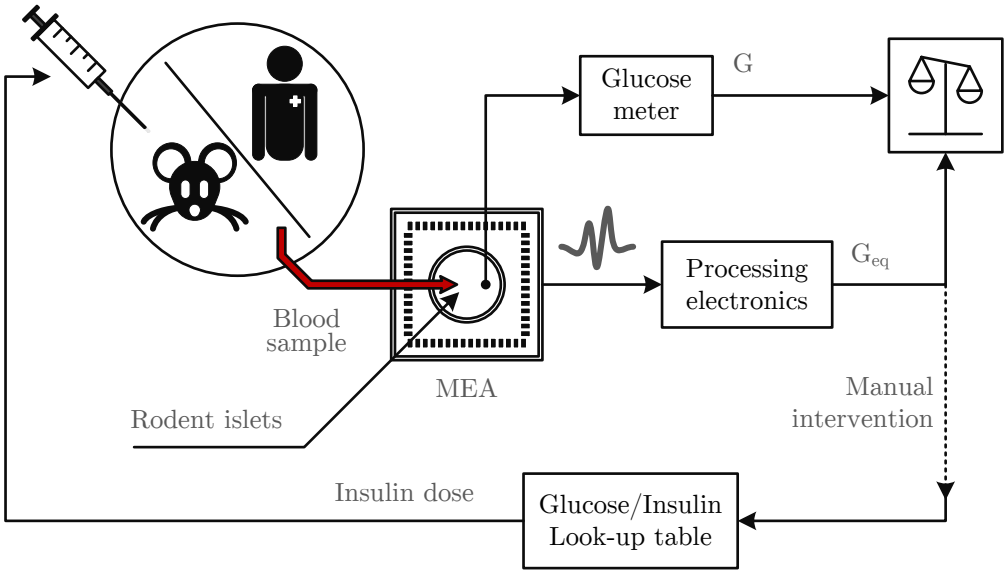

Figure 4.10 – Controllable open-loop (supervised closed-loop) experiment scheme. This will validate the system's ability to perform glucose regulation using the *glucose equivalent* approach. The MEA containing either human of murine cells and the processing electronics constitute the biosensor. It computes a glucose equivalent measurement in real-time on regular blood samples. A glucose sensor assesses the real glucose concentration for comparison. Using glucose equivalent measurements, and with critical assessment of the difference with actual glucose levels, the experimenter will refer to insulin dosage tables to inject insulin to the subject.

Conclusion

> *"If the doors of perception were cleansed every thing would appear to man as it is, Infinite. For man has closed himself up, till he sees all things thro' narrow chinks of his cavern"*
>
> - William Blake, *The Marriage of Heaven and Hell*

This thesis summarizes three years of research in exploiting extracellular recordings of pancreatic islets in a biosensor, following three main approaches: drug screening for pharmacological applications, islet screening for clinical applications, and hormone-sensitive sensing of insulin demand for the artificial pancreas. After assessing the specificities of the biological activity patterns of islets, an FPGA-based signal processing system was developed. It is capable of real-time multichannel processing and can measure parameters related to action potentials and slow potentials. Measurements were conducted on pancreatic islets and cells, and experimental results were used to produce a model of the biosensor. To open prospects into true physiological sensing of insulin demand, this model was simulated to regulate an *in silico* patient's glycaemia, and glucose-equivalent measurement taking into account glucose and hormone (GLP-1 and Adrenaline) levels was proposed.

Synthesis

Chapter 1: The first chapter reviewed the necessary knowledge regarding T1D pathophysiology, β cell electrophysiology, and methods of recording extracellular activity with MEAs. In particular, it revealed that extracellular measurements of electrical potential on pancreatic cells could be exploited to sense changes in nutrient or hormone levels. The recorded signals exhibited action APs and SPs that could be analysed not only to extract information on cell electrophysiology, but also to integrate physiological, hormone-sensitive insulin demand. The need for a real-time processing system that transduces biosignals recorded on MEAs into usable information was therefore introduced. Applications for a biosensor thus formed include pharmacological drug screening, clinical islet screening, and sensing for the artificial pancreas.

Chapter 2: The second chapter gave a detailed description of the electronics developed to process pancreatic islet signals. It is capable of processing 64 channels in real-time (submillisecond latency) with dedicated algorithms. Functions include signal filtering (Infinite Impulse Response (IIR) and wavelet), event detection (APs, SPs and bursts), electrode sorting, and parameter measurements (AP frequency, SP frequency, SP amplitude, burst Fraction Of Plateau Phase (FOPP)). The processing architecture was embedded in an FPGA, mounted on a custom acquisition board, *Multimed*. The latter was designed for either research applications or chip-ready processing architecture prototyping. It has VGA live display, SD card

storage, UART control, and MCS-compatible analogue input interfaces. Implementation of the architecture was made to promote evolutivity and transferability. The system was designed to be utilized by clinicians and biologists and is therefore supplied with a user-friendly software tools.

Chapter 3: The third chapter presented a series of experimental results making use of Multimed or its processing algorithms (online and offline). It established that SPs and APs exhibit glucose-dependent frequencies. In particular, one experiment showed that SP frequency variations were sufficient to distinguish between three physiological glucose concentrations. Hormone effects were also shown, focusing on the inhibiting effect of adrenaline and the potentiating effect of GLP-1. Then, endogenous islet algorithms were investigated: asymmetrical response to glucose and secretion-like biphasic activation were identified. Insight in islet electrophysiology was given by measurements of time correlation between SPs within a single islet, as well as correlation between SPs and APs. Finally, a protocol for islet quality control was proposed.

Chapter 4: The fourth chapter proposed a data-based model of the biosensor. Separate static effects of glucose, adrenaline, and GLP-1 were modelled, as well as dynamic (two-phase and hysteretic) response to glucose. The produced model was then integrated in a closed-loop scenario to demonstrate its ability to regulate the glycaemia of an *in silico* T1D patient. Finally *glucose equivalent* measurement was proposed: it modulates glucose concentration with adrenaline and GLP-1 levels to help achieve automatic hormone-dependent insulin dosage.

Perspectives

Multimed

Multimed was successfully utilized to host a new branch of dedicated processing: algorithms were specifically written for the analysis of pancreatic signals, implemented, and utilized during experiments. This further demonstrates the versatility of the system and its ability to adapt to various contexts. As advertised, it has proven to be an efficient prototyping platform, and despite its versatility has achieved submillisecond processing. However, it is apparent that in several aspects of its hardware, Multimed falls short of its fellow analysis platforms: while some attain up to a thousand acquisition channels and 50 kHz sampling rate, Multimed proposes a fixed, modest amount of 64 channels at 10 kHz.

This design choice is inherited from the previous version of Multimed and remained unchanged because more acquisition channels were not needed for our applications. Should future projects demand it, and in the line of recent trends towards higher electrode densities, future hardware upgrades should revisit the data acquisition card. To Multimed's credit however, attention is particularly attached to designing scalable VHDL architectures, which is currently difficult to demonstrate without significant hardware development.

Embedded processing

Algorithms have successfully been implemented for pancreatic biosignal processing: SPs are detected by the analysis of local extrema, APs are detected with wavelet filtering and adaptive thresholding, and parameter measurements are conducted in real-time using low-resource IIR filters on detected SPs and APs.

With the very few experiments exhibiting APs however, one could argue that the algorithmic cost per detected AP is ludicrously oversized when compared to that of SPs. Plus, correlation between the two types of events suggests that one could supplant the other: whether AP detection should be kept in the system is therefore debatable. Indeed, focusing measurements on SPs only would dramatically reduce implementation costs as well as the required sampling frequency and data rate, without seemingly sacrificing information. In bench experiments,

this question does not stand, as neither resources, nor power consumption, nor storage space are an issue. In a perspective of integration however, the relevance of APs can be disputed. Yet, one important argument in favour of APs is that they are the only detectable cell activity in low-glucose situations: in these conditions, they are fired by α cells and reflect glucagon demand, which makes them a marker for hypoglycaemia risks. Since MIMO modelling of islet response will be done in bench conditions, AP contribution can be evaluated. When the time comes to design a closed-loop controller, the measured contribution of APs will decide their fate in the final biosensor.

The biosensor

Online measurements of cell activity using Multimed have shown that a biosensor using pancreatic islets is feasible: glucose- and hormone-dependence variations can be measured in real-time with sufficient resolution. Variability between preparations strongly suggests that periodic calibration will be required in closed-loop scenarios, not unlike classic CGMs. In bench experiments, the biosensor is ready to be utilized: whether it is islet screening or drug screening, measurements can be conducted with moderate training.

In any case, progressing to either an implantable device or a lab-on-chip approach still requires miniaturization work. Integration of the processing electronics is ensured by digital synthesis tools. By design, Multimed is a prototyping system for digital architectures, taking advantage of synthesis possibilities offered by VHDL. The processing chain can be transformed into a physical circuit with very few modifications (essentially, the CPU needs reprogramming to accommodate modified interfaces). The portion of the transducer that actually requires re-designing for miniaturization is the acquisition chain: the front-end preamplifier (currently a commercial product) and A/D conversion (discrete electronics).

In the long term, integrating the biosensor and making it wearable will also require tackling important issues beyond electronics. First, the type of cells must be determined, and more specifically their origin and their species: because of the already-existing difficulties to acquire human primary cells and the authorizations required to utilize differentiated stem cells, the only possibility to use human cells is with clonal cells. As for animal, primary cells have better coupling than clonal and constitute a strong alternative. One can argue that human and animal cells could exhibit different behaviour, and supplementary data needs to be gathered.

Of course, because cultured cells have a limited lifespan and need periodic replacement, the biosensor would not be fully implanted. It would instead be a wearable receiving interstitial fluid and taking advantage of osmotic pressure in the interstitium. Because it permits continuous flow of medium, development of microfluidic MEAs is a step towards this approach, but cell adhesion must still be improved to prevent electrode loss and provide the best possible signal quality. Finally, the biosensor requires proper encapsulation that ensures both biocompatibility and viability of the cells.

Closed-loop regulation

The biosensor has sufficiently matured to, for the first time, project animal experiments aiming at closing the loop on glucose regulation. New projects are being planned to identify, using state of the art control theory methods, an accurate model of islet response to physiological media. This so-called MIMO identification will take into account various nutrients and hormones (multiple inputs) and integrate the different activity patterns of pancreatic islets (multiple outputs). It will also characterise activity dynamics, noise, and coupling.

This identification process will in turn permit the development of an optimal $\mathcal{H}_\infty$ controller that efficiently compensates for sensor dynamics and body dynamics. It is robust to noise and errors, compatible with MIMO approaches, and can be reduced to a low order, easily integrated controller.

This controller approach however does not negate the need for the *glucose equivalent* measurement. It is a valid approach to investigate regulation with classic controllers, and provides an important measurement with true physiological meaning to patients and carers.

Islet quality control

A complete bundle was developed to facilitate quality control experiments: the processing electronics was made accessible to personnel with modest training thanks to a simple user interface and data import/conversion tools. An experimental protocol and measurement charts were also produced to generate and interpret data.

Data was produced at the measuring site in Bordeaux and transportation from the isolation centre (Geneva) deteriorated cell activity, except for one experimental session conducted *in situ*: this was on opportunity to install a measuring setup there and train clinical personnel to use the system. Even with a readily usable system however, quality measurement results cannot be obtained immediately: success of the transplant is indicated by long-term viability and durable insulin-independence. Quality measurements therefore require months to years of follow-up to produce correlation data.

Afterword

Bioelectronics is a place of interaction between many domains of expertise, and hopefully this thesis reflects that extensively. While studying the interface between two disciplines may only require a two-sided partnership, every possible aspect of the research must include precise insight from expert partners.

In the process of reaching our implantable device for insulin demand sensing, abiding regulations and customer needs will require many domains of research and engineering expertise: from cell culture to device encapsulation through electrode coating, microdevice manufacturing, signal acquisition and processing, and patient compliance, perspectives of the presented work will only come to life with a sufficiently broad circle of partners.

In hindsight, it seems evident that collaborations such as these do not automatically equal the sum of their parts; in domains that share very little common ground, dialog can be a delicate art to master for information to be shared accurately. It is – in my opinion – vital to extend this area of mutual understanding and not limit one's expertise to his/her domain exclusively. This is especially true for project managers, but also for the «small hands »that do the practical work. They need to know and *understand* the needs of their collaborators to not only minimize frustrating misunderstandings, but also help generate joint ideas: collaborations with deep mutual understanding can invent entirely new lines of research.

"While I remained ambitious, punctual, and hedonistic at home, I had learned to better appreciate the timeless beauties and blessings of nature, to value sincerity as a cardinal virtue and reject the Western reverence for affectation and hypocrisy, and to make my frantic life pause for sunrises, sunsets, and full moons."

- Neil Peart, *Traveling Music: The Soundtrack to My Life and Times*

Appendix A

SP detection validation on β cell signals

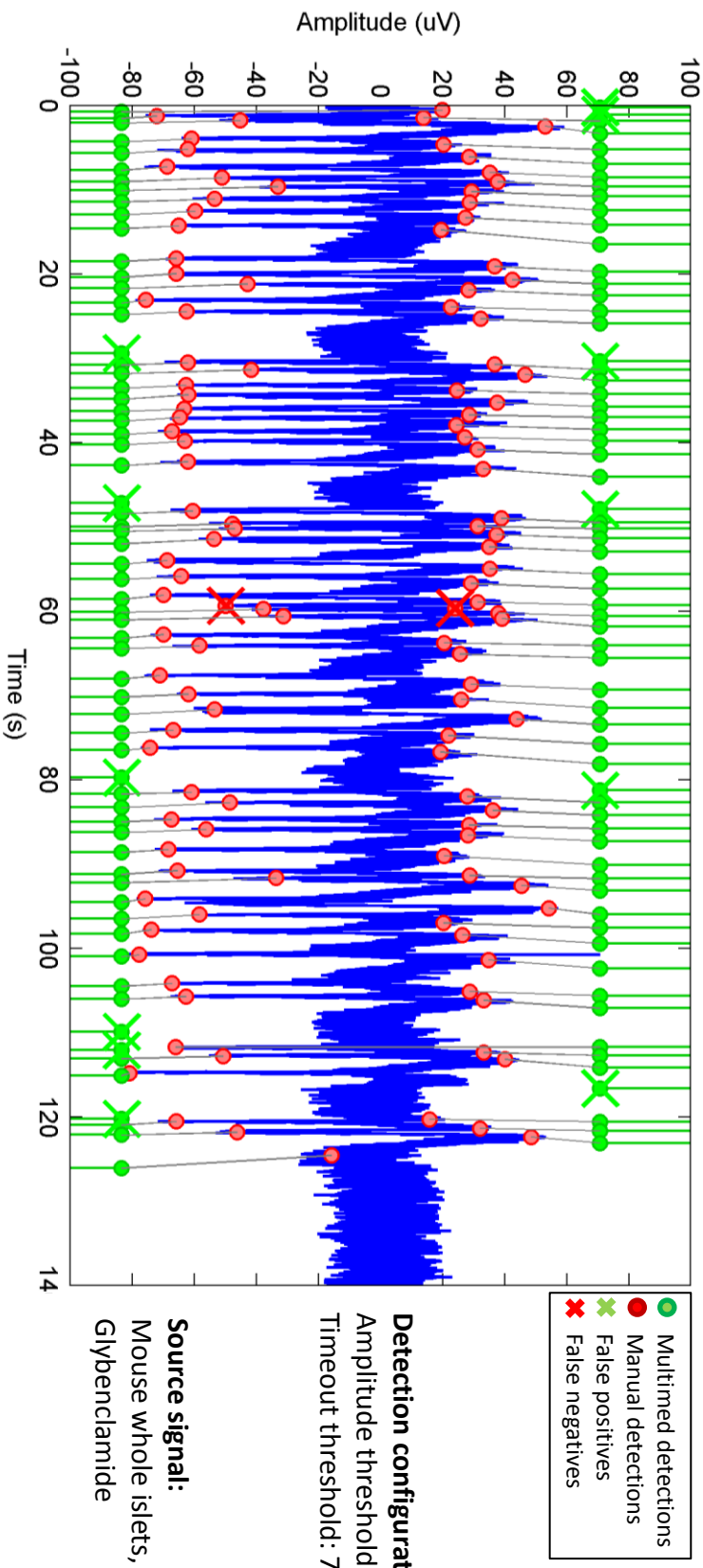

Figure A.1 – Validation of SP detection on mouse whole islets.

Appendix B

Electrode sorting validation data

The sorting module was tested using synthetic signals to validate its function. Input signals were calibrated to ensure 100% event detection rates prior to sorting. They were generated to feature the typical signatures represented in Fig. B.1 and evoke similar event detection. This included low-frequency (0.3-0.8 Hz) sine waves and fast (5-10 Hz) biphasic pulses. The signals were chosen to demonstrate and validate each sorting criterion, i.e. two synchronized signals, a fast pulsing signal, a saturating signal, and two valid. As represented in Fig. B.1B-C, the sorting paradigm included all four sorting cells. Cell #0 detected electrodes with either Action Potential (AP) or SP activity, cell #1 detected synchronized SPs , cell #2 detected rapid pulsing, and cell #3 detected saturation. The inclusion/exclusion rule stated that electrodes with SP or AP activity were included and electrodes with synchronization, excessive AP firing, or saturation were excluded. The sorting module successfully detected the two "normally-behaving" electrodes (Fig. B.1C), and all sorting cells accurately detected electrodes meeting their criteria (Fig. B.1B).

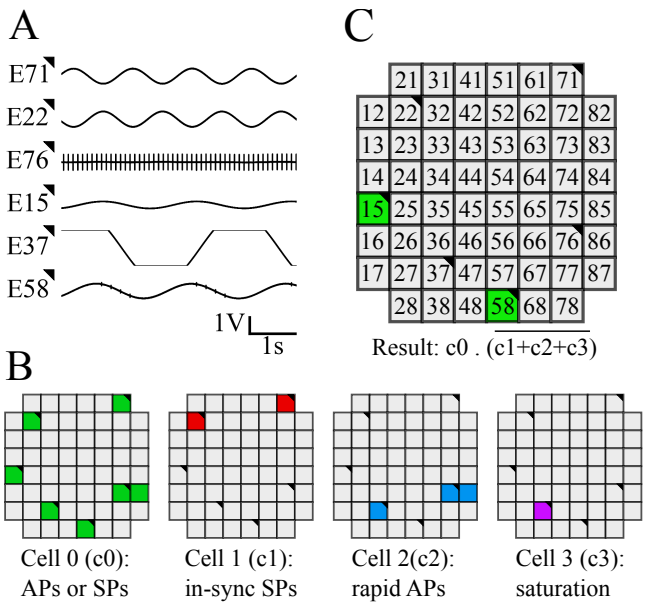

Figure B.1 – Validation of sorting algorithms on test signals, applied on six electrodes marked on the MEA matrix with black corners. **A**: Test signals used. E71 and E22 were 0.8 Hz, 0.9 Vpp sine waves in phase opposition. E76 was a 10 Hz continuous burst of 0.9 Vpp biphasic pulses. E15 was a 0.5 Hz, 200 mVpp sine wave. E37 was a 0.3 Hz, 4 Vpp sine wave, clipped at ± 1 V by the input converters. E58 was a 0.5 Hz, 0.8 Vpp sine wave with bursts of 5 Hz pulses on the descending phase of the sine wave. **B**: Intermediary sorting results returned by the module on four sorting cells. Cell 0 flagged electrodes that had more than 30 APs or 3 SPs in 30 s. Cell 1 flagged electrodes that had 7 synchronized SPs within a 20 ms window in 10 s. Cell 2 flagged electrodes that had 100 APs or more in 10 s. Note that electrode 86 was flagged due to crosstalk with electrode 76 and electrode 37 was flagged because its saturation caused multiple AP detections. Cell 3 flagged electrodes which signal saturated. **C**: Final sorting result returned by the module. The LUT was configured to flag electrodes that had APs or SPs , did not have synchronized SPs , did not have unphysiological AP firing, and which signals did not saturate, hence the logical equation: $c0 \cdot (c1 + \bar{c2} + c3)$. The two remaining electrodes (E15 and E58) are indeed the only two normally-behaving electrodes.

Appendix C

Storage formats

C.1 Raw data

Raw data have a simple format of 64 16 b samples (16 bit signed, big-endian), stored as described in Fig. C.1A. The subsequent bitrate is 1280000 B/s or 1.22 MB/s, adding up to a maximum recording time of 07:27:23 on 32 GB SD cards.

C.2 Processed data

Processed data, unlike raw data, have multiple sources and multiple sampling frequencies, and require a more complex format. The system must be able to differentiate between sources and permit single stream reconstruction during readback.

Each data frame is 64 bytes long, starting with a 4 B header. The two first bytes contain a 16 b packet number (PN) and the last two a 16 b identifier number (ID). The remaining 60 bytes are reserved for data. Multiple sources, either events or samples, may be written in this reserved space. Figure C.1B shows a summary of the chosen data formats for event data and multi- or single- channel measurement data.

Event data are recorded as a series of 64 b groups (1 b per channel), sampled at 1 kHz. Single channel measurement data (average AP frequency, average SP frequency, average FOPP) offer high-resolution average measurement of multiple channels, recorded on 16 b at 1 kHz (except average SP frequency, which is only 10 Hz). Note that these data are not recorded if the electrode sorting result is blank. Finally, multichannel measurement data (AP frequency, SP frequency, and FOPP on all electrodes) are downsampled at 1 Hz. For a more efficient use of space, the dummy channels (electrodes 11, 18, 81, 88) are not recorded, leaving only 60 16-bit channels to record. For a more homogeneous recording format, MSBs and LSBs of these data are recorded separately (with different IDs), meaning that each measurement is stored as two 64 B frames, one of which contains all 60 MSBs and the other all 60 LSBs.

The complete description of processed data formats and list of IDs can be found in section C. Note that despite all data formats being represented with a single data type (e.g. events), they are extremely flexible; indeed, neither the recording architecture nor the data conversion tools prevent from mixing types (e.g. events and streams) within a data frame.

To handle all incoming sources and avoid data collision, a writing buffer was implemented. It buffers all connected inputs separately, and cycles through the buffers, checking for pending data to write. Its state machine is represented in Fig. C.2. Contrarily to the upstream data formatters, this buffer does not wait for specific data: it blindly writes whatever is sent, meaning that it is possible to shut down some of its sources. This permits choosing which processed data are and are not recorded. In practice, only high-resolution processed data (averaged measurements) are considered non-essential and may be discarded by the user. The subsequent possible bitrates are 129280 B/s (including high-resolution data) or 64640 B/s

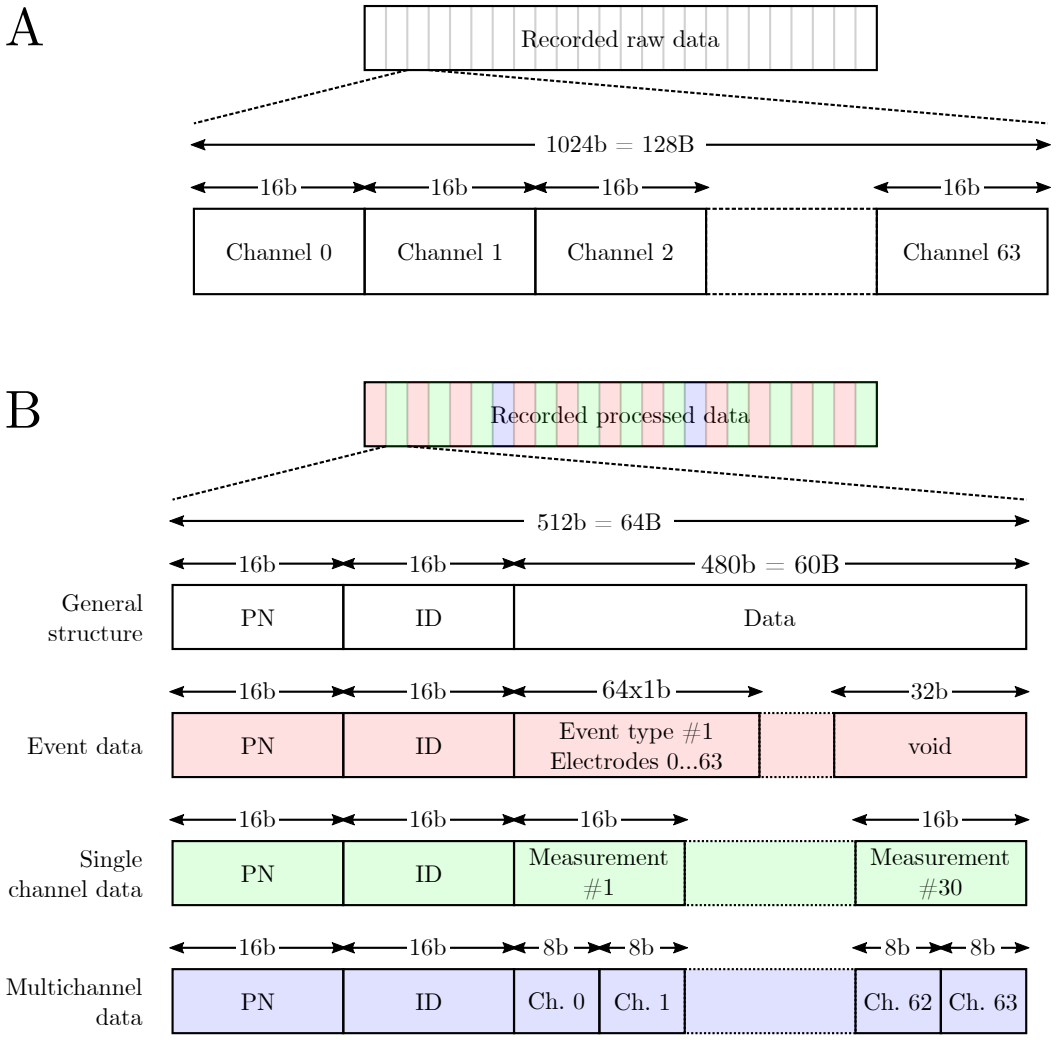

Figure C.1 – **A**: Raw data format. 16-bit data is big-endian. **B**: Processed data format.

(excluding high-resolution data). These respectively amount to around 70 hours or 140 hours of recording time on 32 GB SD cards.

C.3 Processed data IDs and properties

Table C.1 – Processed data storage format

ID	Data structure				Fs (Hz)
	size (B)	Name	Type	Channels	
00001	2	Packet number	System		N/A
	2	ID	System		
	1	PGA gain	Configuration		
	59	void			
10010	2	Packet number	System		10
	2	ID	System		
	2	SP frequency (averaged)	Samples	1	
	58	void			
11000	2	Packet number	System		1000
	2	ID	System		
	8	APs	Events	64	
	8	Burst starts	Events	64	
	8	Burst ends	Events	64	
	8	SP maxima	Events	64	
	8	SP minima	Events	64	
	20	void			
21000	2	Packet number	System		1000
	2	ID	System		
	2	AP frequency (averaged)	Samples	1	
	2	FOPP (averaged)	Samples	1	
	56	void			
10101	2	Packet number	System		1
	2	ID	System		
	60	AP frequency MSB	Samples	60	
10201	2	Packet number	System		1
	2	ID	System		
	60	AP frequency LSB	Samples	60	
20101	2	Packet number	System		1
	2	ID	System		
	60	SP frequency MSB	Samples	60	
20201	2	Packet number	System		1
	2	ID	System		
	60	SP frequency LSB	Samples	60	
30101	2	Packet number	System		1
	2	ID	System		
	60	FOPP MSB	Samples	60	
30201	2	Packet number	System		1
	2	ID	System		

Continued

ID	size (B)	Name	Type	Channels	Fs (Hz)
	60	FOPP LSB	Samples	60	
40101	2	Packet number	System		1
	2	ID	System		
	60	Positive peak amplitude MSB	Samples	60	
40201	2	Packet number	System		1
	2	ID	System		
	60	Positive peak amplitude LSB	Samples	60	
40301	2	Packet number	System		1
	2	ID	System		
	60	Negative peak amplitude MSB	Samples	60	
40401	2	Packet number	System		1
	2	ID	System		
	60	Negative peak Amplitude LSB	Samples	60	

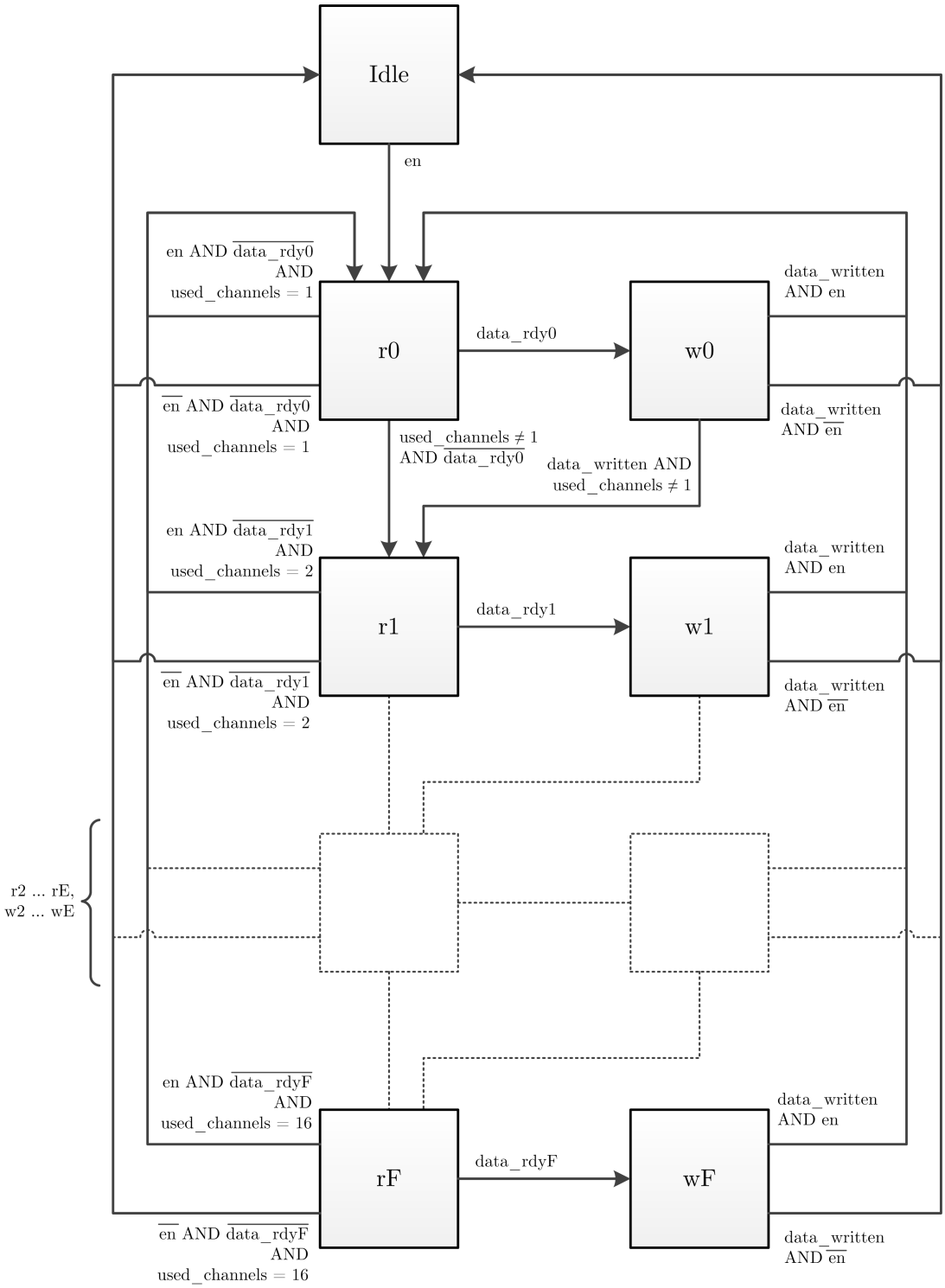

Figure C.2 – State machine of the recording buffer used to handle multiple sources. "r" states (r1-rF) are reading states, where buffers are checked for pending data. "w" states (w1-wF) are writing states, where pending data is pushed out of the buffer.

Appendix D

Functional Blocks

D.0.1 Spatial display of detected events

The ISLET-CHIP project has brought up the need to use multiple types of MEAs that do not all have the same layout. Traditionally, the 60-electrode 8×8 grid was used, but alternative designs, with two groups of 30 electrodes and a completely different layout, were also tested to fit specific constraints on microfluidics 3.1.1. To accommodate for this and help visualize the true location of detected events, a layout manager was added to the system. It consists of a 8×16 8-bit memory that stores a channel number at its x/y coordinates. Channel numbers 0 through 254 are valid. Storing 255 in a memory slot marks the absence of a channel at the associated x/y coordinates. The memory is accessible for writing, meaning that layouts may be changed while in operation. As an illustration, Fig. D.1 shows two memory configurations that accommodate for the layouts used in ISLET-CHIP .

A

y \ x	0	1	2	3	4	5	6	7	8	9	10	11	12	13	14	15
0	255	**8**	**16**	**24**	**32**	**40**	**48**	255	255	255	255	255	255	255	255	255
1	**1**	**9**	**17**	**25**	**33**	**41**	**49**	**57**	255	255	255	255	255	255	255	255
2	**2**	**10**	**18**	**26**	**34**	**42**	**50**	**58**	255	255	255	255	255	255	255	255
3	**3**	**11**	**19**	**27**	**35**	**43**	**51**	**59**	255	255	255	255	255	255	255	255
4	**4**	**12**	**20**	**28**	**36**	**44**	**52**	**60**	255	255	255	255	255	255	255	255
5	**5**	**13**	**21**	**29**	**37**	**45**	**53**	**61**	255	255	255	255	255	255	255	255
6	**6**	**14**	**22**	**30**	**38**	**46**	**54**	**62**	255	255	255	255	255	255	255	255
7	255	**15**	**23**	**31**	**39**	**47**	**55**	255	255	255	255	255	255	255	255	255

B

y \ x	0	1	2	3	4	5	6	7	8	9	10	11	12	13	14	15
0	255	**34**	**35**	**41**	**48**	255	255	255	**60**	**52**	**44**	255	**59**	255	255	255
1	255	**32**	**40**	**49**	**42**	255	255	255	255	255	255	255	255	255	255	255
2	**25**	**24**	**33**	**9**	**50**	**57**	255	**12**	**61**	**62**	**45**	**46**	**47**	255	255	255
3	**26**	**27**	**8**	**10**	**43**	**58**	255	**5**	**20**	**53**	**55**	**36**	**37**	255	255	255
4	**16**	**17**	**18**	**1**	**2**	**51**	255	**6**	**13**	**54**	**30**	**39**	**38**	255	255	255
5	255	255	255	255	255	255	255	255	**21**	**14**	**23**	**31**	255	255	255	255
6	**4**	255	**19**	**11**	**3**	255	255	255	**15**	**22**	**28**	**29**	255	255	255	255
7	255	255	255	255	255	255	255	255	255	255	255	255	255	255	255	255

Figure D.1 – Memory configurations for two different MEA layouts. **A**: Standard 60-electrode layout. **B**: Custom microfluidic MEA layout.

D.1 High-level communication interfaces

The softcore microcontroller is the main communication organ. It offers high-level solutions to translate user instructions to modulate configuration and vice-versa. Rather than having dedicated hardware communication interfaces, accessing a module's properties is as easy as setting or reading microcontroller register values. This section describes in more detail the mechanisms of this protocol.

D.1.1 Microcontroller-VHDL blocks communication

Configuration is performed through a system bus mastered by the main softcore processor (CPU (Central Processing Unit)), which systematically associates data exchanges with a destination (address). Each module is connected to the CPU's address and data busses (Fig. D.2), and has a unique address. Therefore all modules simultaneously receive the data, but one, and only one reacts in consequence when the CPU's address bus matches his. Generally, to each address corresponds either an instruction to modify a processing parameter or a request for data readback. Since only one module is able to send readback data at a time, all read outputs are connected to a logical OR, that returns a single value to the CPU(see Fig. D.2).

In reality, because they have multiple parameters, modules have a series of consecutive [1] addresses, all unique, that serve different purposes. Following this design, each module has one address per modifiable parameter (the address gives the parameter name and the data gives the parameter value) and one readout address per output (the address gives the output name and the data gives the channel number).

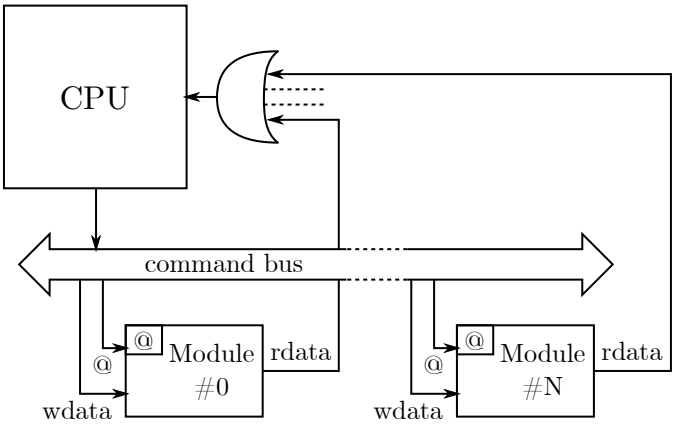

Figure D.2 – Instruction addressing scheme

D.1.2 Microcontroller-User communication

The CPU uses its UART (Universal Asynchronous Receiver/Transmitter) to communicate with the user. The port's settings are detailed in 2.2.2 p. 44.

Instructions are sent to Multimed as ASCII (American Standard Code for Information Interchange) strings composed of either a single-character (for example, to change display options) or a character followed by a number of parameters (to change a module's settings, or to request a data readout on a specific channel). In the latter case, parameters are a series of hexadecimal characters (e.g. `y049B` changes SP detection threshold to $049B_{16} = 1179_{10}$). See appendix E for a list of commands.

1. by convention

Appendix E

Configuring Multimed

E.1 Summary

Table E.1 – Configuration commands of Multimed: Glycaemia V1.3.1

Command		Description	Arguments
	R	Return to bootloader	N/A
	i	Change signal input settings	See E.2.1
	z	Launch/stop recording	See E.2.2
	%	Start comment line (ends with \n)	N/A
	$	Toggle human mode off	N/A
	@	Toggle human mode on	N/A
	E	Echo command	N/A
	V	Returns system version	N/A
	v	Enter VGA configuration	N/A
	e	Enter electrode sorting configuration	N/A
APs	c	Configure wavelet coefficients	See E.2.3
	o	Configure wavelet transform levels	See E.2.4
	I	Configure interspike intervals	See E.2.5
	T	Configure adaptive threshold	See E.2.6
	a	Configure AP frequency measurement	See E.2.7
	p	Configure FOPP measurement	See E.2.8
SPs	x	Configure SP timeout	See E.2.9
	y	Configure SP amplitude threshold	See E.2.10
	F	Configure SP filter	See E.2.11
while in VGA configuration	s	Configure SP frequency measurement	See E.2.12
	1	Select channel to display	See E.2.13
	s	Decrease timescale (slower)	N/A
	f	Increase timescale (faster)	N/A
	m	Change display mode	N/A
	n	Change display bank	N/A
	S	Toggle pause	N/A
	q	Quit VGA configuration	N/A
While in electrode sorting configuration	s	Manually select all electrodes on current cell	N/A
	c	Manually clear all electrodes on current cell	N/A
	a	Configure automatic sorting on current cell	See Table E.2
	m	Manually select electrodes on current cell	See Table E.2
	r	Read results on current cell	N/A
	0	Select sorter cell 0	N/A
	1	Select sorter cell 1	N/A
	2	Select sorter cell 2	N/A
	3	Select sorter cell 3	N/A
	*	Select final result	N/A
	o	Configure LUT output law	See E.2.14
	R	Return to bootloader	N/A
	q	Quit electrode sorting mode	N/A

E.2 Detail

Nomenclature:

— bit 7: msb
— bit 0: lsb

E.2.1 Acquisition configuration

Two hexadecimal characters (8 bits):

— bit 7: enable (1)/disable (0) acquisition
— bit 6-5: N/A
— bit 4: invert signal (1)
— bits 3-1: Gain (0-1-2-5-10-20-50-100)
— bit 0: Use PGAs (1) or in-built signals (0)

E.2.2 Recording setup

Two hexadecimal characters:

— "81": Record
— "80": Stop
— "00": Eject

A more complex (timed) recording management is also possible.

E.2.3 Wavelet coefficient configuration

Five hexadecimal characters (20 bits):

— bit 19: Mother wavelet (0)/ Father wavelet (1)
— bits 18-16: Point number
— bits 15-0: Value

E.2.4 Wavelet levels configuration

Two hexadecimal characters (8 bits):

— bits 7-4: Noise transform level
— bits 3-0: Signal transform level

E.2.5 Interspike interval configuration

Twelve hexadecimal characters (3 groups of 4 characters):

— first group: refractory period
— second group: interspike interval
— third group: interburst interval

E.2.6 Adaptive threshold configuration

Six hexadecimal characters (8+16 bits):

— bits 23-16: Select element to configure (0: configure integrator and filter, 1: configure target, 2: configure loop gain, 3: configure output gain)
— bits 15-0 (modes 1 to 3): value
— bits 7-0 (mode 0): enable integrator (bit 7), filter cutoff frequency (bits 6-0)

E.2.7 AP frequency measurement configuration

Two hexadecimal characters (8 bits):

— bits 7-6: N/A
— bit 5: first order (0) or second order (1)
— bits 4-0: cutoff frequency

E.2.8 FOPP measurement configuration

Two hexadecimal characters (8 bits):

— bits 7-6: N/A
— bit 5: first order (0) or second order (1)
— bits 4-0: cutoff frequency

E.2.9 SP timeout configuration

Two hexadecimal characters ($time\ [s] \times 1000/128$ on 8 bits)

E.2.10 SP detection threshold configuration

Four hexadecimal characters (value on 16 bits)

E.2.11 SP filter configuration

Four hexadecimal characters (16 bits):

— bits 15-8: Filter number
— bits 7-0 (filter number below 8): Cutoff frequency
— bits 7-0 (filter number equal to 16): First high-pass filter number

E.2.12 SP frequency measurement configuration

Two hexadecimal characters (8 bits):

— bits 7-6: N/A
— bit 5: first order (0) or second order (1)
— bits 4-0: cutoff frequency

E.2.13 Displayed channel selection

Two hexadecimal characters (8 bits):

— bit 7: display MSB (0) or LSB (1)
— bit 6: N/A
— bits 5-0: Channel number

E.2.14 Sortin LUT configuration

Four hexadecimal characters (mask on 16 bits)

E.2.15 Electrode sorting

Table E.2 – Format of the electrode sorting configuration two-byte argument

MSB usage

bit 7	Enable sorting
bit 6	Clear results
bits 5-4	Type select (00: None/01: Synchronization/10: Analog/11: Activity)
bit 3	Module select (Activity 0/1, Synchronization 0/1, Analog 0/1)
bits 2-1	Argument select (See below)
bit 0	Keep (0) or overwrite (1) measurement

LSB usage

MSB state		bit 7	bit 6	bit 5	bit 4	bit 3	bit 2	bit 1	bit 0
Type select (bits 5-4)	Argument select (bits 2-1)								
00	00	W[a]	-			Used modules select[b]			
01	00	-			Synchronization occurences threshold				
01	01				Accumulator threshold				
01	10				Accumulator increment			Accumulator decrement	
10	00				Analog threshold MSB				
10	01				Analog threshold LSB				
11	–	-			Accumulator threshold				

[a] When '1', enables the writing of "used modules"

[b] bit 5 is Activity #0, bit 4 is Activity #1, bit 3 is Synchronization #0, bit 2 is Synchronization #1, bit 1 is Analog #0, bit 0 is Analog#1

Appendix F

Setting up Multimed

F.1 Instructions

See Fig. 2.12 for a complete connection diagram [1]. The recommended installation scheme is as follows, with all equipment initially turned off:

- Plug the Multi Channel Systems (MCS) preamplifier (2) to Multimed (1), while being careful to connect, on the Multimed-side, the SCSI68 connector which indicator Light-Emitting Diodes (LEDs) are ON [2] (see paragraph F.2 for more information).
- If an external acquisition device (5) is used, plug it to Multimed's other SCSI68 connector while making sure its indicator LEDs are OFF.
- Plug the thermal controller (3) to the preamplifiers (2)
- Plug the USB (Universal Serial Bus) cables of both Multimed (1) and the external recording equipment (6) to the computer.
- Finally, plug the Video Graphics Array (VGA) monitor (5) to Multimed (1).

If an external filter module (7) needs to be used, be sure to plug it between Multimed (1) and the preamplifiers (2), to have both recording devices (1 and 6) receiving identical signals. It is good practice to keep the described working setup connected at all times, with all power cords (Multimed power supply, monitor power supply, thermal controller power supply, secondary acquisition device power supply and computer power supply) on a single power strip with an ON/OFF switch, acting as the main power switch. This prevents connection errors and early deterioration of regularly plugged/unplugged cables.

F.2 Safety precautions

Attention is particularly brought to the power supplies of the headstage preamplifier. Traditionally, on MCS equipment, three pins on the SCSI68 connectors are reserved for symmetrical power supply. These three same pins are powered by Multimed as indicated by LEDs (lit LEDs indicate power is on, see Fig. F.1) to provide working setups without external power supplies. If MCS equipment is indeed used with Multimed, and that equipment provides power through its connector, it is mandatory that the connection between them is made on the non-energized (indicated by off LEDs) SCSI68 port. Doing otherwise may damage either one of the power supplies.

1. Note that fluidic material (such as pumps and glassware) are not represented, as they do not interact with the electronics.
2. Multimed may be momentarily turned on to verify which connector must be used.

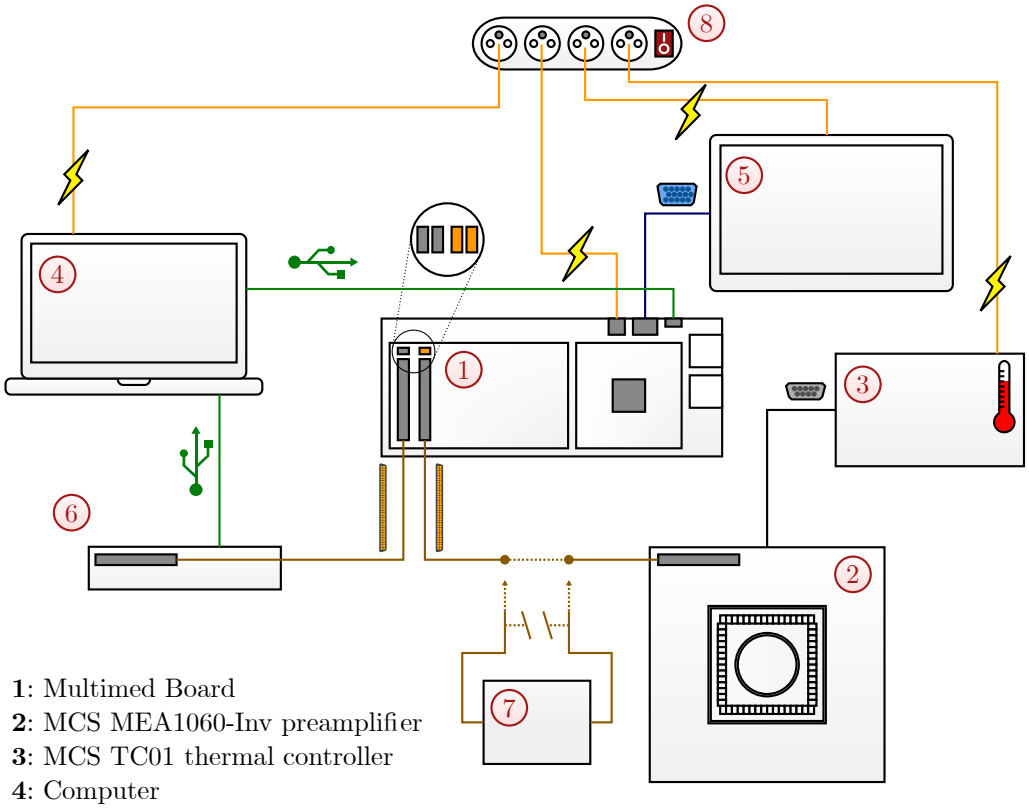

1: Multimed Board
2: MCS MEA1060-Inv preamplifier
3: MCS TC01 thermal controller
4: Computer
5: VGA monitor
6: MCS USB-ME64 acquisition board (optional)
7: Optional filters

power cord VGA connector USB connector
RS232 connector SCSI68 connector

Figure F.1 – Complete setup scheme (identical to Fig. 2.12)

Appendix G

Event correlation computation method

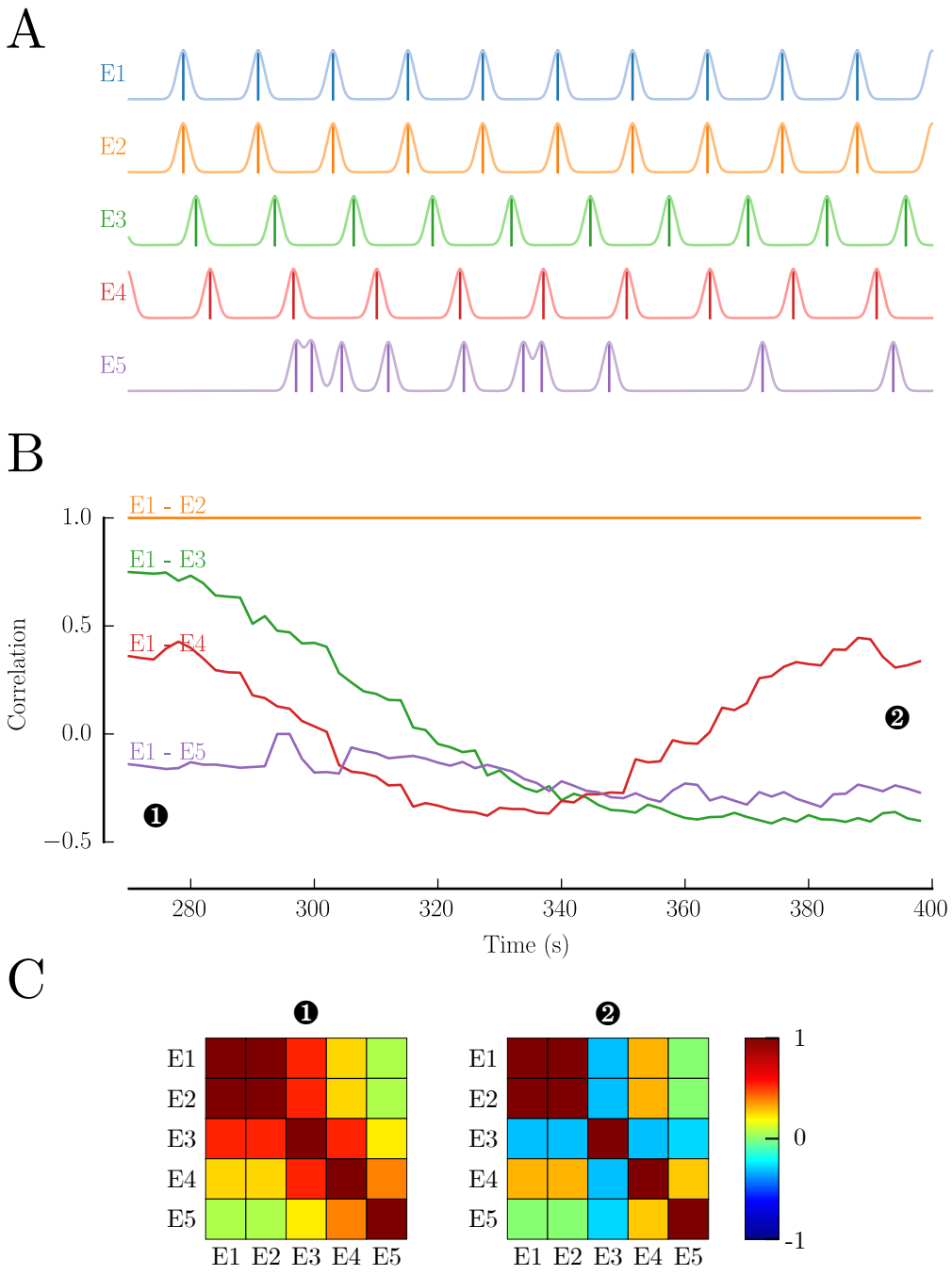

Figure G.1 – Illustration of the method used to compute temporal event correlation, and its matrix representation. **A**: Temporal detection of events (thick lines) and continuous signals constructed by correlating events with a Gaussian (thin, lighter lines). The time axis is shared with **B**. E1 and E2 are identical trains of regular events. E3 is a regular train of events, 95% the speed of E1. E4 is a regular train of events, 90% the speed of E1. E4 is a random train of events. **B**: Time-dependent correlation measurements between E1 and E2-E4. Colours indicate with which signal E1 is correlated, following the colour scheme of **A**. Note that due to frequencies of E1, E3 and E4 being extremely close, synchronization beat occurs. **C**: Matrix representations of correlation at instants ❶ and ❷, as indicated in **B**. each square represents the correlation, between -1 and 1, of the couple of electrodes given by its coordinates (hence the unitary diagonal).

Appendix H

Revised quality control protocol

After several applications, the quality control protocol was revised. Some changes are purely typographic, but others do alter the experiments (see Fig. H.1). Decision tree paths are given relative to the revised protocol:

— The starting condition was changed from G1 to G1 + Diazoxide. Diazoxide is a molecule used to inhibit insulin secretion by opening ATP-sensitive K^+ channels [194, 195]. The experiment is therefore started with a forced – and reversible – inactive state of pancreatic islets instead of plain low glucose.
— The strongly inhibiting Nifedipine condition was removed because it was rendered unnecessary by the Diazoxide condition.
— The absence of activity after G1 + Adrenaline (– +) is no longer a final condition, as it does not test cell response to physiological glucose levels. Instead, it resumes to the remainder of the protocol.
— AP activity is now distinct from SP activity. The distinction is now used in the condition G1 + Adrenaline (– +) where the presence of APs is an indicator of mainly α cell activity.
— A criteria for failure or success of the dose-response was added (at least two conditions significantly different from G1 are needed for success).
— The notation system was changed from `*`–`******` to `0`–`5`, to prevent very poor cultures from having a non-zero grade.
— Outcome labels were slightly changed, with no significant change in meaning.

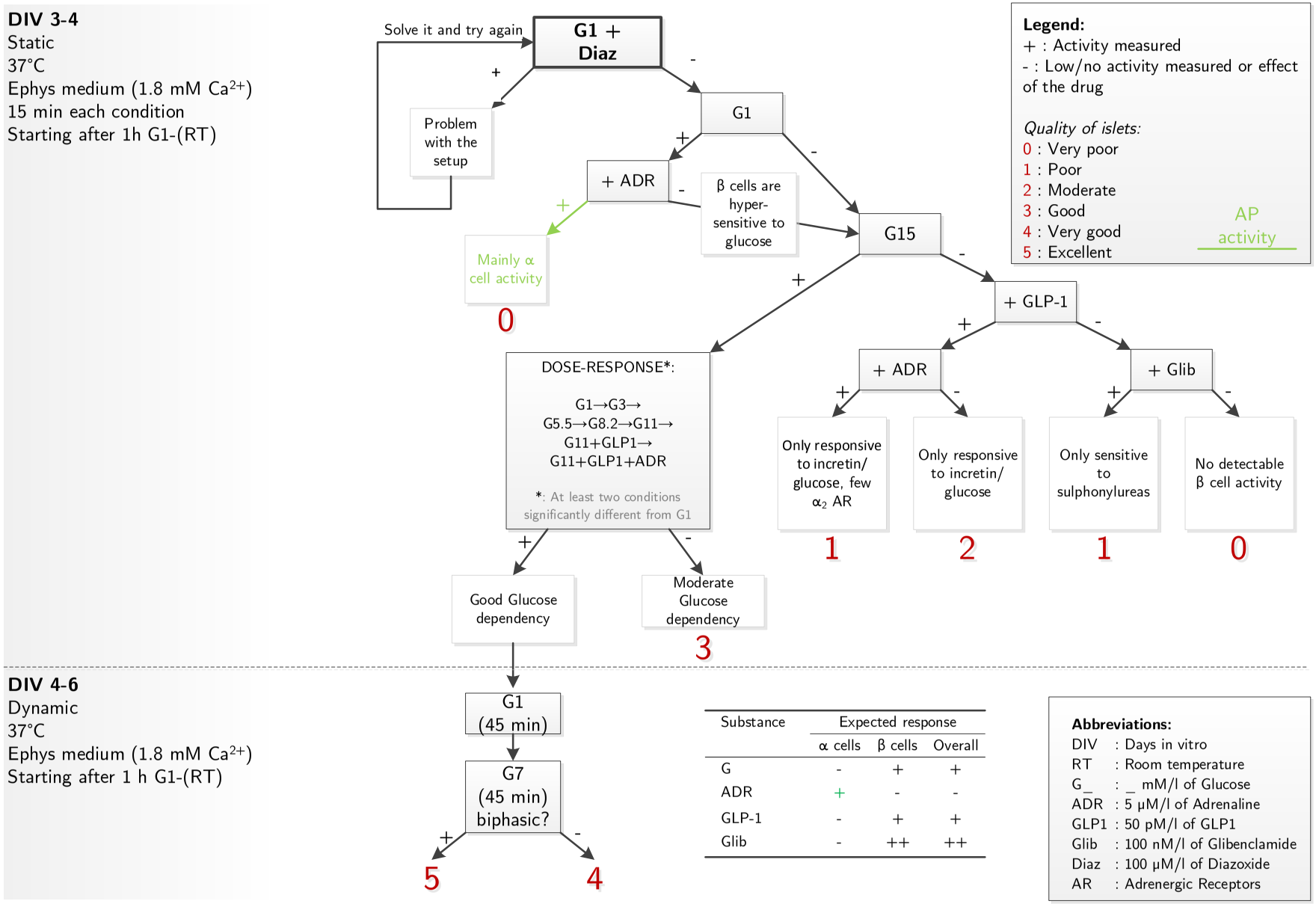

Figure H.1 – Revised islet quality control protocol. Changes were made to the notation system, the starting condition (G1+Diazoxide instead of G1), the Nifedipine condition was removed, some outcomes were modified, and AP activity was discerned from SP activity.

Appendix I

Model equations and parameters

$$\mathscr{A}(G) = \begin{cases} \dfrac{[G - G_0]^n}{[G_{50} - G_0]^n + [G - G_0]^n} & \text{if } G \geq G_0 \\ 0 & \text{otherwise} \end{cases} \tag{I.1}$$

$$f(G) = f_M \times \mathscr{A}(G) \tag{I.2a}$$

$$\gamma(X^\Gamma, G) = \begin{cases} 1 + \dfrac{[X^\Gamma - X_0^\Gamma(G)]^{n^\Gamma(G)}}{[X_{50}^\Gamma(G) - X_0^\Gamma(G)]^{n^\Gamma(G)} + [X^\Gamma - X_0^\Gamma(G)]^{n^\Gamma(G)}} & \text{if } X^\Gamma \geq X_0^\Gamma \\ 1 & \text{otherwise} \end{cases} \tag{I.2b}$$

$$\alpha(X^A) = \begin{cases} 1 - \dfrac{[X^A - X_0^A]^{n^A}}{[X_{50}^A - X_0^A]^{n^A} + [X^A - X_0^A]^{n^A}} & \text{if } X^A \geq X_0^A \\ 1 & \text{otherwise} \end{cases} \tag{I.2c}$$

$$X_0^\Gamma(G) = a_0^\Gamma \times G + b_0^\Gamma \tag{I.3a}$$

$$X_{50}^\Gamma(G) = a_{50}^\Gamma \times G + b_{50}^\Gamma \tag{I.3b}$$

$$n^\Gamma(G) = a_n^\Gamma \times G + b_n^\Gamma \tag{I.3c}$$

$$X^\Gamma = \log_{10}([\text{GLP1}]) \tag{I.3d}$$

$$X^A = \log_{10}([\text{Adr}]) \tag{I.3e}$$

$$\begin{cases} \dfrac{dY_0}{dt}(t) = -\lambda_4 \times Y_0(t) + \hat{\lambda_3}(G) \times R & \text{(I.4a)} \\ \dfrac{dY_1}{dt}(t) = -\hat{\lambda_5}(G) \times Y_1(t) + \lambda_4(t) \times Y_0(t) & \text{(I.4b)} \\ \dfrac{dF}{dt}(t) = -\lambda_2 \times F(t) + \hat{\lambda_5}(G) \times Y_1(t) & \text{(I.4c)} \\ \mathscr{F}(t) = \dfrac{\lambda_1}{\lambda_3} \times \dfrac{\lambda_3 \times \lambda_4}{\lambda_3 + \lambda_4} \times F(t) & \text{(I.4d)} \end{cases}$$

$$\mathscr{N} = \frac{\mathscr{F}}{\lambda_3} \tag{I.5}$$

$$\hat{\lambda_\cdot}(G) = \mathscr{A}(G) \times \lambda_\cdot \tag{I.6}$$

Table I.1 – Model parameters

Parameter	Value	Unit
G_0	5.5	mM
G_{50}	12.63725052	mM
n	1.58236019	.
f_M	0.82027264	Hz
a_0^Γ	5.19461662	.
b_0^Γ	-104.38095093	.
a_{50}^Γ	-0.43138251	.
b_{50}^Γ	-1.93716611	.
a_n^Γ	-1.2006536	.
b_n^Γ	26.00980396	.
X_0^A	-11.0017291	.
X_{50}^A	-8.21733483	.
n^A	10.	.
λ_1	0.36223665221897783	Hz.min
λ_2	0.038841569302492725	min^{-1}
λ_3	0.2888958602068274	min^{-1}
λ_4	0.03107371062811306	min^{-1}
λ_5	10.0	min^{-1}
R	1	.

Publications of the author

Fanny Lebreton, Antoine Pirog, Isma Belouah, Domenico Bosco, Thierry Berney, Paolo Meda, Yannick Bornat, Bogdan Catargi, Sylvie Renaud, Matthieu Raoux, and Jochen Lang. Slow potentials encode intercellular coupling and insulin demand in pancreatic beta cells. *Diabetologia*, pages 1291–1299, 2015. ISSN 0012-186X. doi: 10.1007/s00125-015-3558-z. URL http://link.springer.com/10.1007/s00125-015-3558-z

Eileen Pedraza, Aleksandar Karajić, Matthieu Raoux, Romain Perrier, Antoine Pirog, Fanny Lebreton, Stéphane Arbault, Julien Gaitan, Sylvie Renaud, Alexander Kuhn, et al. Guiding pancreatic beta cells to target electrodes in a whole-cell biosensor for diabetes. *Lab on a Chip*, 15(19):3880–3890, 2015

Catrin F Williams, David Lloyd, Jonathan Lees, Antoine Pirog, Gilles M Geroni, Jordan Pastre, Valentin Kriegel, and Adrian Porch. What the deep sea can tell us about microwaves. In *Microwave Symposium (IMS), 2016 IEEE MTT-S International*, pages 1–4. IEEE, 2016

Catrin F Williams, Gilles M Geroni, Antoine Pirog, David Lloyd, Jonathan Lees, and Adrian Porch. The separated electric and magnetic field responses of luminescent bacteria exposed to pulsed microwave irradiation. *Applied Physics Letters*, 109(9):093701, 2016

Dimitrios A Koutsouras, Romain Perrier, Ariana Villarroel Marquez, Antoine Pirog, Eileen Pedraza, Eric Cloutet, Sylvie Renaud, Matthieu Raoux, George G Malliaras, and Jochen Lang. Simultaneous monitoring of single cell and of micro-organ activity by pedot: Pss covered multi-electrode arrays. *Materials Science and Engineering: C*, 81:84–89, 2017

Matthieu Ambroise, Stefano Buccelli, Filippo Grassia, Antoine Pirog, Yannick Bornat, Michela Chiappalone, and Timothée Levi. Biomimetic neural network for modifying biological dynamics during hybrid experiments. *Artificial Life and Robotics*, pages 1–6, 2017

Bibliography

[1] Marjatta Karvonen, Maarit Viik-Kajander, Elena Moltchanova, Ingrid Libman, RONALD LaPorte, and Jaakko Tuomilehto. Incidence of childhood type 1 diabetes worldwide. diabetes mondiale (diamond) project group. *Diabetes care*, 23(10):1516–1526, 2000.

[2] EAM Gale. Type 1 diabetes in the young: the harvest of sorrow goes on, 2005.

[3] Mark A Atkinson. The pathogenesis and natural history of type 1 diabetes. *Cold Spring Harbor perspectives in medicine*, 2(11):a007641, 2012.

[4] Valma Harjutsalo, Lena Sjöberg, and Jaakko Tuomilehto. Time trends in the incidence of type 1 diabetes in finnish children: a cohort study. *The Lancet*, 371(9626):1777–1782, 2008.

[5] Ilse Weets, Jan Van Autreve, BJ Van der Auwera, FC Schuit, MVL Du Caju, Katelijn Decochez, IH De Leeuw, Bart Keymeulen, Chantal Mathieu, Raoul Rottiers, et al. Male-to-female excess in diabetes diagnosed in early adulthood is not specific for the immune-mediated form nor is it hla-dq restricted: possible relation to increased body mass index. *Diabetologia*, 44(1):40–47, 2001.

[6] Jeffrey P Krischer, David D Cuthbertson, and Carla Greenbaum. Male sex increases the risk of autoimmunity but not type 1 diabetes. *Diabetes Care*, 27(8):1985–1990, 2004.

[7] Dana Dabelea, Ronny A Bell, Ralph B D'Agostino Jr, Giuseppina Imperatore, Judith M Johansen, Barbara Linder, Lenna L Liu, Beth Loots, Santica Marcovina, Elizabeth J Mayer-Davis, et al. Incidence of diabetes in youth in the united states. *Jama*, 297(24): 2716–2724, 2007.

[8] Christina L Vandewalle, Marina I Coeckelberghs, Ivo H De Leeuw, Marc V Du Caju, Frans C Schuit, Daniel G Pipeleers, and Frans K Gorus. Epidemiology, clinical aspects, and biology of iddm patients under age 40 years: Comparison of data from antwerp with complete ascertainment with data from belgium with 40% ascertainment. the belgian diabetes registry. *Diabetes care*, 20(10):1556–1561, 1997.

[9] Christopher C Patterson, Gisela G Dahlquist, Eva Gyürüs, Anders Green, Gyula Soltész, EURODIAB Study Group, et al. Incidence trends for childhood type 1 diabetes in europe during 1989–2003 and predicted new cases 2005–20: a multicentre prospective registration study. *The Lancet*, 373(9680):2027–2033, 2009.

[10] David M Maahs, Nancy A West, Jean M Lawrence, and Elizabeth J Mayer-Davis. Epidemiology of type 1 diabetes. *Endocrinology and metabolism clinics of North America*, 39(3):481–497, 2010.

[11] Maria J Redondo, Pamela R Fain, and George S Eisenbarth. Genetics of type 1a diabetes. *Recent progress in hormone research*, 56:69–89, 2001.

[12] Jason D Cooper, Deborah J Smyth, Adam M Smiles, Vincent Plagnol, Neil M Walker, James E Allen, Kate Downes, Jeffrey C Barrett, Barry C Healy, Josyf C Mychaleckyj, et al. Meta-analysis of genome-wide association study data identifies additional type 1 diabetes risk loci. *Nature genetics*, 40(12):1399–1401, 2008.

[13] MA Atkinson, JA Bluestone, GS Eisenbarth, M Hebrok, KC Herold, D Accili, M Pietropaolo, PR Arvan, M Von Herrath, DS Markel, et al. How does type 1 diabetes develop? the notion of homicide or β-cell suicide revisited (diabetes (2011) 60,(1370-1379)). *Diabetes*, 61(6), 2012.

[14] Daria La Torre and Åke Lernmark. Immunology of β-cell destruction. In *The Islets of Langerhans*, pages 537–583. Springer, 2010.

[15] Jeffrey A Bluestone, Kevan Herold, and George Eisenbarth. Genetics, pathogenesis and clinical interventions in type 1 diabetes. *Nature*, 464(7293):1293, 2010.

[16] Steven L Rabinowe and George S Eisenbarth. Type i diabetes mellitus: a chronic autoimmune disease? *Pediatric Clinics of North America*, 31(3):531–543, 1984.

[17] Meredith S Campbell, Desmond A Schatz, Vincent Chen, Jenise C Wong, Andrea Steck, William V Tamborlane, Jennifer Smith, Roy W Beck, Eda Cengiz, Lori M Laffel, et al. A contrast between children and adolescents with excellent and poor control: the t1d exchange clinic registry experience. *Pediatric diabetes*, 15(2):110–117, 2014.

[18] Scott M Blackman, Dan Raghinaru, Saleh Adi, Jill H Simmons, Laurie Ebner-Lyon, H Peter Chase, William V Tamborlane, Desmond A Schatz, Jennifer M Block, Jean C Litton, et al. Insulin pump use in young children in the t1d exchange clinic registry is associated with lower hemoglobin a1c levels than injection therapy. *Pediatric diabetes*, 15(8):564–572, 2014.

[19] Romesh Khardori and G Griffing. Type 2 diabetes mellitus treatment & management. *Retrieved online July*, 16:2011, 2011.

[20] Sandrine Lablanche, Sophie Borot, Anne Wojtusciszyn, Francois Bayle, Rachel Tétaz, Lionel Badet, Charles Thivolet, Emmanuel Morelon, Luc Frimat, Alfred Penfornis, et al. Five-year metabolic, functional, and safety results of patients with type 1 diabetes transplanted with allogenic islets within the swiss-french gragil network. *Diabetes Care*, 38 (9):1714–1722, 2015.

[21] Nalani Haviland, John Walsh, Ruth Roberts, and Timothy S Bailey. Update on Clinical Utility of Continuous Glucose Monitoring in Type 1 Diabetes. *Current Diabetes Reports*, 16(11):115, 2016. ISSN 1539-0829. doi: 10.1007/s11892-016-0808-5. URL http://dx.doi.org/10.1007/s11892-016-0808-5.

[22] Roy W Beck, Tonya Riddlesworth, Katrina Ruedy, Andrew Ahmann, Richard Bergenstal, Stacie Haller, Craig Kollman, Davida Kruger, Janet B Mcgill, William Polonsky, Elena Toschi, Howard Wolpert, and David Price. Effect of Continuous Glucose Monitoring on Glycemic Control in Adults With Type 1 Diabetes Using Insulin Injections The DIAMOND Randomized Clinical Trial. 33647(4):371–378, 2017. doi: 10.1001/jama.2016.19975.

[23] Felix Aberer, Martin Hajnsek, Markus Rumpler, Sabine Zenz, Petra M Baumann, Hesham Elsayed, Adelheid Puffing, Gerlies Treiber, Thomas R Pieber, Harald Sourij, et al. Evaluation of subcutaneous glucose monitoring systems under routine environmental conditions in patients with type 1 diabetes. *Diabetes, Obesity and Metabolism*, 2017.

[24] Jort Kropff and J Hans DeVries. Continuous glucose monitoring, future products, and update on worldwide artificial pancreas projects. *Diabetes technology & therapeutics*, 18 (S2):S2–53, 2016.

[25] Elena Toschi and Howard Wolpert. Utility of continuous glucose monitoring in type 1 and type 2 diabetes. *Endocrinology and metabolism clinics of North America*, 45(4): 895–904, 2016.

[26] Volker Lodwig, Bernhard Kulzer, Oliver Schnell, and Lutz Heinemann. Current trends in continuous glucose monitoring. *Journal of diabetes science and technology*, 8(2):390–396, 2014.

[27] David C Klonoff, Bruce Buckingham, Jens S Christiansen, Victor M Montori, William V Tamborlane, Robert A Vigersky, and Howard Wolpert. Continuous glucose monitoring: an endocrine society clinical practice guideline. *The Journal of Clinical Endocrinology & Metabolism*, 96(10):2968–2979, 2011.

[28] Paul Zimmet, Catherine Cowie, Jean-Marie Ekoe, and Jonathan Shaw. Classification of diabetes mellitus and other categories of glucose intolerance. *International Textbook of Diabetes Mellitus*, 2004.

[29] Ciara Morris, Colm M O'Grada, Miriam F Ryan, Michael J Gibney, Helen M Roche, Eileen R Gibney, and Lorraine Brennan. Modulation of the lipidomic profile due to a lipid challenge and fitness level: a postprandial study. *Lipids in health and disease*, 14 (1):65, 2015.

[30] Jing Cen, Ernest Sargsyan, and Peter Bergsten. Fatty acids stimulate insulin secretion from human pancreatic islets at fasting glucose concentrations via mitochondria-dependent and-independent mechanisms. *Nutrition & metabolism*, 13(1):59, 2016.

[31] George Dimitriadis, Panayota Mitrou, Vaia Lambadiari, Eirini Maratou, and Sotirios A Raptis. Insulin effects in muscle and adipose tissue. *Diabetes research and clinical practice*, 93:S52–S59, 2011.

[32] Werner Waldhäusl. Circadian rhythms of insulin needs and actions. *Diabetes research and clinical practice*, 6(4):S17–S24, 1989.

[33] Anthony JM Verberne, Willian S Korim, Azadeh Sabetghadam, and Ida J Llewellyn-Smith. Adrenaline: insights into its metabolic roles in hypoglycaemia and diabetes. *British journal of pharmacology*, 173(9):1425–1437, 2016.

[34] Constantin Ionescu-Tirgoviste, Paul A Gagniuc, Elvira Gubceac, Liliana Mardare, Irinel Popescu, Simona Dima, and Manuella Militaru. A 3d map of the islet routes throughout the healthy human pancreas. *Scientific reports*, 5, 2015.

[35] Jochen Lang. Molecular mechanisms and regulation of insulin exocytosis as a paradigm of endocrine secretion. *The FEBS Journal*, 259(1-2):3–17, 1999.

[36] Leonid E Fridlyand, David A Jacobson, and LH Philipson. Ion channels and regulation of insulin secretion in human β-cells: a computational systems analysis. *Islets*, 5(1):1–15, 2013.

[37] Leonid E Fridlyand, DA Jacobson, A Kuznetsov, and Louis H Philipson. A model of action potentials and fast ca 2+ dynamics in pancreatic β-cells. *Biophysical Journal*, 96 (8):3126–3139, 2009.

[38] HP Meissner and H Schmelz. Membrane potential of beta-cells in pancreatic islets. *Pflügers Archiv European Journal of Physiology*, 351(3):195–206, 1974.

[39] Patrik Rorsman, Krister Bokvist, Carina Ämmälä, Per Arkhammar, Per-Olof Berggren, Olof Larsson, and Karin Wåhlander. Activation by adrenaline of a low-conductance g protein-dependent k+ channel in mouse pancreatic b cells. *Nature*, 349(6304):77–79, 1991.

[40] Jonathan E Campbell and Daniel J Drucker. Pharmacology, physiology, and mechanisms of incretin hormone action. *Cell metabolism*, 17(6):819–837, 2013.

[41] Guy A Rutter, Timothy J Pullen, David J Hodson, and Aida Martinez-Sanchez. Pancreatic β-cell identity, glucose sensing and the control of insulin secretion. *Biochemical Journal*, 466(2):203–218, 2015.

[42] Yoram Palti, Galia Ben David, Ela Lachov, Yuval H Mika, Gila Omri, and Rachel Schatzberger. Islets of langerhans generate wavelike electric activity modulated by glucose concentration. *Diabetes*, 45(5):595–601, 1996.

[43] Fanny Lebreton, Antoine Pirog, Isma Belouah, Domenico Bosco, Thierry Berney, Paolo Meda, Yannick Bornat, Bogdan Catargi, Sylvie Renaud, Matthieu Raoux, and Jochen Lang. Slow potentials encode intercellular coupling and insulin demand in pancreatic beta cells. *Diabetologia*, pages 1291–1299, 2015. ISSN 0012-186X. doi: 10.1007/s00125-015-3558-z. URL http://link.springer.com/10.1007/s00125-015-3558-z.

[44] Alan L Hodgkin and Andrew F Huxley. Propagation of electrical signals along giant nerve fibres. *Proceedings of the Royal Society of London. Series B, Biological Sciences*, pages 177–183, 1952.

[45] Erwin Neher and Bert Sakmann. Single-channel currents recorded from membrane of denervated frog muscle fibres. *Nature*, 260(5554):799–802, 1976.

[46] Owen P Hamill, A Marty, Erwin Neher, Bert Sakmann, and FJ Sigworth. Improved patch-clamp techniques for high-resolution current recording from cells and cell-free membrane patches. *Pflügers Archiv European journal of physiology*, 391(2):85–100, 1981.

[47] Luca Berdondini, Kilian Imfeld, Alessandro Maccione, Mariateresa Tedesco, Simon Neukom, Milena Koudelka-Hep, and Sergio Martinoia. Active pixel sensor array for high spatio-temporal resolution electrophysiological recordings from single cell to large scale neuronal networks. *Lab on a Chip*, 9(18):2644–2651, 2009.

[48] Alessandro Maccione, Matteo Garofalo, Thierry Nieus, Mariateresa Tedesco, Luca Berdondini, and Sergio Martinoia. Multiscale functional connectivity estimation on low-density neuronal cultures recorded by high-density cmos micro electrode arrays. *Journal of neuroscience methods*, 207(2):161–171, 2012.

[49] Christina Hassler, Tim Boretius, and Thomas Stieglitz. Polymers for neural implants. *Journal of Polymer Science Part B: Polymer Physics*, 49(1):18–33, 2011.

[50] Raeyoung Kim, Sunghoon Joo, Hyunjun Jung, Nari Hong, and Yoonkey Nam. Recent trends in microelectrode array technology for in vitro neural interface platform. *Biomedical Engineering Letters*, 4(2):129–141, 2014.

[51] Xinyan Cui, Valerie A Lee, Yehoash Raphael, James A Wiler, Jamille F Hetke, David J Anderson, and David C Martin. Surface modification of neural recording electrodes with conducting polymer/biomolecule blends. *Journal of Biomedical Materials Research Part A*, 56(2):261–272, 2001.

[52] Wendy Franks, Iwan Schenker, Patrik Schmutz, and Andreas Hierlemann. Impedance characterization and modeling of electrodes for biomedical applications. *IEEE Transactions on Biomedical Engineering*, 52(7):1295–1302, 2005.

[53] Kip A Ludwig, Jeffrey D Uram, Junyan Yang, David C Martin, and Daryl R Kipke. Chronic neural recordings using silicon microelectrode arrays electrochemically deposited with a poly (3, 4-ethylenedioxythiophene)(pedot) film. *Journal of neural engineering*, 3 (1):59, 2006.

[54] Edward W Keefer, Barry R Botterman, Mario I Romero, Andrew F Rossi, and Guenter W Gross. Carbon nanotube coating improves neuronal recordings. *Nature nanotechnology*, 3(7):434–439, 2008.

[55] Vijay Viswam, David Jäckel, Marco Ballini, Jan Müller, Milos Radivojevic, Urs Frey, Felix Franke, and Andreas Hierlemann. An automated method for characterizing electrode properties of high-density microelectrode arrays. In *Proceedings MEA Meeting 2014: July 1-July 4, 2014, Reutlingen, Germany: 9th International Meeting on Substrate-Integrated Microelectrode Arrays*, volume 9, pages 302–303. NMI Natural and Medical Sciences Institute at the University of Tuebingen, 2014.

[56] Yoonkey Nam and Bruce C Wheeler. In vitro microelectrode array technology and neural recordings. *Critical Reviews^{TM} in Biomedical Engineering*, 39(1), 2011.

[57] Marie Engelene J Obien, Kosmas Deligkaris, Torsten Bullmann, Douglas J Bakkum, and Urs Frey. Revealing neuronal function through microelectrode array recordings. *Frontiers in neuroscience*, 8:423, 2015.

[58] Paul L Nunez and Ramesh Srinivasan. *Electric fields of the brain: the neurophysics of EEG*. Oxford University Press, USA, 2006.

[59] Peter Fromherz. Semiconductor chips with ion channels, nerve cells and brain. *Physica E: low-dimensional systems and nanostructures*, 16(1):24–34, 2003.

[60] Parikha Mehrotra. Biosensors and their applications–a review. *Journal of oral biology and craniofacial research*, 6(2):153–159, 2016.

[61] JJ Pancrazio, JP Whelan, DA Borkholder, W Ma, and DA Stenger. Development and application of cell-based biosensors. *Annals of biomedical engineering*, 27(6):697–711, 1999.

[62] Christiane Ziegler. Cell-based biosensors. *Fresenius' journal of analytical chemistry*, 366 (6-7):552–559, 2000.

[63] CA Corcoran and GA Rechnitz. Cell-based biosensors. *Trends in Biotechnology*, 3(4): 92–96, 1985.

[64] Craig S Nunemaker, Min Zhang, David H Wasserman, Owen P McGuinness, Alvin C Powers, Richard Bertram, Arthur Sherman, and Leslie S Satin. Individual mice can be distinguished by the period of their islet calcium oscillations. *Diabetes*, 54(12):3517–3522, 2005.

[65] Dong Song, Rosa HM Chan, Vasilis Z Marmarelis, Robert E Hampson, Sam A Deadwyler, and Theodore W Berger. Nonlinear modeling of neural population dynamics for hippocampal prostheses. *Neural Networks*, 22(9):1340–1351, 2009.

[66] Adeline Zbrzeski, Yannick Bornat, Brian Hillen, Ricardo Siu, James Abbas, Ranu Jung, and Sylvie Renaud. Bio-inspired Controller on an FPGA applied to Closed-loop Diaphragmatic Stimulation. *Frontiers in Neuroscience*, 10:275, 2016. doi: 10.3389/FNINS.2016.00275.

[67] Stefano Buccelli, Jacopo Tessadori, Yannick Bornat, Valentina Pasquale, Matthieu Ambroise, Timothée Levi, Paolo Massobrio, and Michela Chiappalone. Connecting biological and artificial neural networks.

[68] Arianna Bruzzone, Valentina Pasquale, Przemyslaw Nowak, Jacopo Tessadori, Paolo Massobrio, and Michela Chiappalone. Interfacing in silico and in vitro neuronal networks. In *Engineering in Medicine and Biology Society (EMBC), 2015 37th Annual International Conference of the IEEE*, pages 3391–3394. IEEE, 2015.

[69] J. Lang, B. Catargi, S. Renaud, M. Raoux, G. Charpentier, and Y. Bornat. Capteur pour la mesure de l'activite des cellules .beta.-pancreatiques ou des ilots de langerhans, fabrication et utilisation d'un tel capteur, July 21 2011. URL https://encrypted.google.com/patents/CA2787302A1?cl=ar. CA Patent App. CA 2,787,302.

[70] Adam Quotb, Yannick Bornat, and Sylvie Renaud. Wavelet transform for real-time detection of action potentials in neural signals. *Frontiers in neuroengineering*, 4(July): 7, 2011. ISSN 1662-6443. doi: 10.3389/fneng.2011.00007.

[71] Camillo Ricordi, Derek WR Gray, Bernhard J Hering, Dixon B Kaufman, Garth L Warnock, Norman M Kneteman, Stephen P Lake, Nicholas JM London, Carlo Socci, Rodolfo Alejandro, et al. Islet isolation assessment in man and large animals. *Acta diabetologia latina*, 27(3):185–195, 1990.

[72] Mpm Van der Burg, M Scheringa, I Basir, and E Bouwman. Assessment of isolated islet equivalents. In *Transplantation proceedings*, volume 29, pages 1971–1973. Elsevier, 1997.

[73] Karthik Ramachandran, Han-Hung Huang, and Lisa Stehno-Bittel. A simple method to replace islet equivalents for volume quantification of human islets. *Cell transplantation*, 24(7):1183–1194, 2015.

[74] Peter Girman, Zuzana Berkova, Eva Dobolilova, and Frantisek Saudek. How to use image analysis for islet counting. *The review of diabetic studies: RDS*, 5(1):38, 2008.

[75] Jan Müller, Douglas J. Bakkum, and Andreas Hierlemann. Sub-millisecond closed-loop feedback stimulation between arbitrary sets of individual neurons. *Front. Neural Circuits*, 6(121), 2013.

[76] A versatile electrode sorting module for meas: implementation in a fpga-based real-time system. In *Biomedical Circuits and Systems Conference, 2017, BioCAS 2007. IEEE*. IEEE, 2017.

[77] Paolo Bonifazi, Francesco Difato, Paolo Massobrio, Gian L Breschi, Valentina Pasquale, Timothée Levi, Miri Goldin, Yannick Bornat, Mariateresa Tedesco, Marta Bisio, et al. In vitro large-scale experimental and theoretical studies for the realization of bi-directional brain-prostheses. 2013.

[78] A M Zbrzeski, R. Siu, Y. Bornat, B K Hillen, R. Jung, Senior Member, and S. Renaud. A Versatile Fast-Development Platform applied to Closed-Loop Diaphragmatic Pacing. *2015 7th International IEEE/EMBS Conference on Neural Engineering (NER)*, pages 22–24, apr 2015. doi: 10.1109/NER.2015.7146742. URL http://ieeexplore.ieee.org/document/7146742/.

[79] Sébastien Joucla, Matthieu Ambroise, Timothée Levi, Thierry Lafon, Philippe Chauvet, Lionel Rousseau, Gaëlle Lissorgues, Sylvain Saïghi, Yannick Bornat, Noëlle Lewis, Sylvie Renaud, and Blaise Yvert. Generation of locomotor-like activity in the isolated rat spinal cord by electrical microstimulations driven by an artificial CPG. *2013 IEEE Neural Engineering Short Papers No. 0079*, page 5218, 2013.

[80] Jonathan P. Newman, Riley Zeller-Townson, Ming-Fai Fong, Sharanya Arcot Desai, Robert E. Gross, and Steve M. Potter. Closed-loop, multichannel experimentation using the open-source NeuroRighter electrophysiology platform. *Front. Neural Circuits*, 6(98), 2013.

[81] K. Imfeld, S. Neukom, A. Maccione, Y. Bornat, S. Martinoia, P.-A. Farine, M. Koudelka-Hep, and L. Berdondini. Large-Scale, High-Resolution Data Acquisition System for Extracellular Recording of Electrophysiological Activity. *IEEE Transactions on Biomedical Engineering*, 55(8):2064–2073, aug 2008. ISSN 0018-9294. doi: 10.1109/TBME.2008.919139. URL http://ieeexplore.ieee.org/document/4567617/.

[82] M S Fee, P P Mitra, and D Kleinfeld. Variability of extracellular spike waveforms of cortical neurons. *Journal of neurophysiology*, 76(6):3823–33, dec 1996. ISSN 0022-3077. URL http://www.ncbi.nlm.nih.gov/pubmed/8985880.

[83] K.S Guillory and R.A Normann. A 100-channel system for real time detection and storage of extracellular spike waveforms. *Journal of Neuroscience Methods*, 91(1):21–29, 1999. ISSN 01650270. doi: 10.1016/S0165-0270(99)00076-X.

[84] R.R. Harrison. A low-power integrated circuit for adaptive detection of action potentials in noisy signals. *Proceedings of the 25th Annual International Conference of the IEEE Engineering in Medicine and Biology Society (IEEE Cat. No.03CH37439)*, 4:3325–3328, 2003. ISSN 1094-687X. doi: 10.1109/IEMBS.2003.1280856.

[85] François Rummens, Stéphane Ygorra, Hol C. Mayiss Boussamba, Sylvie Renaud, and Noëlle Lewis. Theoretical study and optimisation of a standard deviation estimator circuit for adaptive threshold spike detection. *International Journal of Circuit Theory and Applications*, 2016. ISSN 00989886. doi: 10.1002/cta.2192.

[86] T. Burdyga and Susan Wray. Action potential refractory period in ureter smooth muscle is set by Ca sparks and BK channels. *Nature*, 436(7050):559–562, jul 2005. ISSN 0028-0836. doi: 10.1038/nature03834. URL http://www.nature.com/doifinder/10.1038/nature03834.

[87] Eileen Pedraza, Aleksandar Karajić, Matthieu Raoux, Romain Perrier, Antoine Pirog, Fanny Lebreton, Stéphane Arbault, Julien Gaitan, Sylvie Renaud, Alexander Kuhn, et al. Guiding pancreatic beta cells to target electrodes in a whole-cell biosensor for diabetes. *Lab on a Chip*, 15(19):3880–3890, 2015.

[88] Micha E Spira and Aviad Hai. Multi-electrode array technologies for neuroscience and cardiology. *Nature nanotechnology*, 8(2):83–94, 2013.

[89] Roy Biran, David C Martin, and Patrick A Tresco. Neuronal cell loss accompanies the brain tissue response to chronically implanted silicon microelectrode arrays. *Experimental neurology*, 195(1):115–126, 2005.

[90] Florian Kölbl. *Design of electrical adaptive stimulators for different pathological contexts: a global approach*. PhD thesis, Université de Bordeaux, 2014.

[91] James Friend and Leslie Yeo. Fabrication of microfluidic devices using polydimethylsiloxane. *Biomicrofluidics*, 4(2), mar 2010. ISSN 1932-1058. doi: 10.1063/1.3259624. URL http://www.ncbi.nlm.nih.gov/pubmed/20697575http://www.pubmedcentral.nih.gov/articlerender.fcgi?artid=PMC2917889.

[92] Takashi DY Kozai, Kasey Catt, Zhanhong Du, Kyounghwan Na, Onnop Srivannavit, M Haque Razi-ul, John Seymour, Kensall D Wise, Euisik Yoon, and Xinyan Tracy Cui. Chronic in vivo evaluation of pedot/cnt for stable neural recordings. *IEEE Transactions on Biomedical Engineering*, 63(1):111–119, 2016.

[93] Xinyan Cui and David C Martin. Electrochemical deposition and characterization of poly (3, 4-ethylenedioxythiophene) on neural microelectrode arrays. *Sensors and Actuators B: Chemical*, 89(1):92–102, 2003.

[94] Andrea Mazzatenta, Michele Giugliano, Stephane Campidelli, Luca Gambazzi, Luca Businaro, Henry Markram, Maurizio Prato, and Laura Ballerini. Interfacing neurons with carbon nanotubes: electrical signal transfer and synaptic stimulation in cultured brain circuits. *Journal of Neuroscience*, 27(26):6931–6936, 2007.

[95] Giada Cellot, Emanuele Cilia, Sara Cipollone, Vladimir Rancic, Antonella Sucapane, Silvia Giordani, Luca Gambazzi, Henry Markram, Micaela Grandolfo, Denis Scaini, et al. Carbon nanotubes might improve neuronal performance by favouring electrical shortcuts. *Nature nanotechnology*, 4(2):126–133, 2009.

[96] Kai Fuchsberger, Alan Le Goff, Luca Gambazzi, Francesca Maria Toma, Andrea Goldoni, Michele Giugliano, Martin Stelzle, and Maurizio Prato. Multiwalled carbon-nanotube-functionalized microelectrode arrays fabricated by microcontact printing: Platform for studying chemical and electrical neuronal signaling. *Small*, 7(4):524–530, 2011.

[97] A Pasquarelli, V Carabelli, Y Xu, Z Gao, A Marcantoni, E Kohn, and E Carbone. Diamond microelectrodes for amperometric detection of secretory cells activity. In *World Congress on Medical Physics and Biomedical Engineering, September 7-12, 2009, Munich, Germany*, pages 208–211. Springer, 2009.

[98] Dimitrios A Koutsouras, Romain Perrier, Ariana Villarroel Marquez, Antoine Pirog, Eileen Pedraza, Eric Cloutet, Sylvie Renaud, Matthieu Raoux, George G Malliaras, and Jochen Lang. Simultaneous monitoring of single cell and of micro-organ activity by pedot: Pss covered multi-electrode arrays. *Materials Science and Engineering: C*, 81: 84–89, 2017.

[99] Quang Vinh Nguyen, Anton Caro, Matthieu Raoux, Adam Quotb, Jean Baptiste Floderer, Yannick Bornat, Sylvie Renaud, and Jochen Lang. A novel bioelectronic glucose sensor to process distinct electrical activities of pancreatic beta-cells. *Proceedings of the Annual International Conference of the IEEE Engineering in Medicine and Biology Society, EMBS*, pages 172–175, 2013. ISSN 1557170X. doi: 10.1109/EMBC.2013.6609465.

[100] Pascal Bucher, Zoltan Mathe, Philippe Morel, Domenico Bosco, Axel Andres, Manfred Kurfuest, Olaf Friedrich, Nicole Raemsch-Guenther, Leo H Buhler, and Thierry Berney. Assessment of a novel two-component enzyme preparation for human islet isolation and transplantation. *Transplantation*, 79(1):91–97, 2005.

[101] Sandrine Lablanche, Sandra David-Tchouda, Sophie Borot, Anne Wojtusciszyn, Jennifer Margier, Rachel Tetaz, Lionel Badet, Charles Thivolet, Fanny Buron, Emmanuel Morelon, et al. A randomized, prospective, medico-economic nationwide french study of islet transplantation in patients with type 1 brittle diabetes: The stabilot study protocol. *Transplant International*, 28:469, 2015.

[102] Susanne Schreiber, Jean-Marc Fellous, D Whitmer, P Tiesinga, and Terrence J Sejnowski. A new correlation-based measure of spike timing reliability. *Neurocomputing*, 52:925–931, 2003.

[103] Teresa Ree Chay and Joel Keizer. Minimal model for membrane oscillations in the pancreatic beta-cell. *Biophysical journal*, 42(2):181–189, 1983.

[104] P Rorsman. The pancreatic beta-cell as a fuel sensor: an electrophysiologist's viewpoint. *Diabetologia*, 40(5):487–495, 1997.

[105] I Atwater, CM Dawson, A Scott, G Eddlestone, and E Rojas. The nature of the oscillatory behaviour in electrical activity from pancreatic beta-cell. *Hormone and metabolic research. Supplement series*, pages 100–107, 1980.

[106] ILLANI Atwater, B Ribalet, and E Rojas. Cyclic changes in potential and resistance of the beta-cell membrane induced by glucose in islets of langerhans from mouse. *The Journal of physiology*, 278(1):117–139, 1978.

[107] Daniel Porte Jr. A receptor mechanism for the inhibition of insulin release by epinephrine in man. *Journal of Clinical Investigation*, 46(1):86, 1967.

[108] Yang Z De Marinis, Albert Salehi, Caroline E Ward, Quan Zhang, Fernando Abdulkader, Martin Bengtsson, Orit Braha, Matthias Braun, Reshma Ramracheya, Stefan Amisten, et al. Glp-1 inhibits and adrenaline stimulates glucagon release by differential modulation of n-and l-type ca 2+ channel-dependent exocytosis. *Cell metabolism*, 11(6):543–553, 2010.

[109] Craig S Nunemaker, David H Wasserman, Owen P McGuinness, Ian R Sweet, Jeanette C Teague, and Leslie S Satin. Insulin secretion in the conscious mouse is biphasic and pulsatile. *American Journal of Physiology-Endocrinology and Metabolism*, 290(3):E523–E529, 2006.

[110] Jean-Claude Henquin, Denis Dufrane, Julie Kerr-Conte, and Myriam Nenquin. Dynamics of glucose-induced insulin secretion in normal human islets. *American Journal of Physiology-Endocrinology and Metabolism*, 309(7):E640–E650, 2015.

[111] Morten Gram Pedersen, Giuliana Cortese, and Lena Eliasson. Mathematical modeling and statistical analysis of calcium-regulated insulin granule exocytosis in β-cells from mice and humans. *Progress in biophysics and molecular biology*, 107(2):257–264, 2011.

[112] Patrik Rorsman, Lena Eliasson, Erik Renström, Jesper Gromada, Sebastian Barg, and Sven Göpel. The cell physiology of biphasic insulin secretion. *Physiology*, 15(2):72–77, 2000.

[113] AM Albisser, BS Leibel, TG Ewart, Z Davidovac, CK Botz, and W Zingg. An artificial endocrine pancreas. *Diabetes*, 23(5):389–396, 1974.

[114] Ali Cinar. Multivariable adaptive artificial pancreas system in type 1 diabetes. *Current Diabetes Reports*, 17(10):88, 2017.

[115] Ishan Ajmera, Maciej Swat, Camille Laibe, Nicolas Le Novere, and Vijayalakshmi Chelliah. The impact of mathematical modeling on the understanding of diabetes and related complications. *CPT: pharmacometrics & systems pharmacology*, 2(7):1–14, 2013.

[116] Victor W Bolie. Coefficients of normal blood glucose regulation. *Journal of Applied Physiology*, 16(5):783–788, 1961.

[117] Richard N Bergman, Lawrence S Phillips, and Claudio Cobelli. Physiologic evaluation of factors controlling glucose tolerance in man: measurement of insulin sensitivity and beta-cell glucose sensitivity from the response to intravenous glucose. *Journal of clinical investigation*, 68(6):1456, 1981.

[118] Richard N Bergman, Y Ziya Ider, Charles R Bowden, and Claudio Cobelli. Quantitative estimation of insulin sensitivity. *American Journal of Physiology-Endocrinology And Metabolism*, 236(6):E667, 1979.

[119] Claudio Cobelli, Chiara Dalla Man, Giovanni Sparacino, Lalo Magni, Giuseppe De Nicolao, and Boris P Kovatchev. Diabetes: models, signals, and control. *IEEE reviews in biomedical engineering*, 2:54–96, 2009.

[120] Andrea De Gaetano and Ovide Arino. Mathematical modelling of the intravenous glucose tolerance test. *Journal of mathematical biology*, 40(2):136–168, 2000.

[121] Hanna E Silber, Petra M Jauslin, Nicolas Frey, Ronald Gieschke, Ulrika SH Simonsson, and Mats O Karlsson. An integrated model for glucose and insulin regulation in healthy volunteers and type 2 diabetic patients following intravenous glucose provocations. *The Journal of Clinical Pharmacology*, 47(9):1159–1171, 2007.

[122] Cornelia B Landersdorfer and William J Jusko. Pharmacokinetic/pharmacodynamic modelling in diabetes mellitus. *Clinical pharmacokinetics*, 47(7):417–448, 2008.

[123] Andrea Mari. Mathematical modeling in glucose metabolism and insulin secretion. *Current Opinion in Clinical Nutrition & Metabolic Care*, 5(5):495–501, 2002.

[124] Tara M Wallace, Jonathan C Levy, and David R Matthews. Use and abuse of homa modeling. *Diabetes care*, 27(6):1487–1495, 2004.

[125] LL Kjems, A Vølund, and Sten Madsbad. Quantification of beta-cell function during ivgtt in type ii and non-diabetic subjects: assessment of insulin secretion by mathematical methods. *Diabetologia*, 44(10):1339–1348, 2001.

[126] R Philip Eaton, RC Allen, DS Schade, KM Erickson, and J Standefer. Prehepatic insulin production in man: kinetic analysis using peripheral connecting peptide behavior. *The Journal of Clinical Endocrinology & Metabolism*, 51(3):520–528, 1980.

[127] Morten Gram Pedersen, Gianna M Toffolo, and Claudio Cobelli. Cellular modeling: insight into oral minimal models of insulin secretion. *American Journal of Physiology-Endocrinology and Metabolism*, 298(3):E597–E601, 2010.

[128] Mingzhan Huang, Jiaxu Li, Xinyu Song, and Hongjian Guo. Modeling impulsive injections of insulin: towards artificial pancreas. *SIAM Journal on Applied Mathematics*, 72 (5):1524–1548, 2012.

[129] Gianluca Nucci and Claudio Cobelli. Models of subcutaneous insulin kinetics. a critical review. *Computer methods and programs in biomedicine*, 62(3):249–257, 2000.

[130] Jiaxu Li and James D Johnson. Mathematical models of subcutaneous injection of insulin analogues: a mini-review. *Discrete and continuous dynamical systems. Series B*, 12(2): 401, 2009.

[131] Naviyn Prabhu Balakrishnan, Gade Pandu Rangaiah, and Lakshminarayanan Samavedham. Review and analysis of blood glucose (bg) models for type 1 diabetic patients. *Industrial & Engineering Chemistry Research*, 50(21):12041–12066, 2011.

[132] Roman Hovorka, Valentina Canonico, Ludovic J Chassin, Ulrich Haueter, Massimo Massi-Benedetti, Marco Orsini Federici, Thomas R Pieber, Helga C Schaller, Lukas Schaupp, Thomas Vering, et al. Nonlinear model predictive control of glucose concentration in subjects with type 1 diabetes. *Physiological measurement*, 25(4):905, 2004.

[133] Chiara Dalla Man, Robert A Rizza, and Claudio Cobelli. Meal simulation model of the glucose-insulin system. *IEEE Transactions on biomedical engineering*, 54(10):1740–1749, 2007.

[134] John Thomas Sorensen. *A physiologic model of glucose metabolism in man and its use to design and assess improved insulin therapies for diabetes*. PhD thesis, Massachusetts Institute of Technology, 1985.

[135] Joseph Tiran, Kurt R Galle, and Daniel Porte. A simulation model of extracellular glucose distribution in the human body. *Annals of biomedical engineering*, 3(1):34–46, 1975.

[136] John R Guyton, Richard O Foster, J Stuart Soeldner, Meng H Tan, Charles B Kahn, L Koncz, and Ray E Gleason. A model of glucose-insulin homeostasis in man that incorporates the heterogeneous fast pool theory of pancreatic insulin release. *Diabetes*, 27(10):1027–1042, 1978.

[137] Puntip Toghaw, Alice Matone, Yongwimon Lenbury, and Andrea De Gaetano. Bariatric surgery and t2dm improvement mechanisms: a mathematical model. *Theoretical Biology and Medical Modelling*, 9(1):16, 2012.

[138] Gerold M Grodsky, D Curry, Herbert Landahl, and L Bennett. Further studies on the dynamic aspects of insulin release in vitro with evidence for a two-compartmental storage system. *Acta diabetologica latina*, 6:554–578, 1969.

[139] Gerold M Grodsky. A threshold distribution hypothesis for packet storage of insulin and its mathematical modeling. *Journal of Clinical Investigation*, 51(8):2047, 1972.

[140] Jeppe Sturis, Kenneth S Polonsky, Erik Mosekilde, and Eve Van Cauter. Computer model for mechanisms underlying ultradian oscillations of insulin and glucose. *American Journal of Physiology-Endocrinology And Metabolism*, 260(5):E801–E809, 1991.

[141] Iva Marija Tolić, Erik Mosekilde, and Jeppe Sturis. Modeling the insulin–glucose feedback system: the significance of pulsatile insulin secretion. *Journal of theoretical biology*, 207(3):361–375, 2000.

[142] R Srinivasan, Arnold H Kadish, and R Sridhar. A mathematical model for the control mechanism of free fatty acid-glucose metabolism in normal humans. *Computers and Biomedical Research*, 3(2):146–165, 1970.

[143] C Cobelli and A Ruggeri. Evaluation of alternative model structures of metabolic systems: two case studies on model identification and validation. *Medical and Biological Engineering and Computing*, 20(4):444–450, 1982.

[144] C Cobelli and A Mari. Validation of mathematical models of complex endocrine-metabolic systems. a case study on a model of glucose regulation. *Medical and Biological Engineering and Computing*, 21(4):390–399, 1983.

[145] ED Lehmann and T Deutsch. A physiological model of glucose-insulin interaction in type 1 diabetes mellitus. *Journal of biomedical engineering*, 14(3):235–242, 1992.

[146] Steen Andreassen, Jonathan J Benn, Roman Hovorka, Kristian G Olesen, and Ewart R Carson. A probabilistic approach to glucose prediction and insulin dose adjustment: description of metabolic model and pilot evaluation study. *Computer methods and programs in biomedicine*, 41(3-4):153–165, 1994.

[147] Chiara Dalla Man, Davide M Raimondo, Robert A Rizza, and Claudio Cobelli. Gim, simulation software of meal glucose—insulin model, 2007.

[148] Claudio Cobelli, Eric Renard, and Boris Kovatchev. Artificial pancreas: past, present, future. *Diabetes*, 60(11):2672–2682, 2011.

[149] Enrique Campos-Náñez, Jennifer E Layne, and Howard C Zisser. In silico modeling of minimal effective insulin doses using the uva/padova type 1 diabetes simulator. *Journal of Diabetes Science and Technology*, page 1932296817735341, 2017.

[150] Marc D Breton, Rolf Hinzmann, Enrique Campos-Nañez, Susan Riddle, Michael Schoemaker, and Guenther Schmelzeisen-Redeker. Analysis of the accuracy and performance of a continuous glucose monitoring sensor prototype: An in-silico study using the uva/padova type 1 diabetes simulator. *Journal of Diabetes Science and Technology*, 11(3):545–552, 2017.

[151] Enrique Campos-Náñez, Kurt Fortwaengler, and Marc D Breton. Clinical impact of blood glucose monitoring accuracy: An in-silico study. *Journal of Diabetes Science and Technology*, page 1932296817710474, 2017.

[152] Jinyu Xie and Qian Wang. A variable state dimension approach to meal detection and meal size estimation: in silico evaluation through basal-bolus insulin therapy for type 1 diabetes. *IEEE Transactions on Biomedical Engineering*, 2017.

[153] Marco Viceconti, Claudio Cobelli, Tarek Haddad, Adam Himes, Boris Kovatchev, and Mark Palmer. In silico assessment of biomedical products: The conundrum of rare but not so rare events in two case studies. *Proceedings of the Institution of Mechanical Engineers, Part H: Journal of Engineering in Medicine*, 231(5):455–466, 2017.

[154] Chiara Toffanin, Roberto Visentin, Mirko Messori, Federico Di Palma, Lalo Magni, and Claudio Cobelli. Towards a run-to-run adaptive artificial pancreas: In silico results. *IEEE Transactions on Biomedical Engineering*, 2017.

[155] Roberto Visentin, Clemens Giegerich, Robert Jäger, Raphael Dahmen, Anders Boss, Marshall Grant, Chiara Dalla Man, Claudio Cobelli, and Thomas Klabunde. Improving efficacy of inhaled technosphere insulin (afrezza) by postmeal dosing: in-silico clinical trial with the university of virginia/padova type 1 diabetes simulator. *Diabetes technology & therapeutics*, 18(9):574–585, 2016.

[156] Stamatina Zavitsanou, Athanasios Mantalaris, Michael C Georgiadis, and Efstratios N Pistikopoulos. In silico closed-loop control validation studies for optimal insulin delivery in type 1 diabetes. *IEEE Transactions on Biomedical Engineering*, 62(10):2369–2378, 2015.

[157] Stephen D Patek, B Wayne Bequette, Marc Breton, Bruce A Buckingham, Eyal Dassau, Francis J Doyle III, John Lum, Lalo Magni, and Howard Zisser. In silico preclinical trials: methodology and engineering guide to closed-loop control in type 1 diabetes mellitus. *Journal of diabetes science and technology*, 3(2):269–282, 2009.

[158] Chiara Dalla Man, Michael Camilleri, and Claudio Cobelli. A system model of oral glucose absorption: validation on gold standard data. *IEEE Transactions on Biomedical Engineering*, 53(12):2472–2478, 2006.

[159] Ewart Carson and Claudio Cobelli. Modelling methodology for physiology and medicine. chapter 11. Newnes, 2013.

[160] Chiara Dalla Man, Francesco Micheletto, Dayu Lv, Marc Breton, Boris Kovatchev, and Claudio Cobelli. The uva/padova type 1 diabetes simulator: new features. *Journal of diabetes science and technology*, 8(1):26–34, 2014.

[161] I Johanna Stamper and Xujing Wang. Mathematical modeling of insulin secretion and the role of glucose-dependent mobilization, docking, priming and fusion of insulin granules. *Journal of theoretical biology*, 318:210–225, 2013.

[162] Archibald Vivian Hill. The possible effects of the aggregation of the molecules of haemoglobin on its dissociation curves. *J Physiol (Lond)*, 40:4–7, 1910.

[163] James D Murray. Mathematical biology. i, volume 17 of interdisciplinary applied mathematics, 2002.

[164] Ferenc Preisach. Über die magnetische nachwirkung. *Zeitschrift für Physik A Hadrons and Nuclei*, 94(5):277–302, 1935.

[165] Rafael Nesher and Erol Cerasi. Modeling phasic insulin release. *Diabetes*, 51(suppl 1): S53–S59, 2002.

[166] Morten Gram Pedersen, Alberto Corradin, Gianna M Toffolo, and Claudio Cobelli. A subcellular model of glucose-stimulated pancreatic insulin secretion. *Philosophical Transactions of the Royal Society of London A: Mathematical, Physical and Engineering Sciences*, 366(1880):3525–3543, 2008.

[167] P Lonnroth, PA Jansson, and U Smith. A microdialysis method allowing characterization of intercellular water space in humans. *American Journal of Physiology-Endocrinology And Metabolism*, 253(2):E228–E231, 1987.

[168] Eda Cengiz and William V Tamborlane. A tale of two compartments: interstitial versus blood glucose monitoring. *Diabetes technology & therapeutics*, 11(S1):S–11, 2009.

[169] Philip J Stout, Nina Peled, Brian J Erickson, Michael E Hilgers, Joel R Racchini, and Thomas B Hoegh. Comparison of glucose levels in dermal interstitial fluid and finger capillary blood. *Diabetes technology & therapeutics*, 3(1):81–90, 2001.

[170] Kerstin Rebrin, Garry M Steil, William P Van Antwerp, and John J Mastrototaro. Subcutaneous glucose predicts plasma glucose independent of insulin: implications for continuous monitoring. *American Journal of Physiology-Endocrinology and Metabolism*, 277(3):E561–E571, 1999.

[171] Kerstin Rebrin and Garry M Steil. Can interstitial glucose assessment replace blood glucose measurements? *Diabetes technology & therapeutics*, 2(3):461–472, 2000.

[172] GM Steil, K Rebrin, F Hariri, S Jinagonda, S Tadros, C Darwin, and MF Saad. Interstitial fluid glucose dynamics during insulin-induced hypoglycaemia. *Diabetologia*, 48(9): 1833–1840, 2005.

[173] Lutz Heinemann and Douglas B Muchmore. Ultrafast-acting insulins: state of the art, 2012.

[174] John Pickup and Harry Keen. Continuous subcutaneous insulin infusion at 25 years. *Diabetes care*, 25(3):593–598, 2002.

[175] B Wayne Bequette. A critical assessment of algorithms and challenges in the development of a closed-loop artificial pancreas. *Diabetes technology & therapeutics*, 7(1):28–47, 2005.

[176] Jacob Jaremko and Otto Rorstad. Advances toward the implantable artificial pancreas for treatment of diabetes. *Diabetes care*, 21(3):444–450, 1998.

[177] Francis J Doyle, Lauren M Huyett, Joon Bok Lee, Howard C Zisser, and Eyal Dassau. Closed-loop artificial pancreas systems: engineering the algorithms. *Diabetes care*, 37 (5):1191–1197, 2014.

[178] Paola Soru, Giuseppe De Nicolao, Chiara Toffanin, Chiara Dalla Man, Claudio Cobelli, Lalo Magni, AP@ home consortium, et al. Mpc based artificial pancreas: strategies for individualization and meal compensation. *Annual Reviews in Control*, 36(1):118–128, 2012.

[179] William L Clarke, Stacey Anderson, Marc Breton, Stephen Patek, Laurissa Kashmer, and Boris Kovatchev. Closed-loop artificial pancreas using subcutaneous glucose sensing and insulin delivery and a model predictive control algorithm: the virginia experience, 2009.

[180] Hyunjin Lee, Bruce A Buckingham, Darrell M Wilson, and B Wayne Bequette. A closed-loop artificial pancreas using model predictive control and a sliding meal size estimator, 2009.

[181] Karl Heinz Kienitz and Takashi Yoneyama. A robust controller for insulin pumps based on h-infinity theory. *IEEE Transactions on Biomedical Engineering*, 40(11):1133–1137, 1993.

[182] MS Ibbini and MA Masadeh. A fuzzy logic based closed-loop control system for blood glucose level regulation in diabetics. *Journal of medical engineering & technology*, 29(2): 64–69, 2005.

[183] Ali Zolghadri, Michel Monsion, David Henry, Christian Marchionini, and O Petrique. Development of an operational model-based warning system for tropospheric ozone concentrations in bordeaux, france. *Environmental Modelling & Software*, 19(4):369–382, 2004.

[184] X Paez, CA Mazzei-Davila, and L Hernandez. Subcutaneous microdialysis: a simple technique for monitoring the extracellular biochemical environment. combination with capillary electrophoresis and laser-induced fluorescence detection. *Investigacion clinica*, 44(3):227–239, 2003.

[185] Yasuhiro Hashiguchi, Michiharu Sakakida, Kenro Nishida, Takero Uemura, Ken-Ichiro Kajiwara, and Motoaki Shichiri. Development of a miniaturized glucose monitoring system by combining a needle-type glucose sensor with microdialysis sampling method: long-term subcutaneous tissue glucose monitoring in ambulatory diabetic patients. *Diabetes care*, 17(5):387–396, 1994.

[186] Chiara Dalla Man, Francesco Micheletto, Airani Sathananthan, Robert A Rizza, Adrian Vella, and Claudio Cobelli. A model of glp-1 action on insulin secretion in nondiabetic subjects. *American Journal of Physiology-Endocrinology and Metabolism*, 298(6):E1115–E1121, 2010.

[187] Galina Smushkin, Matheni Sathananthan, Airani Sathananthan, Chiara Dalla Man, Francesco Micheletto, Alan R Zinsmeister, Claudio Cobelli, and Adrian Vella. Diabetes-associated common genetic variation and its association with glp-1 concentrations and response to exogenous glp-1. *Diabetes*, 61(5):1082–1089, 2012.

[188] Airani Sathananthan, Chiara Dalla Man, Francesco Micheletto, Alan R Zinsmeister, Michael Camilleri, Paula D Giesler, Jeanette M Laugen, Gianna Toffolo, Robert A Rizza, Claudio Cobelli, et al. Common genetic variation in glp1r and insulin secretion in response to exogenous glp-1 in nondiabetic subjects. *Diabetes care*, 33(9):2074–2076, 2010.

[189] Peter Loskill, Sivan G Marcus, Anurag Mathur, Willie Mae Reese, and Kevin E Healy. μorgano: A lego®-like plug & play system for modular multi-organ-chips. *PloS one*, 10 (10):e0139587, 2015.

[190] Johan U Lind, Travis A Busbee, Alexander D Valentine, Francesco S Pasqualini, Hongyan Yuan, Moran Yadid, Sung-Jin Park, Arda Kotikian, Alexander P Nesmith, Patrick H Campbell, et al. Instrumented cardiac microphysiological devices via multi-material three-dimensional printing. *Nature materials*, 16(3):303–308, 2017.

[191] E Ruiz-Velázquez, R Femat, and DU Campos-Delgado. Blood glucose control for type i diabetes mellitus: A robust tracking $\mathcal{H}_\infty$ problem. *Control Engineering Practice*, 12(9): 1179–1195, 2004.

[192] Levente Kovács, Balázs Benyó, József Bokor, and Zoltán Benyó. Induced l 2-norm minimization of glucose–insulin system for type i diabetic patients. *Computer Methods and Programs in Biomedicine*, 102(2):105–118, 2011.

[193] Jessica R Castle, Julia M Engle, Joseph El Youssef, Ryan G Massoud, Kevin CJ Yuen, Ryland Kagan, and W Kenneth Ward. Novel use of glucagon in a closed-loop system for prevention of hypoglycemia in type 1 diabetes. *Diabetes Care*, 33(6):1282–1287, 2010.

[194] Zhen-Ping Shen, Masayoshi Nishimura, Yoshiyuki Tsuura, Shimpei Fujimoto, Eri Mukai, Yuichiro Yamada, and Yutaka Seino. Distinct effect of diazoxide on insulin secretion stimulated by protein kinase a and protein kinase c in rat pancreatic islets. *Diabetes research and clinical practice*, 53(1):9–16, 2001.

[195] Pascal Mariot, Patrick Gilon, Myriam Nenquin, and Jean-Claude Henquin. Tolbutamide and diazoxide influence insulin secretion by changing the concentration but not the action of cytoplasmic ca2+ in beta-cells. *Diabetes*, 47(3):365–373, 1998.

[196] Catrin F Williams, David Lloyd, Jonathan Lees, Antoine Pirog, Gilles M Geroni, Jordan Pastre, Valentin Kriegel, and Adrian Porch. What the deep sea can tell us about microwaves. In *Microwave Symposium (IMS), 2016 IEEE MTT-S International*, pages 1–4. IEEE, 2016.

[197] Catrin F Williams, Gilles M Geroni, Antoine Pirog, David Lloyd, Jonathan Lees, and Adrian Porch. The separated electric and magnetic field responses of luminescent bacteria exposed to pulsed microwave irradiation. *Applied Physics Letters*, 109(9):093701, 2016.

[198] Matthieu Ambroise, Stefano Buccelli, Filippo Grassia, Antoine Pirog, Yannick Bornat, Michela Chiappalone, and Timothée Levi. Biomimetic neural network for modifying biological dynamics during hybrid experiments. *Artificial Life and Robotics*, pages 1–6, 2017.